Titre: Title:	Indirect Measurement of Inter-Particle Forces in a Gas-Solid Fluidized Bed at High Temperature with a Simple Approach
Auteur: Author:	Navid Elahipanah
Date:	2017
Type:	Mémoire ou thèse / Dissertation or Thesis
Référence: Citation:	Elahipanah, N. (2017). Indirect Measurement of Inter-Particle Forces in a Gas-Solid Fluidized Bed at High Temperature with a Simple Approach [Master's thesis, École Polytechnique de Montréal]. PolyPublie. https://publications.polymtl.ca/2624/

UNIVERSITÉ DE MONTRÉAL

INDIRECT MEASUREMENT OF INTER-PARTICLE FORCES IN A GAS-SOLID FLUIDIZED BED AT HIGH TEMPERATURE WITH A SIMPLE APPROACH

NAVID ELAHIPANAH

DÉPARTEMENT DE GÉNIE CHIMIQUE

ÉCOLE POLYTECHNIQUE DE MONTRÉAL

MÉMOIRE PRÉSENTÉ EN VUE DE L'OBTENTION

DU DIPLÔME DE MAÎTRISE ÈS SCIENCES APPLIQUÉES

(GÉNIE CHIMIQUE)

JUIN 2017

UNIVERSITÉ DE MONTRÉAL

ÉCOLE POLYTECHNIQUE DE MONTRÉAL

Ce mémoire intitulé:

INDIRECT MEASUREMENT OF INTER-PARTICLE FORCES IN A GAS-SOLID FLUIDIZED BED AT HIGH TEMPERATURE WITH A SIMPLE APPROACH

présenté par : ELAHIPANAH Navid

en vue de l'obtention du diplôme de : Maîtrise ès sciences appliquées

a été dûment accepté par le jury d'examen constitué de :

M. PERRIER Michel, Ph. D., président

M. CHAOUKI Jamal, Ph. D., membre et directeur de recherche

M. LATIFI Mohammad, Ph. D., membre

ACKNOWLEDGEMENTS

First, my highest appreciation is going to my supervisor, Prof. Jamal Chaouki, who at the first place put his trust on me and consistently allowed me to work freely, but steered me in the right direction whenever he thought I needed it.

The financial support provided by Total E&P, the industrial partner of this research chair and the Natural Sciences and Engineering Research Council of Canada (NSERC) is greatly appreciated.

My sincerest gratitude goes to my dearest colleague, Dr. Jaber Shabanian who guided me through out every step of this work with his priceless experience and vast knowledge.

Special thanks to all my colleagues at PEARL research group, from whom I have learnt a lot during our precious group meetings and friendly discussions.

My deepest appreciation goes to the technicians in the Department of Chemical Engineering, particularly Robert Delisle and Sylvain Simard-Fleury for their excellent technical assistance.

I would like to thank also my dear colleague, El Mahdi Lakhdissi, for the translation of the abstract to French.

Finally, I must express my very profound gratitude to my parents for providing me with unfailing support and continuous encouragement throughout my years of study and through the process of researching and writing this thesis. This accomplishment would not have been possible without them.

Thank you.

Navid Elahipanah

RÉSUMÉ

Le procédé de fluidisation est largement utilisé dans une multitude d'applications et de procédés chimiques et ceci grâce aux avantages qu'il procure tels qu'un traitement facile de la phase solide, une grande qualité de mélangeage des particules solides, un transfert de matière favorisé, une distribution uniforme de la température et une chute de pression réduite. Tous ces avantages rendent la fluidisation un grand concurrent aux réacteurs à lit fixe où tiennent lieu des procédés similaires. Cependant, l'hydrodynamique d'un tel système à hautes température n'est pas bien maitrisée et ceci dû à l'impact des niveaux élevés des forces inter particulaires (FIPs) dans des conditions extrêmes. En d'autres termes, la plupart des modèles et corrélations basées sur l'hydrodynamique et qui sont utilisées n'arrivent pas à prédire correctement les paramètres hydrodynamiques obtenus expérimentalement tels que la vitesse minimale de fluidisation U_{mf} et la vitesse du régime critique U_c car ces modèles et corrélations négligent le rôle des forces inter particulaires à hautes températures. En d'autre part, la demande globale pousse les industriels à utiliser de plus en plus des matières premières de mauvaise qualité et qui ont une grande tendance à causer les phénomènes d'agglomération et de défluidisation à cause des niveaux élevés des forces inter particulaires. Ainsi, l'objectif de ce projet de recherche est d'introduire une nouvelle et simple méthode pour estimer les forces inter particulaires à hautes températures.

Comme première étape, nous avons mis le point sur l'effet de la viscosité et la densité de gaz sur l'hydrodynamique du lit comme U_{mf}, le comportement des bulles et U_c quand le rôle des forces inter particulaires à régir l'hydrodynamique du lit est perceptible. Ceci a été réalisé en mesurant $U_{mf\ et}$ U_c pour différentes températures allant de la température ambiante jusqu'à 650 ºC en utilisant l'air et l'argon comme différentes phases gazeuses et le FCC, les billes de verre, et du sable siliceux grossier et fin comme différentes phases solides. Ces dernières ont différents points de fusion et appartiennent à Geldart A ou B en considérant leur tailles et masse volumiques. Nous avons démontré que pour le sable siliceux fin et grossier l'effet de la température sur les valeurs de U_{mf} et U_c et qui est liée directement à son effet direct sur les propriétés du gaz et le niveau des forces hydrodynamiques FHDs peut être estimé correctement par les corrélations basées sur l'hydrodynamique. Cependant, nous avons trouvé que pour FCC et les billes de verre, les

corrélations hydrodynamiques n'arrivent pas à prédire correctement les valeurs de U_{mf} et U_c obtenues expérimentalement et ceci dû à l'effet significatif des forces inter particulaires. Nous avons aussi démontré que l'ordre de grandeur des forces inter particulaires peut être estimé en faisant la différence entre la valeur de la force de trainée calculée sur la base de U_{mf} mesurée expérimentalement et la valeur de la force de trainée obtenue pour U_{mf} estimée par des considérations purement hydrodynamiques pour une certaine température. Nous avons aussi validé notre estimation en mesurant la hauteur et l'aire sous le pic du graphe qui représente la chute de pression totale du lit en fonction de la vitesse superficielle du gaz pour les billes de verre et les particules FCC. Les résultats démontrent que les forces inter particulaires FIPs jouent un rôle plus important pour des particules qui ont un point de fusion plus bas en considérant la température de fonctionnement et cet effet peut être réduit en exerçant des forces hydrodynamiques plus élevées sur les particules, en l'occurrence, dans le cas de la fluidisation par l'argon.

Nous avons aussi expliqué la variation de U_c en fonction de la température en soulignant l'effet de la température sur le comportement bouillonnant de lits de différents matériaux en considérant le ration FIPs/FHDs. Nous avons trouvé que la taille des bulles et la résistance de la phase d'émulsion à la rupture sont les paramètres principaux qui déterminent la vitesse de transition du gaz.

ABSTRACT

Fluidization process is being broadly used for numerous applications and chemical processes owing to the easy solids handling, high quality mixing of solids, promoted mass transfer, uniform temperature distribution and reduced pressure drop which makes it a promising competitor for similar processes using fixed bed reactors. However, the hydrodynamics of such a system at elevated temperatures is not well understood due to the impact of elevated levels of inter-particle forces (IPFs) at extreme conditions. In other words, most of the available hydrodynamic based models and correlations fail to predict the experimentally obtained hydrodynamic parameters such as U_{mf} and U_c due to neglecting the important role of IPFs at high temperatures. On the other hand, the global demand pushes the industries to increasingly use low quality feedstocks which have higher tendency toward agglomeration and defluidization because of an increased level of IPFs. Thus, in this research our focus is on introducing a new and simple method of estimation of IPFs at high temperature.

As a first step, we highlighted the influence of gas viscosity and density on the bed hydrodynamics such as U_{mf}, bubble behavior and U_c when the role of IPFs in governing the bed hydrodynamics was not discernible. We did so by measuring U_{mf} and U_c at different temperatures from ambient to 650 ºC using air and argon for FCC (86µm), glass beads (71µm), fine (226µm) and coarse silica sand (820µm) particles with different melting points belonging to Geldart group A and B considering their size and density. We showed that for coarse and fine silica sand particles the value of U_{mf} and U_c change by temperature depending on its effect on the gas properties and the magnuitude of HDFs and this trend can be well predicted by the hydrodynamic based correlations. However, we found that for glass beads and FCC particles the experimentally measured U_{mf} and U_c can not be well predicted by the hydrodynamic based correlations due to the significant effect of IPFs. We also showed that by subtracting the values of drag force calculated at the experimentally measured U_{mf} and the one obtained at predicted U_{mf} by purely hydrodynamic considerations we can estimate the magnitude of IPF that is present in the system at a certain temperature. We also validated our estimation by measuring the height and the area of the peak in the plot of total bed pressure drop against increasing superficial gas velocity for glass beads and

FCC particles. The results showed that IPFs plays a more important role for particles with lower melting point considering the operating temperature and this effect would be reduced when higher drag force is applied on the particles i.e. in the case of fluidization with argon.

We also explained the variation of U_c by temperature by explaining the effect of temperature on the bubbling behaviour of beds of different materials considering the ratio of IPFs/HDFs. We found the bubble size and the resistance of the emulsion phase against break-up to be the main parameters to define the transition gas velocity.

TABLE OF CONTENTS

ACKNOWLEDGEMENTS III

RÉSUMÉ IV

ABSTRACT VI

TABLE OF CONTENTS VIII

LIST OF TABLES XI

LIST OF FIGURES XII

LIST OF SYMBOLS AND ABBREVIATIONS XVII

LIST OF APPENDICES XX

CHAPTER 1 INTRODUCTION 1

1.1 Problem Statement and Motivation 1

1.2 Objectives 3

CHAPTER 2 LITERATURE REVIEW 4

2.1 Basics of Fluidization 4

2.2 Application of High Temperature/Pressure Fluidized Bed (HTHP FB) 7

2.3 Hydrodynamic Forces (HDFs) 9

2.3.1 Drag Force 9

2.3.2 Buoyant Force 9

2.4 Inter-Particle Forces (IPFs) 10

2.4.1 Van der Waals 11

2.4.2 Electrostatic 11

2.4.3 Material Bridge 12

2.4.4 Measurement of IPFs 14

2.5 Effect of Temperature on Hydrodynamic Parameters in a Fluidized-Bed with No/Negligible IPFs 17

2.6 Effect of Temperature on Hydrodynamic Parameters in a Fluidized-Bed in the Presence of IPFs 18

2.7 Hydrodynamic-Based Models and Correlations for U_{mf} Prediction 21

CHAPTER 3 EXPERIMENTAL AND METHODOLOGY 25

3.1 Experimental Setup 25

3.2 Materials 30

3.3 Analysis Methods 32

3.3.1 Bed Pressure Drop 32

3.3.2 Standard Deviation 33

3.4 Experimental Procedure 33

CHAPTER 4 RESULTS AND DISCUSSION 35

4.1 Results and Discussion 35

4.1.1 U_{mf} Measurements 35

4.1.2 Indirect Measurement of IPFs 49

CHAPTER 5 CONCLUSION AND RECOMMENDATIONS 58

5.1 Conclusion 58

5.2 Recommendations 59

BIBLIOGRAPHY 61

APPENDIX A – EFFECT OF PRESSURE ON THE HYDRODYNAMICS OF GAS-SOLID FLUIDIZED BEDS 79

APPENDIX B – CORRELATIONS FOR BUBBLING TO TURBULENT TRANSITION VELOCITY (U_C) 84

APPENDIX C – U_C MEASUREMENT RESULTS 86

LIST OF TABLES

Table 2.1: Expected flowability of powders based on angle of repose [64] 15

Table 2.2: Powder classification based on HR [64] 15

Table 3.1: Solid materials used in the experiments 31

Table 3.2: Fluidizing gases used in the experiments 31

LIST OF FIGURES

Figure 2.1: Different fluidization regimes in a fluidized bed.....5

Figure 2.2: Geldart classification of particles 6

Figure 2.3: Summary of more than 100 research done on the hydrodynamics of FBs at high pressure and temperature 8

Figure 2.4: Liquid bridge formed between two identical particles. 12

Figure 2.5: Presentation of various IPFs along with the weight of the particle [33] 13

Figure 2.6: Dependance of Hausner Ratio (HR) for Al_2O_3 (3700 kg/m^3) and TiO_2 (4200 kg/m^3) powders using automatic tapping (HRa) and manual tapping (HRm). [63] 16

Figure 2.7: Variation of U_{mf} by temperature for Geldart group D particles [77].....18

Figure 2.8: Influence of pressure on U_{mf}. ○-ballottini, d= 0.25 mm;.....22

Figure 2.9: Effect of the dependence of ε_{mf} on temperature on the estimation of U_{mf} by Carman-Kozeny equation. — corrected ε_{mf}, - - - ambient ε_{mf} [15].....23

Figure 2.10: Comparison between U_{mf} obtained experimentally and by predictions from Carman-Kozeny for different sizes of silica sand [15]. 24

Figure 3.1: High-temperature fluidized bed drawing. Bed and freeboard sections. 25

Figure 3.2: Filter design 26

Figure 3.3: Schematic drawing of the perforated distributor plate: (a) side view, (b) Top view, (c) Bottom view 28

Figure 3.4: Pre-heating elements and heating jacket.....28

Figure 3.5: Total bed pressure drop vs. superficial gas velocity plot in: (a) decreasing pass and (b) increasing pass.....33

Figure 4.1: Variation of total bed pressure drop in the decreasing superficial gas velocity pass at different temperatures for CS820 fluidized by Air. 36

Figure 4.2: Variation of minimum fluidization velocity of CS820 by the temperature compared to the prediction achieved by the Chitester et al.'s correlation [118].....37

Figure 4.3: Variation of total bed pressure drop in the decreasing superficial gas velocity pass at different temperatures for FS226 fluidized by Air at $1 < U_g < 5$ cm/s.....38

Figure 4.4: Variation of total bed pressure drop in the decreasing superficial gas velocity pass at different temperatures for FS226 fluidized by Air at $U_g > 5$ cm/s.....38

Figure 4.5: Variation of minimum fluidization velocity of FS226 by temperature compared to the prediction achieved by theWen-Yu (W-Y) Eq. [119].....39

Figure 4.6: Variation of total bed pressure drop in the increasing superficial gas velocity pass at different temperatures for Cooked FCC86 fluidized by Air at $0.2 < U_g < 1$ cm/s.....40

Figure 4.7: Variation of Minimum fluidization velocity of Cooked FCC86 by temperature compared to the predictions achieved by the Wen-Yu (W-Y) [119] and Carman-Kozeny (C-K) [121] correlation as well as the C-K correlation with a corrected value of ε_{mf} by temperature [15], [96].....40

Figure 4.8: Condensation of water at the outlet of HTFB at temperatures higher than 500ºC causing the particles to stick to the filter.....41

Figure 4.9: TGA results of Fresh and Cooked FCC86.....42

Figure 4.10: Variation of total bed pressure drop by increasing the superficial gas velocity at different temperatures for GB71 fluidized by Air at $0 < Ug < 2$ cm/s.....43

Figure 4.11: Variation of total bed pressure drop by increasing the superficial gas velocity at different temperatures for GB71 fluidized by Air at $Ug > 1$ cm/s.....43

Figure 4.12: Variation of minimum fluidization velocity of GB71 by temperature fluidized with air compared to Carman-Kozeny (C-K) [121] and C-K with corrected value of ε_{mf} by temperature [15], [96].....44

Figure 4.13: Evolutions of in-bed and total bed pressure drops and the in-bed temperature readings (T4, T5, T6 and T7 respectively at 5, 12.5, 15 and 17.5 cm from the distributor plate) through a defluidization test for GB71 at U_g=1.1 cm/s. 45

Figure 4.14: Formation of hard agglomerates of GB71 after full defluidization at 500ºC. 46

Figure 4.15: Variations of the viscosities of Air and Argon (Ar) by temperature [81], [127]. 47

Figure 4.16: Variation of minimum fluidization velocity by temperature when fluidizing the particles with Air and Ar in the decreasing pass for: (a) FS226, (b) FCC86 and (c) GB71. .48

Figure 4.17 : Variation of minimum fluidization velocity of GB71 (●) by temperature fluidized with (a) air and (b) argon compared to the predictions achieved by the C-K equation (- - -). 48

Figure 4.18: Variation of total bed pressure drop in the increasing superficial gas velocity pass at different temperatures for GB71 fluidized by Ar at 0 < Ug < 1 cm/s. 49

Figure 4.19: Cubic stacking structure of particles with N_c = 6 51

Figure 4.20: Individual IPFs value obtained for: (a) GB71 fluidized with Air, (b) FCC86 fluidized with Air, (c) GB71 fluidized with Argon and (d) FCC86 fluidized with Argon. 53

Figure 4.21: IPF/W value obtained for: (a) GB71 fluidized with Air, (b) FCC86 fluidized with Air, (c) GB71 fluidized with Argon and (d) FCC86 fluidized with Argon. 54

Figure 4.22: Peak area evaluation as a qualitative estimation of IPFs. GB71 fluidized with air at 400 ºC. 55

Figure 4.23: The variation of normalized peak height and peak area in the plot of total bed pressure drop against increasing gas velocity with temperature for: (a) GB71 fluidized with Air, (b) FCC86 fluidized with Air, (c) GB71 fluidized with Argon and (d) FCC86 fluidized with Argon. 56

Figure 4.24 : The variation of normalized peak area and IPFs/W with temperature for: (a) GB71 and (b) FCC86 fluidized with air. 57

Figure 0.1: Variation of U_{mf} with pressure for 0.7 mm sand particles.....79

Figure 0.2: Variation of bubble size by pressure for 400 µm char particles fluidized by air [157]. 80

Figure 0.3: Summary of the effect of pressure and temperature on simple hydrodynamic parameters of fluidization in the absence of IPFs.....81

Figure 0.4: Summary of the effect of pressure and temperature on simple hydrodynamic parameters of fluidization in the presence of IPFs for fine particles. 83

Figure 0.1: Variation of the standard deviation of gauge pressure signals by superficial gas velocity for FS226 fluidized by Air at different temperatures. 86

Figure 0.2: Variation of U_c by temperature for FS226 fluidized by Air compared to the predicted value by Chehbouni et al. [183]. 87

Figure 0.3: Variation of the standard deviation of gauge pressure signals by superficial gas velocity for CS820 fluidized by Air at different temperatures. 88

Figure 0.4: Variation of the standard deviation of gauge pressure signals by superficial gas velocity for FCC86 fluidized by Air at different temperatures. 89

Figure 0.5: Variation of U_c by temperature for FCC86 fluidized by Air compared to its value estimated by Chehbouni et al. [183].....90

Figure 0.6: Variation of the standard deviation of gauge pressure signals by superficial gas velocity for FCC86 fluidized by Air at T > 350 ºC and $U_g > U_c$.....91

Figure 0.7: Variation of the standard deviation of gauge pressure signals by superficial gas velocity for GB71 fluidized by Air at different temperatures. 92

Figure 0.8: Variation of U_c by temperature for GB71 fluidized by Air compared to its value estimated by Chehbouni et al. [183].....92

Figure 0.9 : Variation of the standard deviation of gauge pressure signals by superficial gas velocity for FS226 at different temperatures fluidized by: (a) air and (b) argon 93

Figure 0.10: Variation of U_c of: (a) FS226 (b) FCC86 and (c) GB71 by temperature for fluidization with Air and Ar. 94

Figure 0.11: Variation of U_c by temperature for FCC86 fluidized by Air compared to its value estimated by: (a) Chehbouni et al. [183], (b) Cai et al. [163] and (c) Horio et al. [181]. 95

LIST OF SYMBOLS AND ABBREVIATIONS

Acronyms

CS820 Coarse Sand (d_p = 820 µm)

FB Fluidized Bed

FCC86 FCC (d_p = 86 µm)

FS226 Fine Sand (d_p = 226 µm)

GB71 Glass Beads (d_p = 71 µm)

HDF Hydrodynamic Force

HPHT High Pressure High Temperature

HR Hausner Ratio

HTFB High Temperature Fluidized Bed

IPF Inter-Particle Force

MSDS Material Safety Data Sheet

PSD Power Spectral Density

Symbols

A Bed Section, (m^2)

Ar Archimedes Number, (-)

C_d Drag Coefficient, (-)

D Column Diameter, (m)

d_p Particle Size, (m)

F_b Buoyancy Force, (N)

F_c Capillary Force, (N)

F_d Total Drag Force, (N)

f_d Single Particle Drag Force, (N)

$F_{d\varepsilon}$ Total Drag Force Considering the Bed Voidage, (N)

F_{vdw} Van der Waals Force, (N)

g Gravitational Acceleration, (m/s^2)

H Bed Height, (m)

H_r Hardness of the softer particle, (N/m^2)

$h\omega$ Liftshits-Van der Waals Coefficient, (J)

N_c Coordination Number, (-)

P Pressure, (Pa)

$\bar{p}$ Mean Value of Pressure Data Points, (Pa)

q Electric Charge, (C)

R Particle Radius, (m)

R_{as} Radius of Asperity, (m)

Re_{mf} Reynolds Number at U_{mf}, (m)

Re_p Particle Reynolds Number, (-)

STD Standard Deviation of Pressure, (Pa)

T Temperature, (ºC)

U_c Transition to turbulent, (m/s)

U_g Superficial Gas Velocity, (m/s)

U_{mb} Minimum Bubbling Velocity, (m/s)

U_{mf} Minimum Fluidization Velocity, (m/s)

U_{tr} Transition to Transport Regime Velocity, (m/s)

W Weight of the Particle, (N)

W_b Buoyancy Weight, (N)

Z Working Distance of Van der Waals Force, (m)

ΔP Pressure Drop, (Pa)

Greek Letters

μ Gas Viscosity, (Pa.s)

ε Bed Voidage, (-)

ε_{mf} Bed Voidage at U_{mf}, (-)

γ Surface tension, (N/m)

ϵ Permittivity, (F/m)

θ Angle of Repose, (rad)

ρ_f Fluid Density, (kg/m^3)

ρ_{fb} Density of a Fluidized Bed, (kg/m^3)

ρ_p Density of Particle, (kg/m^3)

σ Standard Deviation, (-)

τ Sintering Time, (s)

φ Sphericity, (-)

LIST OF APPENDICES

Appendix A – Effect of Pressure on the Hydrodynamics of Gas-Solid Fluidized Beds.....79

Appendix B – Correlations for Bubbling to Turbulent Transition Velocity (U_c) 84

Appendix C – U_c Measurement Results.....86

CHAPTER 1 INTRODUCTION

1.1 Problem Statement and Motivation

Fluidized bed (FB) reactor are being used in a variety of applications in pharmaceutical, food, chemical, and petrochemical, due to their unique gas-solid mixing characteristics [1]–[3]. This feature provides FB reactors with enhanced mass and heat transfer quality [4]–[6]. In general, there are six well-known flow regimes i.e. fixed bed, homogeneous fluidization, bubbling, turbulent, circulating fluidization and pneumatic transport, each of which being separated by a certain gas velocity known as the minimum fluidization gas velocity (U_{mf}), minimum bubbling gas velocity (U_{mb}), transition to turbulent gas velocities (U_c and U_k) and the transition to transport regime(U_{tr}) [7], [8]. Having a thorough vision of the value of these characteristic gas velocities leads us to a better understanding of the hydrodynamics of our FB system. For example, knowing the value of U_{mf} provides us with an estimate of the amount of gas available in the emulsion phase according to the two-phase theory which plays a great role in assessing the reaction performance of a catalytic FB reactor [9]. On the other side, U_c and U_k are important to avoid undesired solid loss due to a maladjustment of operating gas velocity, mostly critical when expensive catalysts are involved or damage to the internal sections of the reactor such as cyclones and spargers [10]–[12]. Along with the gas velocity, gas properties also play an important role in defining the hydrodynamics of FB systems. Gas properties, namely gas density and viscosity, has a direct effect on the level of hydrodynamic forces (HDFs) exerted by the fluidizing gas on the solid particles [13]–[15]. Considering a system working at ambient conditions (pressure and temperature), it is simply the balance between HDFs that defines the fluidization state of the system. In more details when the drag force exerted by the fluidizing gas overcomes the weight of the solid particles it marks the start of fluidization or U_{mf} [4], [16].

But not all the applications that we are dealing with in the industry is being held at ambient condition. Specifically speaking, processes such as FCC regeneration [1], [17], Coal combustion/gasification [18]–[21], polymerization [22]–[24] and mineral processing [25] happens at a considerably broad range of temperature up to 1700 °C and pressure up to 30 bars [26].

Changing the working pressure and temperature directly affects the gas properties which then also changes the level of HDFs working in the FB system. In a glance, the viscosity of fluidizing gas (μ_g) changes by T^n $0.6 < n < 1.0$ and the density of the fluidizing gas (ρ_g) changes inversely by temperature [27], [28].

In addition to the properties of the fluidizing gas, one should also consider the properties of the solid particles as they introduce another type of force, known as interparticle forces (IPFs), into the force balance along with the HDFs. These properties are also affected by the operating temperature. At high temperature and in the case of fluidization of fine particles or for the particles with low melting point compared to the temperature of the process, an increase in the level of IPFs can be observed. However, the change in the level of IPFs should be carefully analyzed by considering different types of IPFs and their dependance on temperature. In a nutshell, Van der Waals forces are mainly due to electrical charges on solid particles which will be decreased by increasing the temperature. On the other hand, IPFs sourced from the formation of liquid bridges and/or Higher contact surface due to the softening of low melting point solids could increase by temperature [29]–[36]. All the above-mentioned phenomena happening at the same time at extreme conditions makes it more and more complicated to predict the behavior of the FB system at extreme conditions.

Investigation of the hydrodynamics of an FB system can be accomplished through different measurement techniques widely used by researchers. Monitoring the temperature, pressure [32], vibration [37] and electrostatic charges [38] all along with visual, X-ray radiography [39]–[41], radioactive particle tracking [32], [42]–[45] and optical fiber measurements give us a more and more clear picture of what happens in an FB system at different working conditions [46]. As a result, models and correlations are being proposed based on HDFs most of which fail to precisely predict the behavior of the FB system at an elevated temperature where IPFs also play and important role, depending on the type of particle in use which imposes the need for modification. This task is not possible unless we have an approach to measure the value of IPFs at different temperatures. The available measurement techniques such as shear cell and AFM techniques fail to well represent the real conditions in a fluidized bed as they are applied outside of a fluidized bed within a limited range of operating temperature. Moreover, qualitative methods such as Hausner

ratio and angle of repose measyrements can not quantify the value of IPFs and can not be used to develop correlations to predict the value of hydrodynamic parameters. Based on the mentioned problems and lack of knowledge we define the objectives of this work below.

1.2 Objectives

In this thesis, we review the models that are widely in use to investigate the behavior of gas-solid FB systems and compare them with the data obtained from our experiments at high temperature, using a variety of particles and fluidizing gases with different properties. As a result, the following objectives will be completed:

1. Measuring the simple hydordynamic parameters of fluidization ,U_{mf} and U_c, at high temperature
2. Evaluation of the precision of available hydrodynamic-based correlations to predict the behavior of an FB system using different solid particles and fluidizing gasses.
3. Indirect measurement of interparticle forces at high temperature

To achieve our aforementioned objectives we conduct a decent literature review on the effect of temperature in the presence and absence of IPFs in chapter 2. Chapter 3, presents the adopted methodology, experimental setup, and measurement techniques. Chapter 4 consists of a detailed presentation of results and our explanation. Finally, in Chapter 5 the conclusion of this work, as well as recommendations for future studies will be discussed. All references used are also listed at the end of Chapter 5.

CHAPTER 2 LITERATURE REVIEW

2.1 Basics of Fluidization

When a fluidizing gas suspends a fixed-bed of solid particles in a form that they act as a body of liquid, an FB system forms. For a better distribution of gas and to provide the initial energy for the gas to fluidize the solid particles, use of a distributor plate is mandatory [4], [16]. This liquid-like behavior of solid particles, which function as catalysts in most of the industrial applications, provides us with unique properties such as high gas-solid contact and high mass and heat transfer[16]. As the fluidizing gas passes through the bed, depending on the gas velocity and operating conditions, which directly affect the gas-solid and solid-solid interactions, different regimes take place in an FB system presented in Figure 2.1.

These regimes can be explained as follows:

Fixed-bed: This state is present in an FB system when the forces exerted by the fluidizing gas on the particles are not enough to overcome the resisting forces (Simply, the weight of the particles in the absence of IPFs). In this state, there is no mixing and temperature is also not uniformly distributed along the bed.

Particulate Fluidization: This is the state where the gas velocity is just enough to lift the particles. In another word, the forces exerted on the body of the particles can overcome their weight and the IPFs, if present and particles can move freely. The start of this state is marked by U_{mf} and the system is only consisted of emulsion phase.

Bubbling: By increasing the gas velocity in the case of fluidization of Geldart group A particles at the minimum bubbling velocity (U_{mb}), the emulsion phase gets saturated and the excess amount of gas appears in the system as bubbles. In this state, bubbles carry with them the bed material to the top of the bed, burst and particles fall again into the lower levels of the bed.

Turbulent regime: As the bubble size and velocity increases by superficial gas velocity through bubble coalescence, emulsion phase becomes diluted due to high level of entrainment and breaks up at the transition gas velocity, U_c. This is also accompanied by a higher rate of bubble break up

and a high intensity of gas-solid mixing which adds to the turbulency of the system. This regime is favorable in many applications such as FCC regeneration, due to its high gas-solid mixing, high gas hold-up, and uniformity of flow. It is note worthy that for beds with high H/D ratio as soon as the bubble size grows to the the diameter of the bed slug formation occurs which can be characterized by large fluctuations in bed pressure drop.

Fast fluidization and pneumatic transport: At very high gas velocities transition to fast fluidization occurs with high level of particle entrainment and annulus flow of gas. This regime is marked by U_{tr} [4], [16].

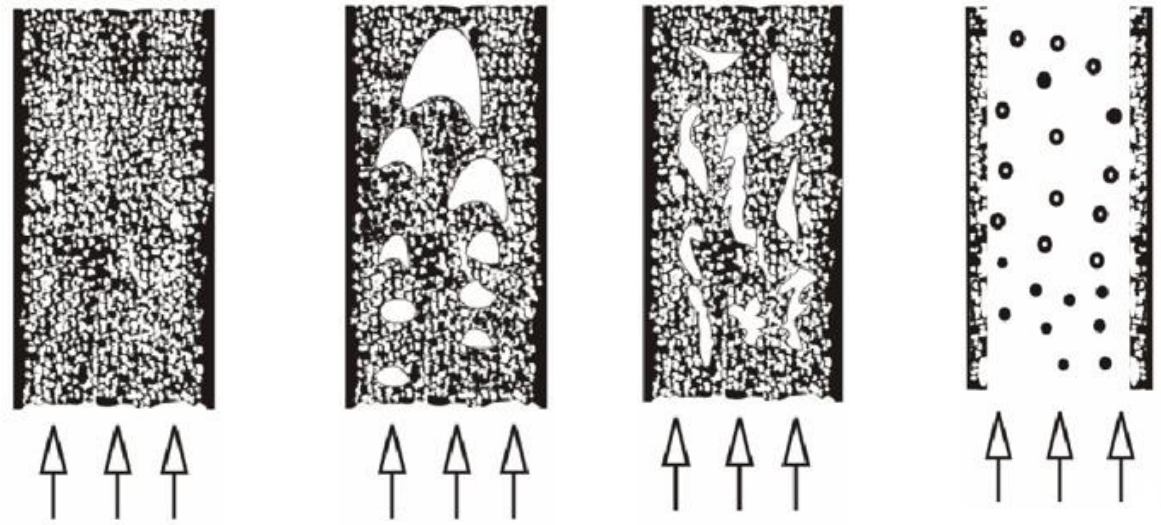

Particulate Fluidization Bubbling Turbulent Regime Fast fluidization

Pneumatic transport

Figure 2.1: Different fluidization regimes in a fluidized bed

What can determine the occurrence of the above-mentioned regimes are gas velocity, gas and particle properties and the level of IPFs. A well-known classification of fluidizing particles from A to D has been done by Geldart based on the size and density of particles [47]. This classification is presented in Figure 2.2.

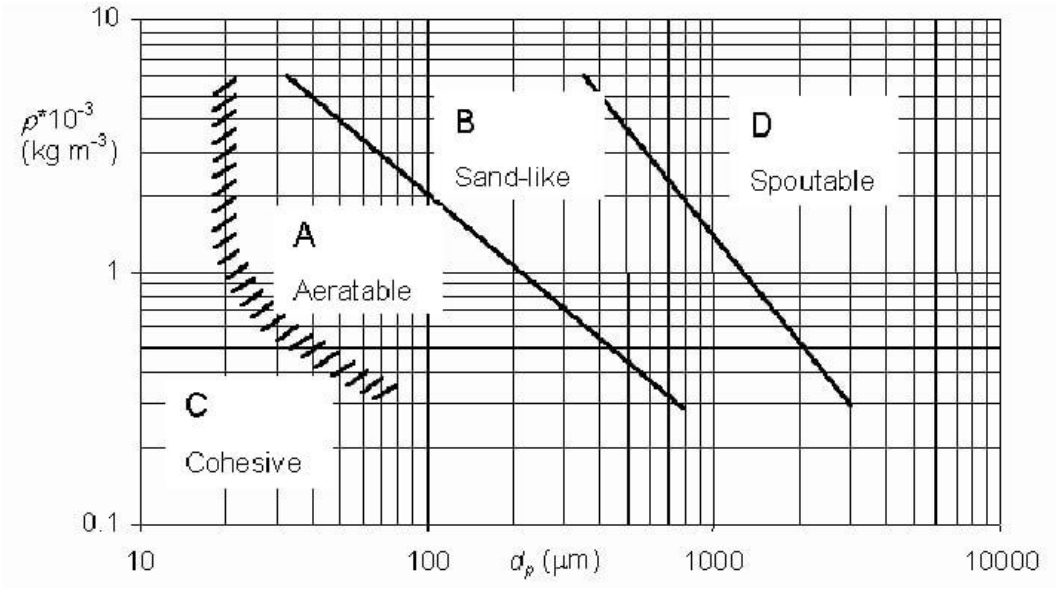

Figure 2.2: Geldart classification of particles

Geldart group C: Cohesive particles with very low flowability and high level of IPFs compared to their weight can be placed in this group. Bubbles do not appear in the fluidization of these particles. Instead, channel or slugg formation will occure by increasing the gas velocity. As a result, assisted fluidization methods should be applied to guarantee a uniform fluidization of these particles. Most of the particles smaller than 20 microns belong to this group.

Geldart group A: Most of the commercial catalysts belong to this group. These powders show a moderate level of IPFs depending on the working condition and the melting point of the particles. Also it is for this group of particles that dense phase expands after U_{mf} and before U_{mb} when bubble start to form ($U_{mb} / U_{mf} > 1$). In the fluidization process of these partices, due to a constant bubble coalescence and break up, bubbles grow to a maximum size and the fluidization quality is very smooth.

Geldart group B: The characteristic behavior of this group is that bubbles start to form as soon as the bed reaches to the fluidization state. In other word there is no dense phase expansion before the bubble formation set point. ($U_{mb} / U_{mf} = 1$). In contrast to group A particles, bubble size can grow up to the bed diameter by increasing the gas velocity.

Geldart group D: Large particles such as rice, nuts and vgetables in food industry are classified in this group. Large bubble formation makes the fluidization of these particles very poor with large pressure fluctuations. The fluidization of these particles is being carried out in spouted bed reactors.

It should be expressed that by moving from Geldart group D towards C, the level of IPFs increases which, as mentioned before, affects the fluidization state as well as the hydrodynamics. Also an increased level of IPFs for any of these groups can change the fluidization behaviour and quality. For instance group A particles with an elevated level of IPFs can exhibit the characteristic behaviors of group C powders.

Knowing the above-mentioned basics of fluidization, it is time to do a more detailed explanation of effective factors in the fluidization process in the next section.

2.2 Application of High Temperature/Pressure Fluidized Bed (HTHP FB)

Pressure and temperature are the most important parameters which can alter the behavior of an FB system. As a result of a growing market and an increasing need for a more efficient process, especially in biomass and energy section, nowadays there are less and less FB reactors working at ambient conditions.

The mining industry also benefits from FB reactors working at elevated pressures and temperatures. Specifically, in the gold refinery, application of high pressure and temperature oxidation eliminates fusion and formation of agglomerates [4].

Higher pressure not only reduces the size of the equipmnet in use by reducing the vlolume of the gas but also reduces the reaction time[48]. In the gasification process, it also eliminates some downstream steps such as compression units and also reduces the CO_2 emission when high-pressure boilers are put into action [49]. The temperature range of gasification process is set to be below the softening point of the coal particles, 950-1100 °C, and biomass, 800-950 °C[50].

In another example, comparing a low and high-pressure process in the production of methanol and ammonia shows higher coal consumption and lower power requirements in the compression unit.

In polyolefin production temperatures in the range of 40-120 °C is required which is relatively high considering the sintering/melting point of the feedstock (polyethylene). Pressures as high as 500 psig is also favorable to increase the heat transfer due to an increase in the unit volume heat capacity of the gas [23], [50].

In the production of Vinyl Chloride Monomer, the building block of PVC, is made through a thermal cracking process of ethylene dichloride in the presence of alumina-supported copper oxide catalysts which belongs to Geldart group A at 450–600 °C and 10–35 bar. To avoid agglomeration of the catalyst the temperature control is very essential [50].

Chemical looping for CO_2 capture is highly in the center of attention due to the growing effect of CO_2 emission on global warming and environmental ctastrophies. A bubbling bed built in Instituto de Carboquimica using alumina based copper oxide catalyste in the size range of 100-500 µm and working at 800 °C to avoid agglomeration of catalyst particles can achieve this goal with full conversion of the fuel to CO_2 was obtained at CuO/Fuel molar flow ratios of higher than 1.4 [50].

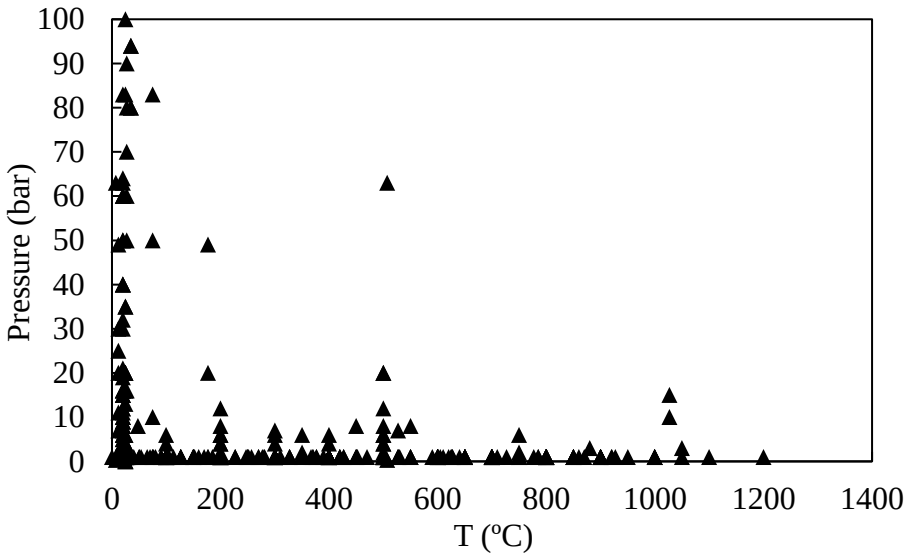

Figure 2.3: Summary of more than 100 research done on the hydrodynamics of FBs at high pressure and temperature

Although high pressure/temperature gas-solid fluidized beds are attracting more attention for industrial applications, there is limited understanding of bed hydrodynamics under extreme

conditions in the literature. A summary of more than hundred studies presented in Figure 2.3 shows that most of the work on high pressure/temperature FBs have either been conducted at low pressure and high temperature or at high pressure and low temperature.

2.3 Hydrodynamic Forces (HDFs)

To better understand the effect of operating conditions on the hydrodynamics of a gas-solid fluidized it is necessary to define different forces that is acting in such a system. Below you can find the definition of these forces along with their formulation.

2.3.1 Drag Force

The drag force exerted by the flowing gas on solid particles can be formulated as in Equation (1)

$$F_d = C_D \frac{\pi d_p^2}{4} \frac{\rho_f U_g^2}{2} \quad (1)$$

In this equation d_p is the diameter of the fluidized particle, U_g is the superficial gas velocity of the fluidizing gas and C_D is the is the drag coefficient which is a function of Reynolds number.

$$Re_p = \frac{\rho_f U_g d_p}{\mu} \quad (2)$$

where ρ_f and μ are the density and viscosity of the fluid, i.e., the fluidizing gas. Considering the voidage of the bed, ε, the drag force on a single particle can be calculated by Equation (3) [51], [52].

$$F_{d\varepsilon} = C_D \frac{\pi d_p^2}{4} \frac{\rho_f U_g^2}{2} \varepsilon^{-3.8} \quad (3)$$

2.3.2 Buoyant Force

It is observed that a fluidized bed of particles act as a body of liquid with a density formulated as in Equation (4) [53].

$$\rho_{fb} = \varepsilon\rho_f + (1-\varepsilon)\rho_p \quad (4)$$

with ρ_p being the density of the particle. The buoyant force exerted on the particles and the buoyant weight can be calculated as in Equations (5) and (6) [54].

$$F_b = \frac{\pi d_p^3}{6}\rho_{fb}g = \frac{\pi d_p^3}{6}(\rho_f + (1-\varepsilon)\rho_p)g \quad (5)$$

$$W_b = \frac{\pi d_p^3}{6}(\rho_p - \rho_f)\varepsilon g \quad (6)$$

where, g is the gravitational constant.

By knowing the definition of different HDFs acting in a fluidized bed now we can have a global picture of the effect of pressure and temperature on the fluidization process. For Geldart group A where $Re_p << 1$ the viscous effect becomes more dominant than the inertia effect and according to the drag coefficient, $C_D = \frac{24}{Re_p}$, density of the gas is responsible for any change in the level of HDFs [55]. Thus, the magnitude of the drag force increases by pressure and decreases by temperature. For Geldart group B drag force increases by pressure. While, increasing the temperature has a dual effect; temperature increases the gas viscosity while it has a decreasing effect on the gas density. So, the behavior of the bed in the presence of these particle is between group D and A particles with no IPFs [26]. The above-mentioned effects on the level of HDFs working in such systems affect the simple hydrodynamic parameters. A summary of the observed effects is presented in sections 2.5 and 2.6.

2.4 Inter-Particle Forces (IPFs)

There are different types of forces categorized as IPFs in the systems dealing with solid particles. Each type of these forces can be present or negligible in a certain working condition. In this section, we explain three type of IPFs known as Van der Waals, electrostatic and material bridge [33].

2.4.1 Van der Waals

Formation of dipoles due to orbiting electrons is responsible for Van der Waals forces leading to the nonideal behavior of gases. These dipoles change rapidly and form an electric field which also changes the polarity of a neighboring atom. The overall effect of this phenomena in the atomic scale can be transferred also to macroscopic scale, i.e., solid particles, resulting in attractive forces between them [56].

This type of attractive force can be formulated as Equation (7) [57], [58]:

$$F_{vdw} = \frac{h\omega}{8\pi Z^2} R \left(1 + \frac{h\omega}{8\pi^2 Z^3 H_r}\right) \quad (7)$$

where $h\omega$ is the Liftshits-van der waals coefficient, which depends on the nature of the solid particles, and the contact medium and H_r is the hardness of the softer particle (10^8 N/m^2 for undeformable particles). Z is the distance where the Van der Waals force reaches to its maximum (usually 4 Å [57]) and R can be calculated as $\frac{R_1 R_2}{R_1 + R_2}$ for two spherical particles with different radii R_1 and R_2. Considering the asperities of in-contact particles a value of R_{as} = 0.1 µm should be considered in the evaluation of R [57], [58].

In a fluidized bed with solid particles smaller than 100 µm and in a condition that the moisture content is negligible, Van der Waals forces play an important role compared to other types of IPFs and even gravitational forces. This size range can be extended to even higher particle sizes in the presence of porous particles, deformable particles or the contact surface characteristics (contact area).

2.4.2 Electrostatic

Electrostatic forces are also present in the fluidized bed processing of nonconduction particles in a dry environment [57], [59], [60]. Charged particles in such systems can affect the flow properties in a gas-solid system. Coulomb's law describes the force between two charged particles as in Equation (8):

$$F_e = \frac{1}{4\pi\epsilon}\frac{q_1 q_2}{s^2} \quad (8)$$

where q1 and q2 are the electric charges of the particles, s is the distance between the particles, and ϵ is the permittivity of the medium. This type of force has much smaller magnitude compared to the Van der Waals force and becomes negligible or zero in humid systems [60].

2.4.3 Material Bridge

2.4.3.1 Capillary or Liquid Bridge

When the moisture content of the fluidizing gas becomes condensed on the particles, a bridge of liquid will form in the small gap between the particles in contact as shown in Figure 2.4.

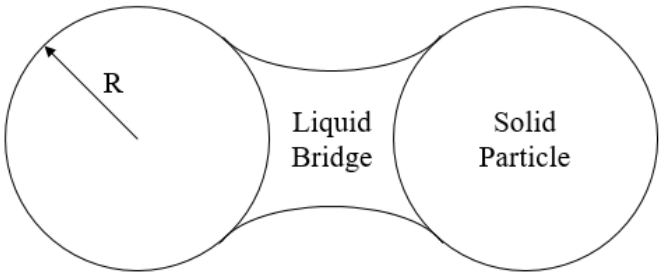

Figure 2.4: Liquid bridge formed between two identical particles.

This bridge due to the capillary effect in liquids exerts an attractive force on the particles keeping them from moving [58], [60], [61]. In a simplified method, the magnitude of capillary force can be calculated by Equation (9):

$$F_c = 2\pi\gamma R \quad (9)$$

where γ is the surface tension of the bridged liquid and R is the particle radii. As before, asperities could be taken into consideration for a better approximation of this force.

To have a better picture of the importance of the IPFs in respect to the particle size the following schematic has been prepared by Seville et al. [33] for a particle with 0.1 μm asperities and density

of 3×10^{-3} kg/m^3. We can see in Figure 2.5 that for a 100 µm particle, Van der Waals force is equal to the weight of the particle and also when the capillary force is present its magnitude is higher than the Van der Waals force.

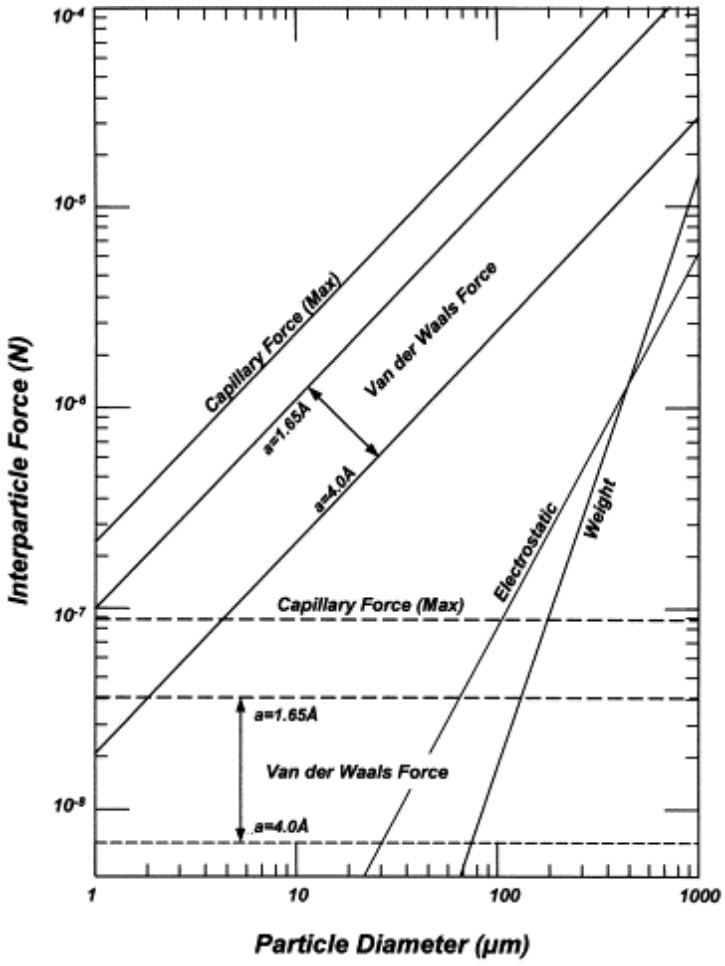

Figure 2.5: Presentation of various IPFs along with the weight of the particle [33]

2.4.3.2 Solid Bridge or Sintering

Another type of material bridge which forms due to diffusion in solid state or other mechanisms is referred to as sintering. This bridge grows with time according to Equation (10), in which x is the neck radii and τ is time and k is defined depending on the neck formation mechanism.

$$(\frac{x}{R})^2 = k\tau \quad (10)$$

In a fluidized bed, a value of k can be calculated by Frenkel equation in Equation (11) for viscous sintering. This neck can be so strong to resist the high-intensity movement of solids in such a system and result in defluidization in a high-temperature process i.e. ash sintering in combustion, gasification and reduction of iron[33].

$$k = \frac{3\gamma}{2R\mu} \quad (11)$$

2.4.4 Measurement of IPFs

To date, different methods have been applied to evaluate the level and the importance of IPFs in systems dealing with solid particles such as Hausner Ratio and measurement of angle of repose [62]–[64], shear test [2], [65]–[67], Atomic Force Microscopy (AFM) approach [64], [66] and, torque measurement in fixed/fluidized bed of particles[67]–[69] none of which gives reliable and repeatable results or fail to fully represent the conditions in an FB.

Hakim et al. [64] classified cohesive properties of nanopowders by a classification system based on the measurement of repose angle and Hausner Ratio (HR) (Table 2.1 and

Table 2.2) with the HR being the ratio of the tapped bulk density to the loose bulk density. Loose bulk density is the density of the bulk body of loosely packed particles and tapped bulk density is referring to the bulk density after tapping the bed and settlement of the particles.

Fatah [63] Showed in his work that measurement of HR is highly dependant on the method used to tap the column of particles as presented in Figure 2.6 clearly expressing the uncertainty of this measurement technique which has also been approved by [70].

Table 2.1: Expected flowability of powders based on angle of repose [64]

Angle of repose (θ)	**Expected flowability**
$55 < \theta < 70$	Very cohesive
$45 < \theta < 55$	Cohesive
$38 < \theta < 45$	Low flowability
$30 < \theta < 38$	Medium flowability
$25 < \theta < 30$	High flowability

Table 2.2: Powder classification based on HR [64]

Hausner Ratio (HR)	**Geldart's classification**
HR > 1.4	Type C powder
HR < 1.2	Type A powder
1.2 < HR < 1.4	May show the behavior of both Type A and Type C powders

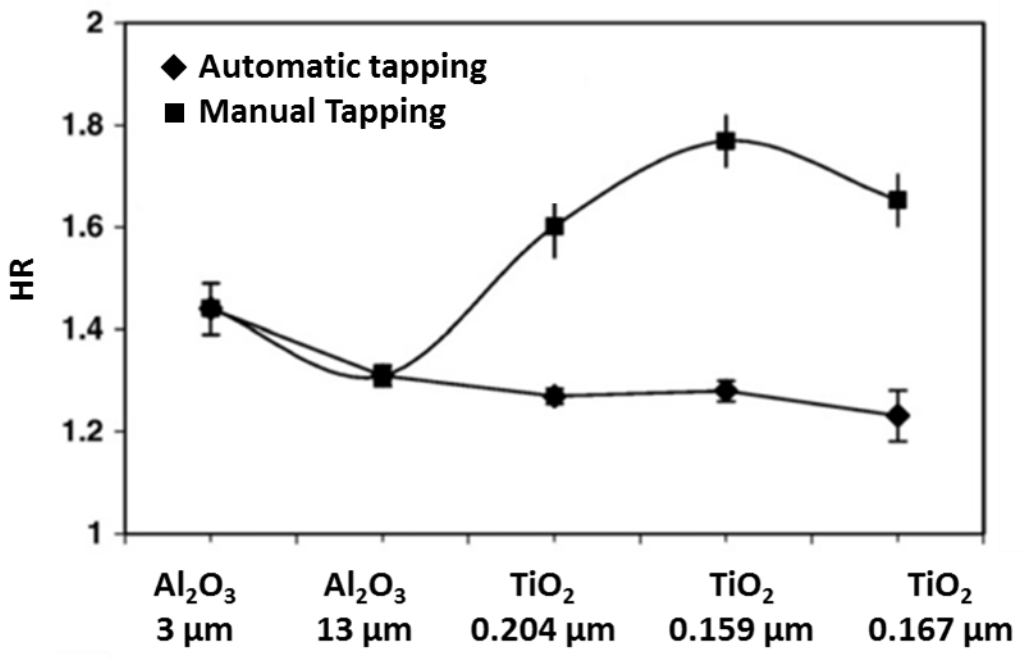

Figure 2.6: Dependance of Hausner Ratio (HR) for Al_2O_3 (3700 kg/m^3) and TiO_2 (4200 kg/m^3) powders using automatic tapping (HRa) and manual tapping (HRm). [63]

Rasteh et al. [71] did a thorough joint study of the level of interparticle forces measured by AFM technique and hydrodynamic study of tapered fluidization. They showed that the smaller the particles, the higher the level of inter-particle forces will be. They also put an stress on the importance of IPFs for smaller particles.

However, this study has been done at ambient temperature due to limitations of AFM technique. Bruni et al. [67], [68] used a novel technique by coupling torque measurement and pressure measurement in a fluidized bed testing particles with different fines content. However, this intrusive method breaks up the solid structure formed because of IPFs and is not a good representative of the real fluidization process.

2.5 Effect of Temperature on Hydrodynamic Parameters in a Fluidized-Bed with No/Negligible IPFs

In an FB system held at dry and ambient conditions consisting of Geldart Group B/D powders the ratio of IPFs/HDFs is negligible or zero. It is worth mentioning that large particles processed at high temperatures considering their melting point are not of the interest of this study and will not be discussed in this section.

In such system, the level of HDFs is more dominant compared to the IPFs. This means that one can easily predict the behavior of the bed according to the available hydrodynamic-based models considering the variation of gas properties by pressure and temperature [72]. These effects have been discussed in details in the following sections.

The effect of temperature in systems with no considerable ratio of IPFs/HDFs, i.e., Geldart group B and D, the dependence of U_{mf} is based on the size of the particles. For group D particles U_{mf} increases by temperature due to a decrease in the density of the fluidizing gas [73]–[77] while, for smaller particles close to group B/D boundary it becomes independent of temperature as the flow regime is also at the border of viscous/inertia regime [15], [78], [79].

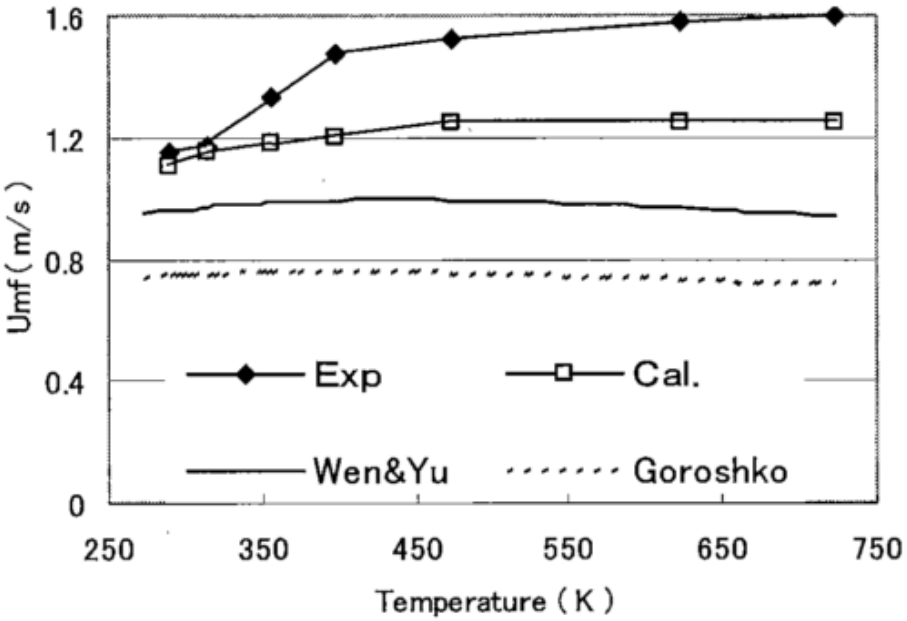

Figure 2.7: Variation of U_{mf} by temperature for Geldart group D particles [77].

For the latter case by increasing the operating pressure, flow regime shifts towards the dominance of the inertia effect and as a consequence, U_{mf} increases by temperature [80]. For lower Reynolds numbers, i.e., small Group B particles, the dominance of the viscous flow regime results in a decrease of U_{mf} by temperature as the viscosity of the gas increases [15], [73]–[75], [79]–[83]. As drag force decreases with temperature in the case of using group D or very coarse group B particles, indentation formation on the roof of the bubbles enhances so that bubble break-up increases. This mechanism leads to a decreasing trend for the bubble size by increasing the temperature [84], [85]. Low energy bubbles, due to a lower gas density at high temperature, and higher rates of bubble break-up reduces the mixing quality and delays the transition to the turbulent regime [86]–[88].

2.6 Effect of Temperature on Hydrodynamic Parameters in a Fluidized-Bed in the Presence of IPFs

As described in 2.4 IPFs are present in systems dealing with solid particles. The level of electrostatic IPFs can change at extreme conditions as conductivity increases [89]–[92]. However, temperature increases Van der Waals forces by increasing the dipole pulsation at the contact point

[57], [93]. Formation of solid-solid material bridge also increases due to softening of particles and also higher diffusion rate in the solid-state [1], [94], [95]. But the effectiveness of these forces depends solely on the magnitude of the ratio between IPFs and HDFs; For systems consisting of particles from group C, A and even coarser particles with specific characteristics, i.e., low melting/sintering point or soft particles, the magnitude of IPFs becomes so pronounced compared to HDFs that they cannot be neglected anymore [33], [36]. However, available models to predict the hydrodynamic behavior of the bed are not considering the effect of IPFs especially when it comes to extreme conditions, e.g., high temperature. Thus, most of the models fail to reproduce the experimental data obtained in such conditions as they only consider the modification of gas properties in extreme conditions and not the solid properties.

At high temperature effect of IPFs is present even before the fluidization state. An increase in the bed voidage in complete fixed-bed state ε_0 and just before fluidization ε_{mf} has been observed in many cases [36], [44], [96]–[99]. It was also reported that for such systems with moderate levels of IPFs, U_{mf} can be delayed to higher values [15], [17], [67], [100], [101] and bubble-free fluidization can be extended for Group B particles [98], [102]–[107]. This change of behavior from group B to group A or even C was reported repeatedly in the literature [17], [36], [98], [104], [105], [107] at a constant gas velocity. High degree IPFs also result in a more viscous emulsion phase which can hinder bubble growth and also bubble rise velocity. As a result, experiments which have been done at this condition usually report smaller bubble size, higher bed expansion, and bed voidage [36], [44], [86], [97], [108], [109]. Increasing the level of IPFs decreases the frequency of bubble movements in the bed, and hence, the rate of bubble break-up. [84], Uc is also delayed until higher gas velocities and entrainment is controlled [26]. On the other hand at the high level of IPFs, the formation of previously mentioned indentations decreases and bubbles grow larger. It was also observed that the bubble behavior of beds affected by IPFs can be different at moderate and high gas velocities so that at moderate gas velocities above U_{mb} bubble size is lower compared to systems unaffected by IPFs and at high gas velocity well-above U_{mb} and close to U_c bubbles are larger compared to systems with no IPFs [17], [36], [85].

In this section, we will report different hydrodynamic observations in FB systems in which IPFs should be considered to clearly show the contradictory which is basically based on ignoring or underestimating the level of IPFs at extreme conditions.

The effect of temperature if it does not affect the level of IPFs has been explained in 2.5 for coarse particles where inertia flow regime is mainly dominant. However, when fine particles are in use and the level of IPFs is not negligible, the effect of temperature can be described using the magnitude of the ratio of IPFs/HDFs. In this case, an increase in temperature also increases the level of Van der Waals and solid-solid bridge IPFs [15], [96], [109]–[114].

From the hydrodynamic point of view, by increasing the operating temperature viscosity of the gas increases by T^n $0.6<n<1.0$. Knowing that for fine particles the viscous regime is dominant, the magnitude of drag force increases due to an increase in the gas viscosity. It can be concluded that U_{mf} decreases by this change. Temperature also increases the bed voidage in the fixed bed and minimum fluidization state due to the reduced flowability and change in the packing behaviour of particles as a consequence of increased IPFs [15], [102], [110], [114], [115]. In other words, in the absence of IPFs particles can slip on each other and reach to a more packed state compared to the case in which high level of IPFs reduce the mobility of particles. Bubbling regime was also found to be affected by temperature so that the bubble size/frequency increases by temperature [116]. This was explained by a lower formation of indentations on the roof of the bubbles and a reduced bubble break-up which leads to a decreased U_c [116], [117].

Some literature did not only consider the variation in gas viscosity and the drag force but also the modification required due to an enhanced level of IPFs to explain the behavior of the bed [109]. When the temperature goes higher than a certain value the effect on the magnitude of the IPFs is higher than its effect on the gas viscosity. In this case, the hydrodynamics of the bed cannot be well determined by the variation of HDFs.

2.7 Hydrodynamic-Based Models and Correlations for U_{mf} Prediction

As previously mentioned the effect of pressure and temperature on the fluidization properties cannot be determined without considering the particle size. It is because of the particle size and of course the gas velocity that we can distinguish between inertia and viscous flow regimes to determine if the gas viscosity is important or the gas density. It is also the particle size that can dramatically affect the ratio of IPFs/HDFs at different operating conditions. This is also the case when it comes to using the proper correlations to predict the hydrodynamic parameters of fluidization, namely U_{mf} and U_c, so that, for every group of particles and ranges of operation a certain number of correlations become handy and the other ones are over/under predicting the parameter in question. In this section, we covered the most useful correlations and models for the prediction of U_{mf}.

Chitester et al. [118]**:** For coarse particles, the following modification of Eregun's equation can be used.

$$Re_{mf} = \sqrt{(28.7)^2 + 0.0494\,Ar} - 28.7 \qquad (12)$$

Wen - Yu [119]**:** The correlation proposed by Wen and Yu is widely used to predict U_{mf} and different working conditions. However, this correlation under predicts this parameter at high temperature since they did not consider the augmented level of IPFs at high temperature. At this state gas, velocity should be increased to maintain the fluidization state [94].

The general form of this correlation is presented in Equation (13).

$$Ar = 1650Re_{p,mf} + 24.5\left(Re_{p,mf}\right)^2 \qquad (13)$$

For small particles ($Re_{p,mf} < 20$), we can simplify this correlation as in Equation (14).

$$U_{mf} = \frac{d_p^2(\rho_p - \rho_g)g}{1650\mu_g} \quad (14)$$

For this range of particles, U_{mf} decreases by temperature and is unaffected by pressure. For large particles ($Re_{p,mf}$ >1000), we can rewrite Equation (13) as Equation (15).

$$U_{mf}^2 = \frac{d_p(\rho_p - \rho_g)g}{24.5\rho_g} \quad (15)$$

The only term that is affected by temperature and pressure for this range of particles is the gas density. Sobreiro et al. [120] tested the validity of this equation by comparing their experimental results with the value obtained from Wen-Yu presented in Figure 2.8.

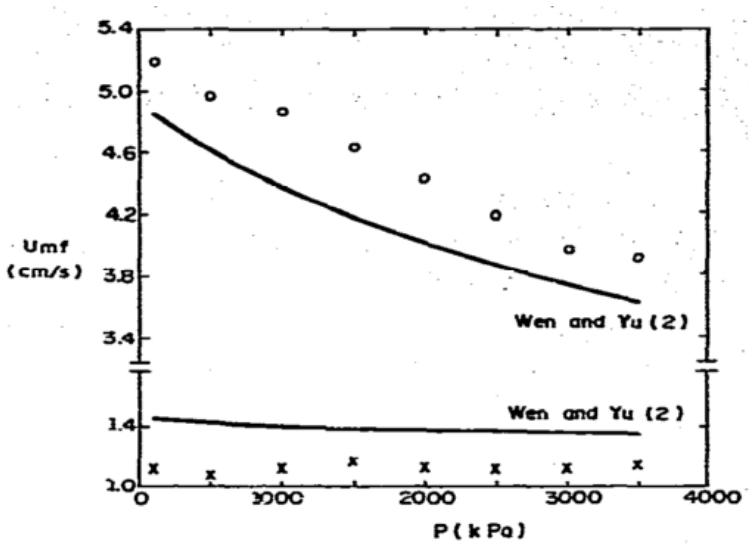

Figure 2.8: Influence of pressure on U_{mf}. ○-ballottini, d= 0.25 mm;

x-alumina,d= 0.125mm [120]

Carman – Kozeny [121], [122]**:** This correlation (Equation (16)) along with the Ergun equation (Equation (17)) is being used in the case of large particles i.e. Geldart group B and D.

$$U_{mf} = \frac{(\varphi d_p)^2}{180}\frac{\rho_p - \rho_g}{\mu_g} g\left(\frac{\varepsilon_{mf}^3}{1-\varepsilon_{mf}}\right) \quad (16)$$

$$150\frac{\mu_g U_{mf}}{(\varphi d_p)^2}\frac{(1-\varepsilon_{mf})^2}{\varepsilon_{mf}^3} + 1.75\frac{\rho_g {U_{mf}}^2}{\varphi d_p}\frac{1-\varepsilon_{mf}}{\varepsilon_{mf}^3} = (\rho_p - \rho_g) g (1-\varepsilon_{mf}) \quad (17)$$

In these equations, φ is the shape factor or sphericity of the particles and ε_{mf} is the bed voidage which is a function of temperature. If the bed voidage is considered unaffected by temperature, there will be a considerable underestimation of U_{mf} at high temperature as shown by Formisani et al. [15] in Figure 2.9.

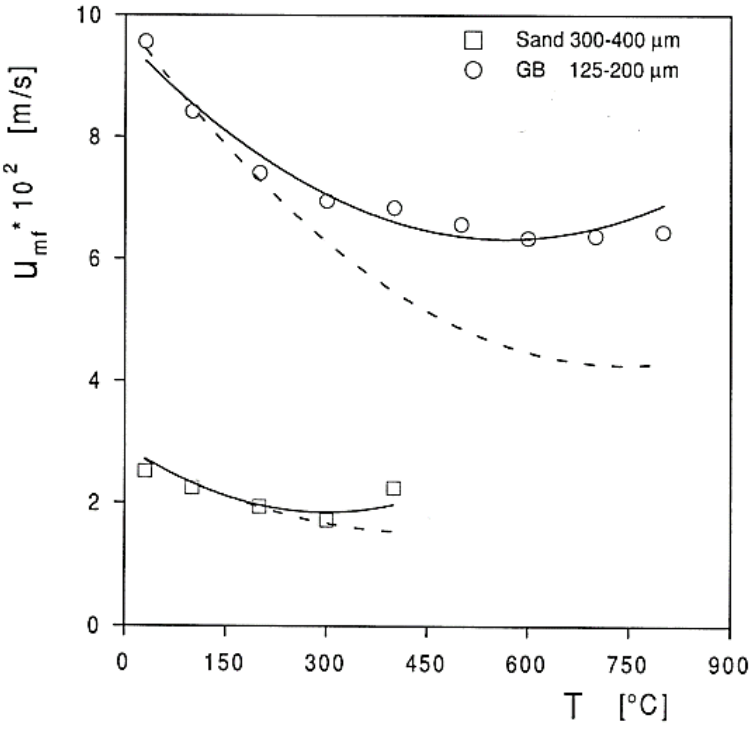

Figure 2.9: Effect of the dependence of ε_{mf} on temperature on the estimation of U_{mf} by Carman-Kozeny equation. — corrected ε_{mf}, - - - ambient ε_{mf} [15].

Formisani et al. [15] tested the validity of this equation by comparing their experimental results with the value obtained from Carman-Kozeny equation with a corrected value of ε_{mf} by temperature presented in Figure 2.10.

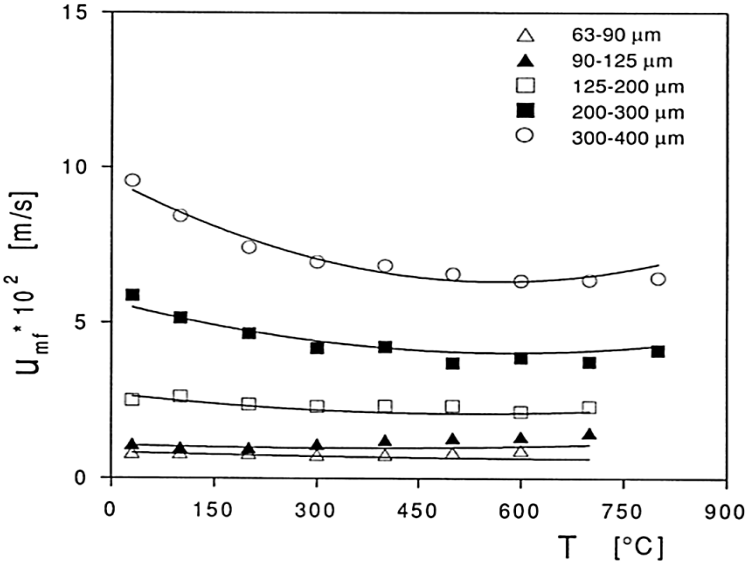

Figure 2.10: Comparison between U_{mf} obtained experimentally and by predictions from Carman-Kozeny for different sizes of silica sand [15].

An elaborated list of other models and correlations is presented by Wu and Baeyens [28], Lin et al. [123] and Jiliang et al.[124] however, they are valid in a limited range of operating conditions and for a certain range of particle size.

CHAPTER 3 EXPERIMENTAL AND METHODOLOGY

3.1 Experimental Setup

The hydrodynamic study was attempted at ambient pressure in a high-temperature fluidized bed (HTFB) capable of operating at temperatures as high as 800 ºC with a total height of 105 cm and an internal diameter of 5.25 cm (2 inches) for the fluidization section as shown in Figure 3.1.

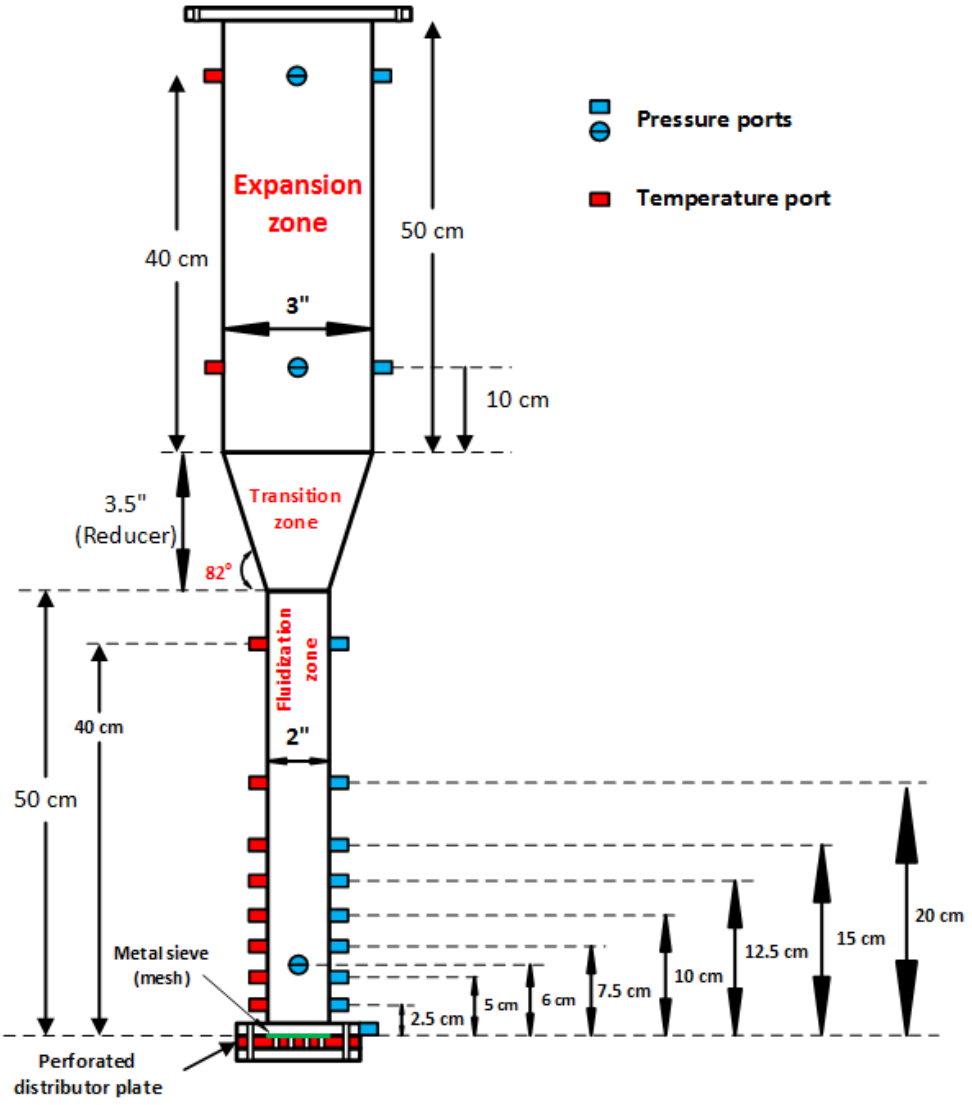

Figure 3.1: High-temperature fluidized bed drawing. Bed and freeboard sections.

At the outlet, we mounted a perforated steel pipe which was covered with glass wool to keep the particles from leaving the reactor at high gas velocity. To decrease the pressure drop caused by the filter we increased the filtering surface by choosing a 65 cm perforated steel pipe with an external diameter of 3.81 cm (1.5 inches) presented in Figure 3.2.

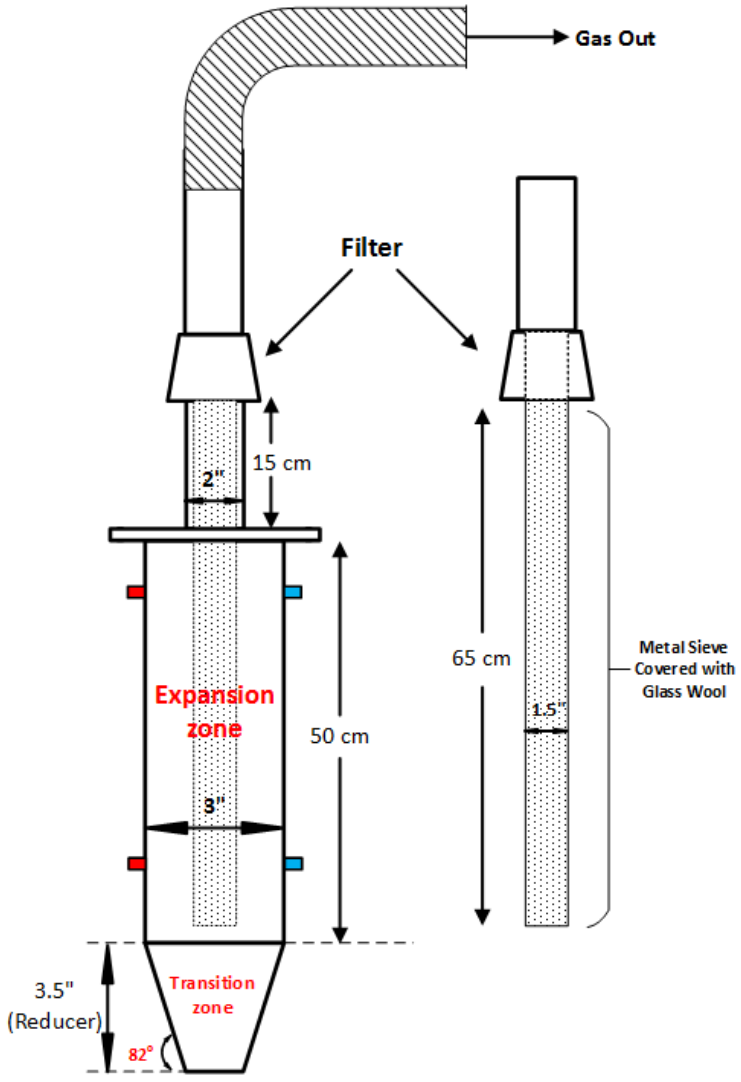

Figure 3.2: Filter design

The distributor plate was made out of a 0.635 cm (1/4 inch) thick aluminum plate with 19 holes with a large hole diameter of 3.175 mm on the top side and a smaller hole diameter of 0.5 mm on

the bottom side to simultaneously provide the high-pressure drop needed to uniformly fluidize the particles and diminish the chance of formation of long high velocity jets at the distributor plate (Figure 3.3). To avoid weepage of particles into the wind-box we also placed a 20 µm metal mesh on top of the distributor plate. We also filled the wind box (50 cm height and 5.25 cm diameter) with 5-10 mm sand particles to provide enough residence time for the passing gas to be adequately heated by the electrical heater.

(a)

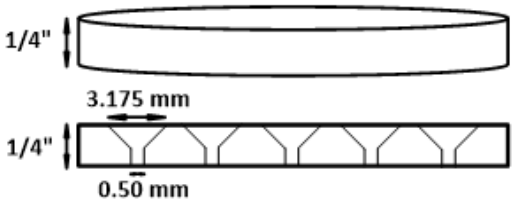

(b)

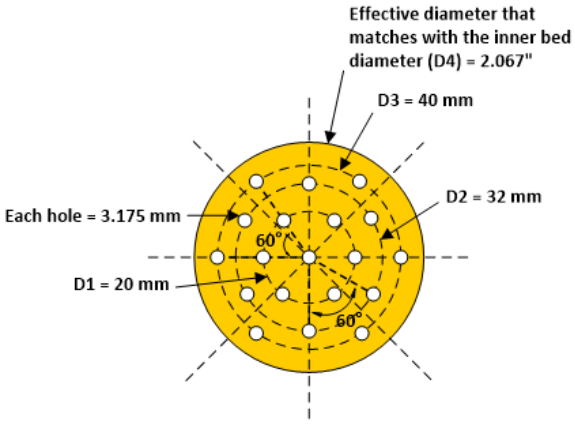

(c)

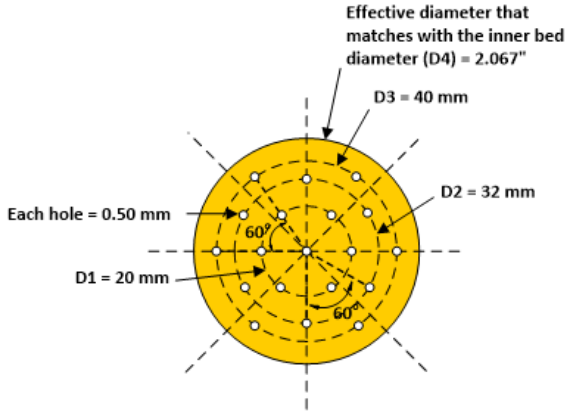

Figure 3.3: Schematic drawing of the perforated distributor plate: (a) side view, (b) Top view, (c) Bottom view

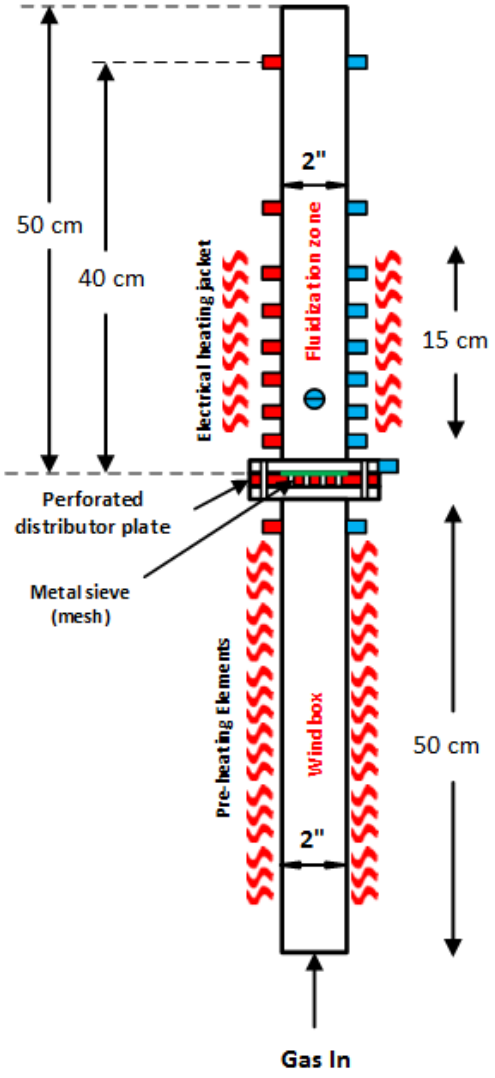

Figure 3.4: Pre-heating elements and heating jacket

We heated up the fluidizing gas by a pre-heating electrical furnace (LINDBERG, 54332, 2070watts, T_{max}=1200ºC) before entering the fluidized bed. We set the temperature of this section according to the desired temperature set point of each experiment with the help of a 16 bit A/D data acquisition board using the LabVIEW v.12 program. The temperature of the pre-heating zone

was based on the readings from an OMEGA, type K thermocouple located at the bottom of the distributor plate. For a better temperature control, we also placed two electrical heating jackets (OMEGA, CRWS-123/120-A, 850 watts, T_{max}=1000ºC) around the fluidization zone. The heating power of these heating jackets was adjusted considering the readings of an OMEGA type K thermocouple located at 6 cm above the distributor plate. Also 6 OMEGA type K thermocouples were recording the temperature of the bed at 2.5, 5, 7.5, 10, 40 and 63.5 cm above the distributor plate during the experiments.

We controlled the gas flow by four calibrated rotameters to cover a wide range of gas velocities in the bed with different precision (0.0001 – 0.578 m/s at 25 ºC). The input flow control system can switch between air and argon as the fluidizing agent.

At each experimental temperature, we adjusted the gas velocity in increasing and decreasing passes with the purpose of hydrodynamic study through the global and local measurements of pressure signals. To do so, we used two differential pressure transducers, one gauge, and one absolute pressure transducer installed at different pressure measurement taps of the HTFB with the following orientation. We used a differential pressure transducer (JUMO, 404304/000-414-415-28-298, 0-100 mbar) to approximately measure the total bed pressure drop with the high and low-pressure ports installed respectively at 7 mm and 97.8 cm above the distributor plate. Also, another differential pressure transducer (JUMO, 404304/000-412-415-28-298, 0-50 mbar) with the high and low pressure ports was installed respectively at 6.3 and 12.5 cm above the distributor plate to measure the in-bed pressure fluctuations. The readings from this pressure transducer give us the ability to monitor the pressure fluctuations in the bed between the two ports of this device [125] considering a bed height of 15 cm. We installed a gauge pressure transducer (OMEGA, PX309-002G5V, 0-2 Psig) and an absolute pressure transducer (OMEGA, PX309-100A5V, 0-100 Pisa) installed respectively at 9.3 cm above and 3.3 cm below the distributor plate to monitor pressure signals in the dense bed and wind-box. Using an in-bed gauge pressure transducer monitors every pressure fluctuation that occurs within the bed [125] we used it to get the global picture of what is happening inside the bed. We set the sampling frequency of the pressure signal measurements at 400 Hz and we recorded the data used for U_{mf} measurements for 1 minute and 2 minutes for the U_c

measurements with the help of a 16 bit A/D data acquisition board using the LabVIEW v.12 program.

3.2 Materials

In this research, we studied the fluidization behavior of different powders by the application of different fluidizing gas listed in

Table 3.1 and Table 3.2. We used different powders from Geldart group A , A/B, B and B/D with high and low melting points to investigate the effect of temperature on the hydrodynamic behavior of the bed and its effect on the level of IPFs.

We also used two different types of gas, air and argon, with different viscosity to see the effect of different level of HDFs, namely drag force, on the fluidization behavior and its impact on the importance of IPFs.

All the materials depending on their melting point and observations that we had were tested at ambient, 150, 250, 350, 450, 550 and 650 ºC at ambient pressure by the application of Air and Ar. A bed height equal to 15 cm has been fed into the reactor at each experiment.

We measured the loose bulk density ($\rho_{b,loose}$) and the tapped bulk density ($\rho_{b,tapped}$) of the particles which are reported in Table 3.1.

Table 3.1: Solid materials used in the experiments

Material	**Code**	**Geldart Classification**	**ρ_p (kg/m^3)**	**d_p (µm)**	**$\rho_{b,loose}$ (kg/m^3)**	**$\rho_{b,tapped}$ (kg/m^3)**	**T_m[1] (ºC)**
Fine Sand	FS226	B	2656	226	1383	1503	~1700
Coarse Sand	CS820	B/D	2650	820	1313	1423	~1700
Glass Beads	GB71	A	2485	71	1405	1530	~700
FCC[2]	FCC86	A	1460	86	820	900	> 900
Alumina (Smelter Grade)	SGA72	A	1875	72	1000	1155	~2000

[1]From MSDS.

[2] Cooked FCC particles, explained in 4.1.1 in more details.

Table 3.2: Fluidizing gases used in the experiments

Material	**Code**	**ρ_g @ 20 ºC (kg/m^3)**	**μ_g @ 20 ºC ×10^{-5} (Pa.s)**
Air	Air	1.20	1.81
Argon	Ar	1.66	2.22

Density and viscosity of Air and Ar calculated according to Equations (18) - (21) [126], [127]

$$\mu_{Air} = 1.46 * 10^{-6} \frac{T^{1.504}}{(T + 120)} \quad (18)$$

$$\rho_{Air} = 1.2 \left(\frac{293}{T}\right) \quad (19)$$

$$\mu_{Ar} = 44.997 + 0.63892\,T - 0.00012455\,T^2 \quad (20)$$

$$\rho_{Ar} = \frac{PMM_{Ar}}{RT} \quad (21)$$

3.3 Analysis Methods

As in this series of experiments we were using an opaque system we were not able to obtain any results by visual observations. Analysis of pressure fluctuations can provide information on different hydrodynamic phenomenon happening inside the fluidized bed if we use a high enough sampling frequency. This information, include the bubbling behavior i.e. bubble break-up and coalescence, and mixing characteristics of the solid particles [46], [128]–[132]. To remove the effect of gas flow fluctuations on the analysis data we subtracted the moving average with 0.2 Hz from the recorded data.

3.3.1 Bed Pressure Drop

The simple plot of the variation of the total bed pressure drop versus decreasing gas velocity was used for the determination of U_{mf} as in Figure 3.5 (a). Also, the simple plot of the variation of the total bed pressure drop versus increasing gas velocity can be used for the evaluation of the level of IPFs for group A particles since it is for this group of particles that an overshoot of the value of the total bed pressure drop at U_{mf} indicates the extent of IPFs in the bed [33], [36] as in Figure 3.5 (b).

(a) (b)

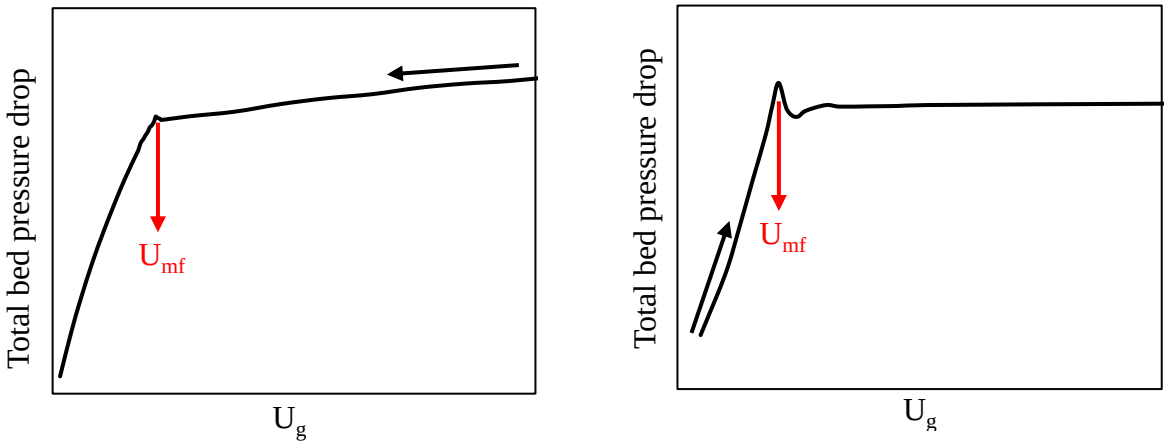

Figure 3.5: Total bed pressure drop vs. superficial gas velocity plot in: (a) decreasing pass and (b) increasing pass

3.3.2 Standard Deviation

Standard deviation is the most common mode of evaluation of pressure signals in the time domain. The standard deviation of a series of pressure data points p_i can be calculated by Equation (22).

$$\sigma = \sqrt{\frac{1}{N-1}\sum_{i=1}^{N}(p_i - \bar{p})^2} \qquad (22)$$

In this equation N is the number of data points and $\overline{p}$ is the mean value of pressure data points[133]. The value of standard deviation (STD) has direct relation with the mean bubble size leading us also to the determination of the turbulent transition velocity U_c [36], [134]–[138].

3.4 Experimental Procedure

To start each experiment, we calculated the exact amount of solid particles to have 15 cm of bed height based on the loose bulk density of powders presented in Table 3.1. Then, we were pouring the bed material into HTFB at a minimum gas velocity only to avoid weepage of particles into the wind-box.

We had to adjust the temperature separately in the wind-box and bed section. We were choosing the preheating temperature 100 ^{o}C above the desired operating temperature and the temperature of the bed section based on the average temperature along the bed. All the calculations of gas velocity were also based on this value. For each operating temperature, the bed was kept in the fluidized state for 2-3 hours for the reactor to reach to the set point temperature before starting the measurements. We recorded the pressure signals in both increasing and decreasing passes for several U_g points.

After every experiment, we removed the filter and particles and refilled the required amount of particles to make sure that we have an equal amount of bed material in every set of experiment.

CHAPTER 4 RESULTS AND DISCUSSION

4.1 Results and Discussion

4.1.1 U_{mf} Measurements

Variation of total bed pressure drop in the decreasing superficial gas velocity pass is presented in Figure 4.1 for CS820. As can be observed, there is a little change in the slope of the fixed bed section due to an increased air viscosity by temperature. However, this change is not leading to a significant change in the values of U_{mf} as presented in Figure 4.2.

For CS820 particles at superficial gas velocities around $U_{mf,}$ the value of Reynolds number was around 25 at room tempoerature, which is appreciably higher than the corresponding value for the creeping flow regime ($Re \ll 0.1$) [51] where the gas viscosity defines the level of drag force exerted on the particles. However, this Reynolds number is not also high enough to satisfy the flow characteristics of inertia regime ($Re > 540$) [51]. Thus, there is a competing effect of an increased gas viscosity and a decreased gas density by temperature leading to a minor change in the magnitude of drag force and U_{mf} at different temperatures according to Equitation (23).

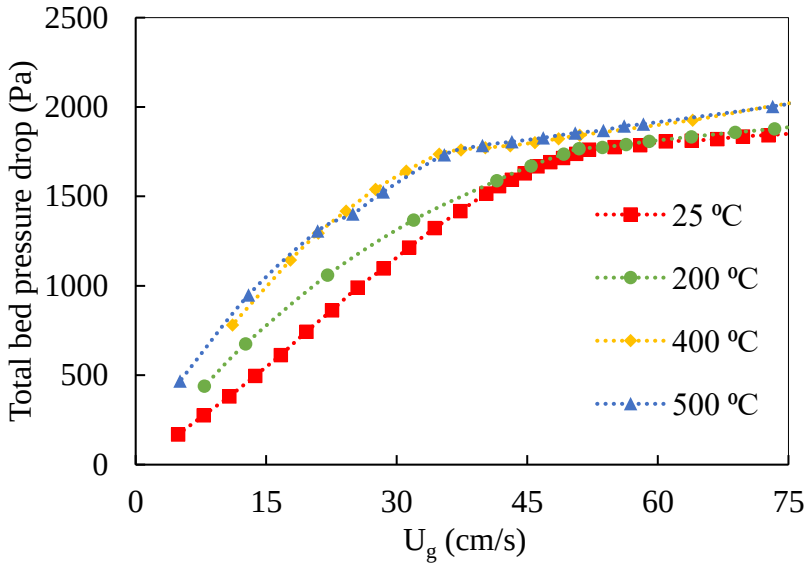

Figure 4.1: Variation of total bed pressure drop in the decreasing superficial gas velocity pass at different temperatures for CS820 fluidized by Air.

This is in a good agreement with the values predicted by the correlation proposed by Chitester et al. [118].

$$F_d = \frac{C_d\,\rho_g\,U_g^2}{2}\times\pi\frac{d_p^2}{4}\times\varepsilon^{-3.8}\,,C_d = \left(0.63+\frac{4.8}{Re_p}\right)^2 for\ \ all\ Re_p \qquad (23)$$

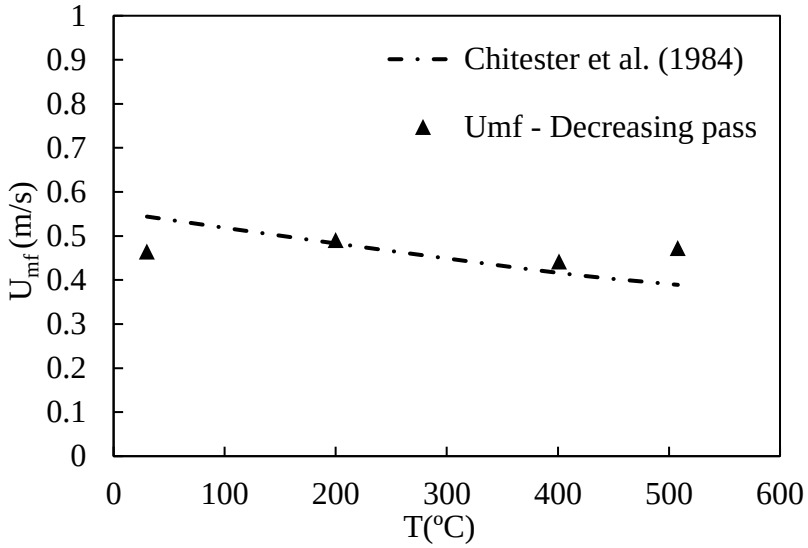

Figure 4.2: Variation of minimum fluidization velocity of CS820 by the temperature compared to the prediction achieved by the Chitester et al.'s correlation [118].

In contrast with CS820, when we look at the variation of total bed pressure drop by superficial gas velocity for FS226 we can see a clear increase of slope in the fixed bed section by increasing the operating temperature from 25 to 650 °C in Figure 4.5.

Moreover, the Reynolds number becomes very close to the creeping flow regime ($Re < 1$) for this size of particles around U_{mf}. Thus, the viscosity is the only gas property that defines the variation of drag force applied on the particles in such a system. As viscosity increases by temperature, the air exerts a higher drag force on the particles and can make them fluidized at a lower gas velocity according to Equation (23). At higher gas velocity well above the minimum fluidization state, the values of total bed pressure drop remains the same at different temperatures as in Figure 4.4. This observation is believed to be due to the absense/negligible effect of IPFs in the case of FS226. This will be compared and explained in detail with the results of GB71 where IPFs are playing an important role.

The decrease of U_{mf} with temperature is in a good agreement with the values predicted by Wen-Yu correlation [119] in Figure 4.5.

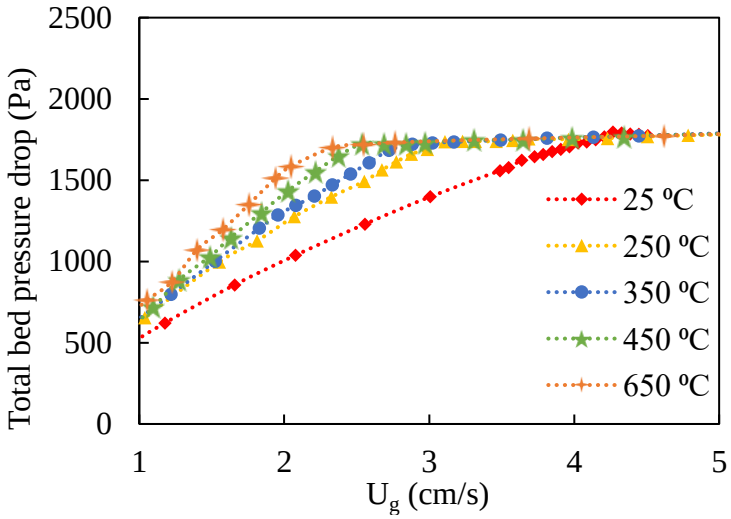

Figure 4.3: Variation of total bed pressure drop in the decreasing superficial gas velocity pass at different temperatures for FS226 fluidized by Air at $1 < U_g < 5$ cm/s.

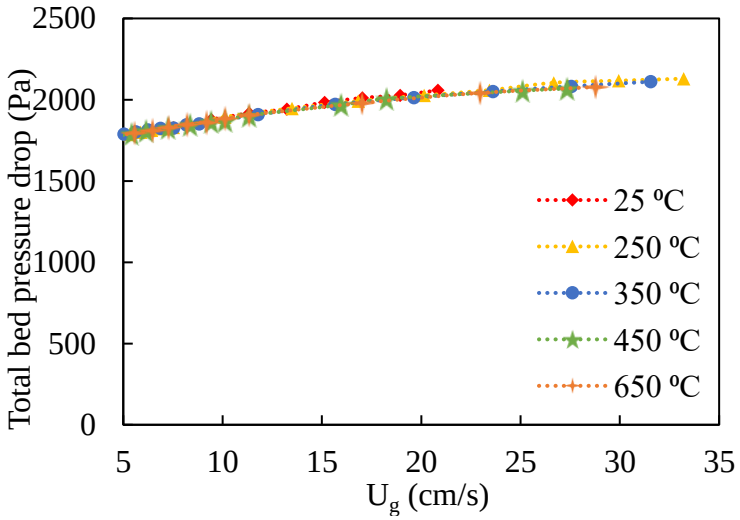

Figure 4.4: Variation of total bed pressure drop in the decreasing superficial gas velocity pass at different temperatures for FS226 fluidized by Air at $U_g > 5$ cm/s.

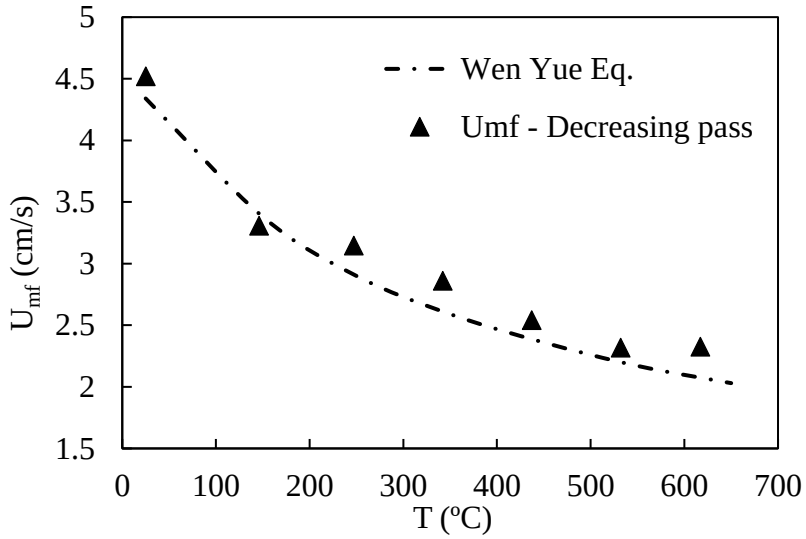

Figure 4.5: Variation of minimum fluidization velocity of FS226 by temperature compared to the prediction achieved by theWen-Yu (W-Y) Eq. [119].

For Cooked FCC86 fluidization by air, looking at the variation of total bed pressure drop in Figure 4.6, one can notice the overshoot happening at around U_{mf}. This is a typical observation for Geldart group A particles due to their higher ratio of IPFs/HDFs at fixed bed state. As soon as the bed is fluidized the value of pressure drop also levels down. Comparing this overshoot at low and high temperature also shows that the level of IPFs are higher when we increase the temperature. Thus, the minimum fluidization state happens at a higher flow of gas.

The same explanation as that for FS226 can be used also here. Gas viscosity is still the key gas property to define the level of drag force in the system and we expect that U_{mf} values decrease by temperature. However, this is not the case due to the mentioned effect of IPFs. As presented in Figure 4.7, values of U_{mf} increases slightly by temperature. Experimental values are not in agreement with those calculated by Wen-Yu [119] or Carman-Kozney [121] correlations. However, the predictions from Carman-Kozney can be ameliorated by considering the effect of temperature on the bed voidage in fixed bed state as proposed by Formisani et al. [15], [96]. According to their study, the value of bed voidage increases by temperature due to a change in the stacking of the particles because of higher IPFs. This increase provides more pourosity in the bed and less pressure drop which shifts the estimated U_{mf} towards higher values at high temperature.

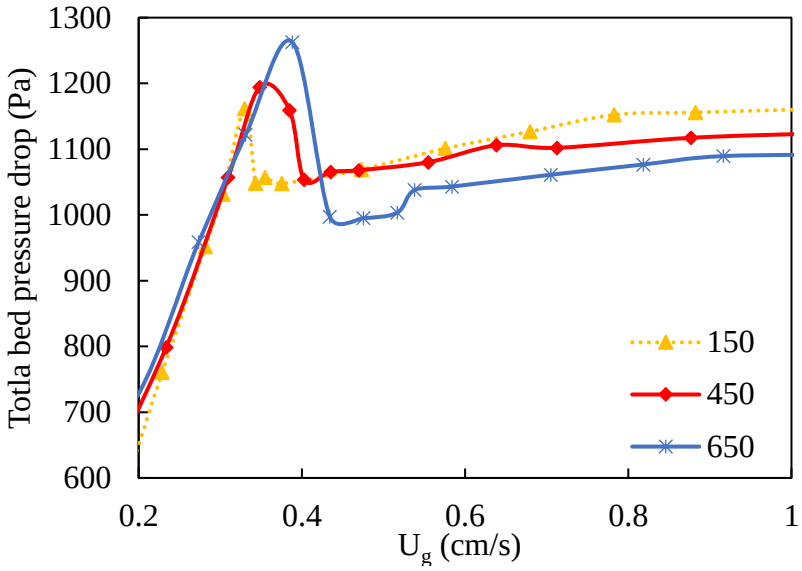

Figure 4.6: Variation of total bed pressure drop in the increasing superficial gas velocity pass at different temperatures for Cooked FCC86 fluidized by Air at $0.2 < U_g < 1$ cm/s.

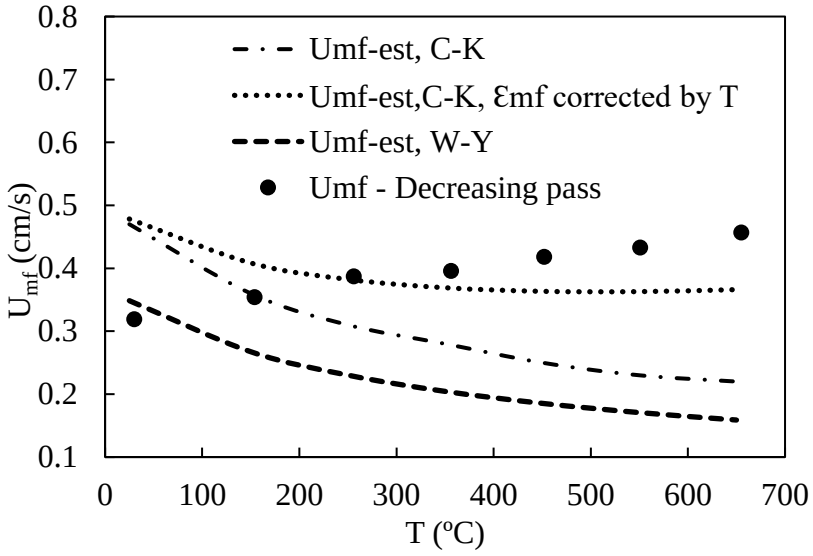

Figure 4.7: Variation of Minimum fluidization velocity of Cooked FCC86 by temperature compared to the predictions achieved by the Wen-Yu (W-Y) [119] and Carman-Kozeny (C-K) [121] correlation as well as the C-K correlation with a corrected value of ε_{mf} by temperature [15], [96].

The term, Cooked, is deployed here due to a problem that we encountered while doing experiments with fresh FCC particles. At temperatures around 500 ºC, we noticed from the values of total bed pressure drop that there is a sensible weight of the particle is lost when we return to fixed bed state after recording data at high gas velocities. This was also confirmed when we opened the reactor and observed that particles are stuck on the filter and there is condensed water on the inner wall of the reactor as presented in Figure 4.8. In general, moisture can be captured by the porous particles i.e. FCC in a humid climate as one that we have in Montreal. However, as we repeated the experiments we noticed that this condensation does not happen at lower temperatures in contrast with the fact that the aforementioned moisture will be released at 100 ºC. TGA results of fresh FCC particles also confirmed that there is a 2% weight loss at around 100 ºC followed by a 10% weight loss at around 500 ºC (Figure 4.9). This is believed to be due to the dehydroxylation of kaolinite content of FCC particles that occurs usually in the range of 400 to 540 ºC [139], [140]. The related weight loss is disappeared when we repeated the TGA test for the same sample. This water loss at high-temperature leads to a change in the properties of our FCC particles and also particle loss at high temperature which makes the data incomparable at a low and high temperature. As a result, all of the FCC particles used in this study are cooked at 500 ºC in a fully fluidized state and stored in dry condition to avoid the condensation problem.

Figure 4.8: Condensation of water at the outlet of HTFB at temperatures higher than 500ºC causing the particles to stick to the filter.

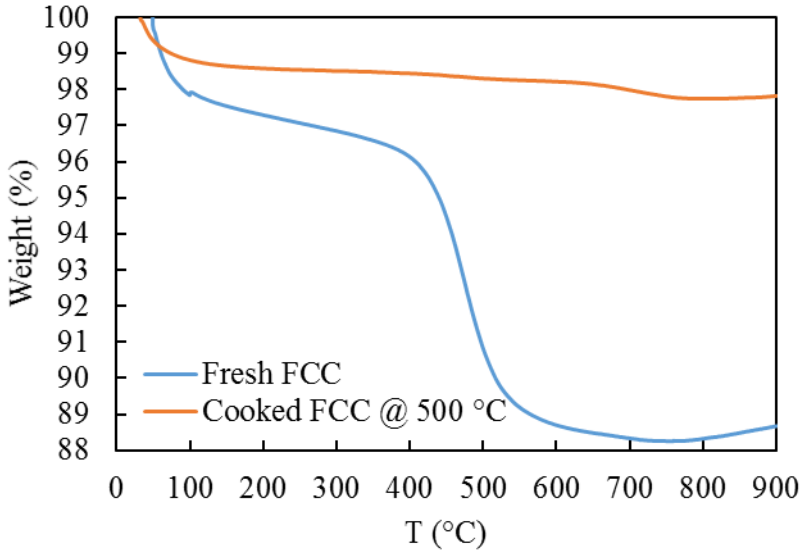

Figure 4.9: TGA results of Fresh and Cooked FCC86

Sample size: 8.5 mg, Heating rate: 5 ºC/min

The effect of IPFs is more pronounced in the case of GB71 particles as they have the lowest melting point among adopted particles. This effect can be observed in the variation of total bed pressure drop against U_g in Figure 4.10 and Figure 4.11. The typical overshoot of pressure drop around U_{mf} increases by temperature for these particles. Moreover, it is at 400 ºC that we have a double-peak which is a sign of channeling and slug formation in the bed. It is worth mentioning that this behavior can be captured only if small enough steps have been chosen to increase the superficial gas velocity through the increasing pass. Moreover, this increase in the level of IPFs results in a delayed full fluidization state and also explains the sudden increase in the values of U_{mf} by temperature in Figure 4.12. Morover, the value of total bed pressure drop was lower at a higher operating temperature when $U_g \geq 1$ cm/s. This is a sign of formation of agglomerates at higher temperatures. These agglomerates have larger size than the original particles which provides more free space for the gas to pass through the bed with a redused resistance against its flow.

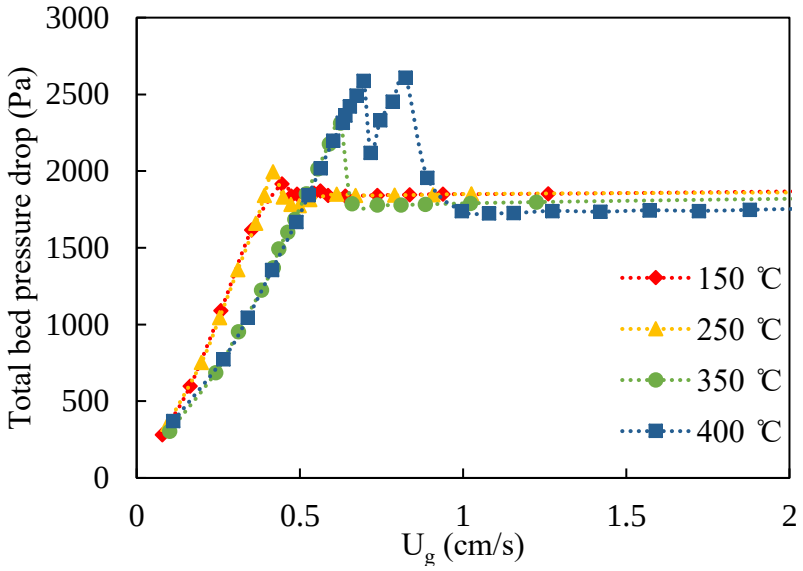

Figure 4.10: Variation of total bed pressure drop by increasing the superficial gas velocity at different temperatures for GB71 fluidized by Air at 0 < Ug < 2 cm/s.

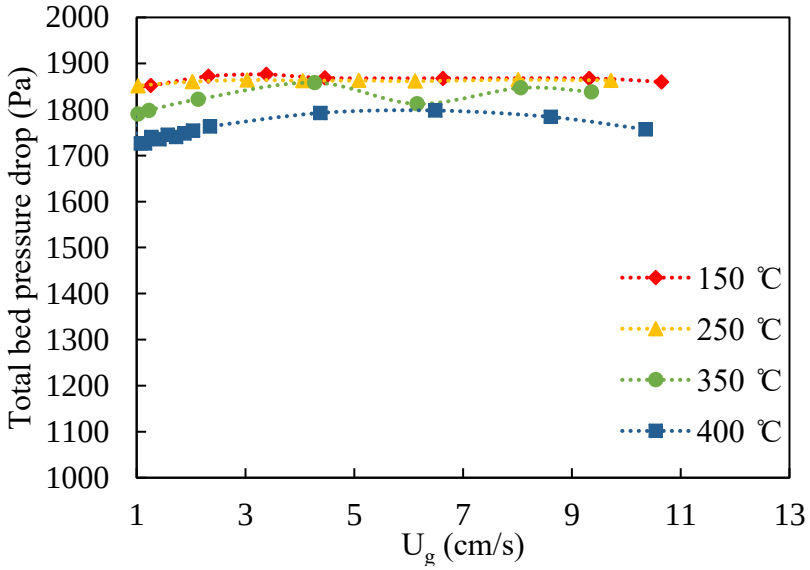

Figure 4.11: Variation of total bed pressure drop by increasing the superficial gas velocity at different temperatures for GB71 fluidized by Air at Ug > 1 cm/s.

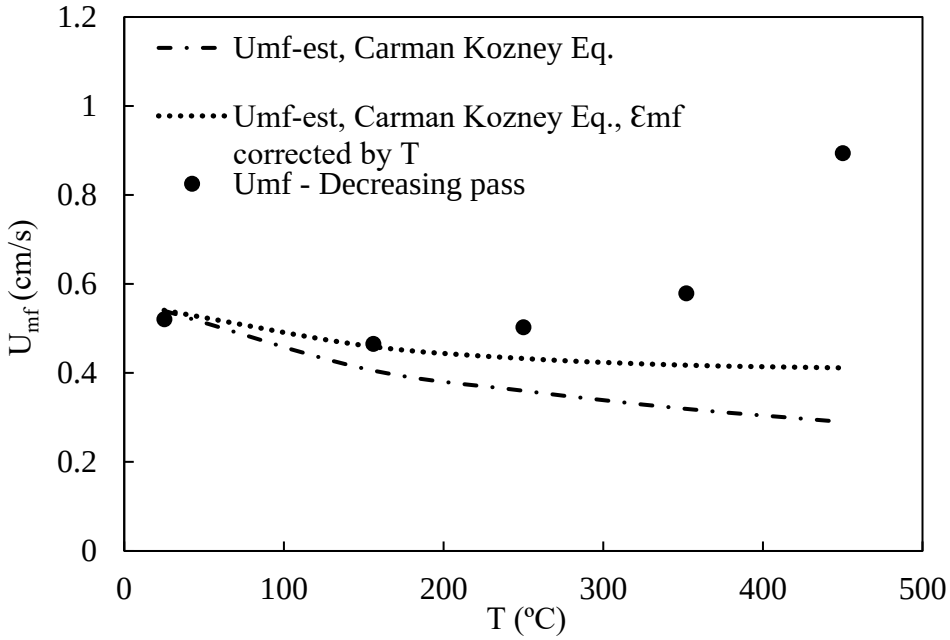

Figure 4.12: Variation of minimum fluidization velocity of GB71 by temperature fluidized with air compared to Carman-Kozeny (C-K) [121] and C-K with corrected value of ε_{mf} by temperature [15], [96].

Compared to what we had in the case of FCC86 particles in Figure 4.7, there is not a good agreement between experimental results and estimated values obtained from Carman-Kozeny correlation for GB71 fluidized with air. Even correcting the value of the bed voidage by temperature is not a good approach to consider the effect of IPFs in this case due the high ratio of IPFs/HDFs. This is a clear confirmation for our argument that hydrodynamic-based models and correlations are not predicting the experimental results in the case of fluidization of fine particles under extreme temperatures where the effect of IPFs is considerably high.

For fine powders, as in the case of GB71, a further increase of the operating temperature leads to full defluidization of particles and shutdown of the system if it is not being taken care of. To show this, we kept the superficial gas velocity constant at 1.1 cm/s at all temperatures which is well above the value of U_{mf} at ambient condition ($U_{mf,\ ambient}$ = 0.5 cm/s) to keep particles at an acceptably well fluidized state and we recorded the total and in-bed pressure drops and temperatures all along the bed as is presented in Figure 4.13.

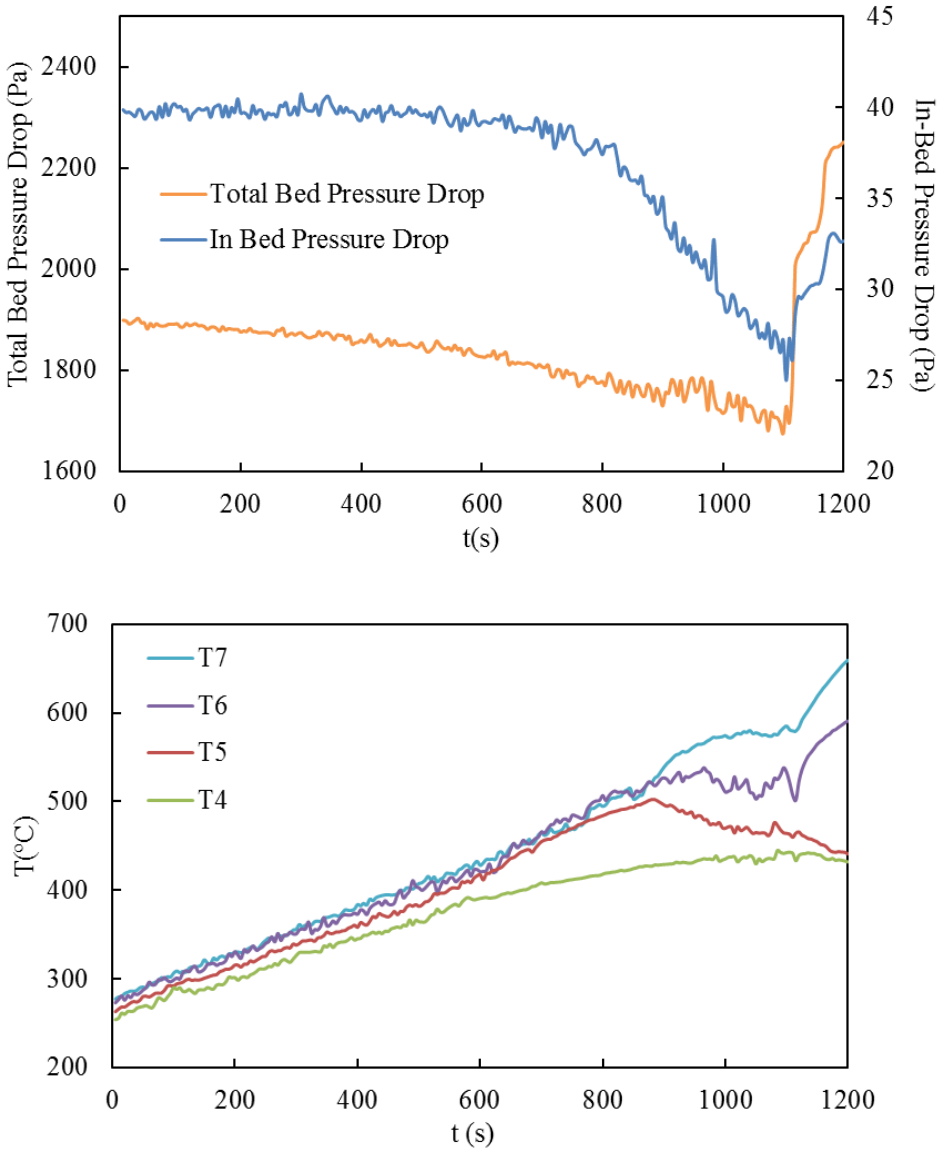

Figure 4.13: Evolutions of in-bed and total bed pressure drops and the in-bed temperature readings (T4, T5, T6 and T7 respectively at 5, 12.5, 15 and 17.5 cm from the distributor plate) through a defluidization test for GB71 at U_g=1.1 cm/s.

As temperature increases, the values of pressure drop for both total and in-bed measurements decrease gradually first because of a decrease in the gas density (in the first 600 seconds) and later as a sign of formation of agglomerates which is accompanied with a slight sign of temperature

irregularity along the bed. However, it is at around 500 ºC (t = 850 s) that the value of both pressure drops start to increase suddenly and at the same time, temperature recordings along the bed start to deviate from their normal increasing trend. This is a typical observation for a bed going through a defluidization process. It was in this state that we stopped heating and increased the gas velocity to avoid full defluidization. However, we could not manage to save the bed from defluidization and we ended up with the formation of big chunks of sticky agglomerates as is presented in Figure 4.14.

To examine the effectiveness of introducing a higher level of HDFs to counter balance the effect of IPFs during the fluidization of particles at high temperature, we employed argon as the fluidizing gas, which has a higher viscosity compared to air as is presented in Figure 4.15.

Figure 4.14: Formation of hard agglomerates of GB71 after full defluidization at 500ºC.

This increase in the level of HDFs clearly decreased the U_{mf} with no or a slight change in its trend of variation by temperature as is clear in Figure 4.16 (a), (b) and (c). To highlight this effect the experimentally obtained values of U_{mf} is compared with the estimated value calculated by the C-K equation at different temperatures in Figure 4.17. Comparing the U_{mf} values at 450 ºC obtained from fluidization with air and argon we can clearly see the absence of the extreme overshoot that

we observed in the case of fluidization with air when we deployed argon. This can only be explained by the effect of an increased level of HDFs.

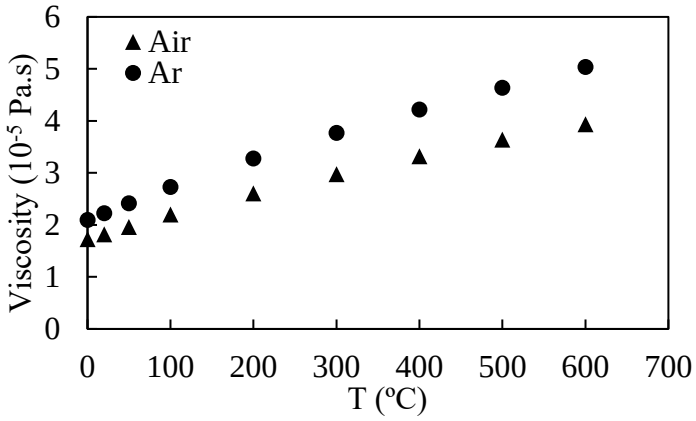

Figure 4.15: Variations of the viscosities of Air and Argon (Ar) by temperature [81], [127].

(a)

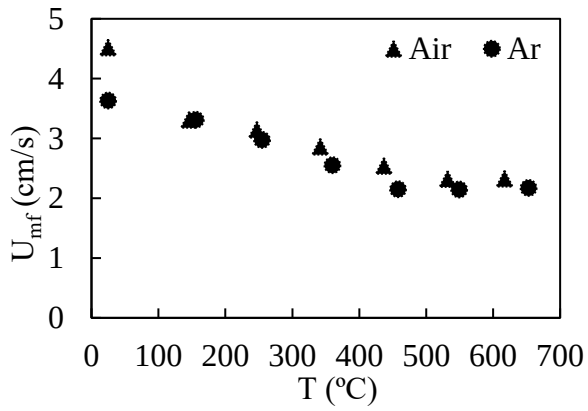

(b)

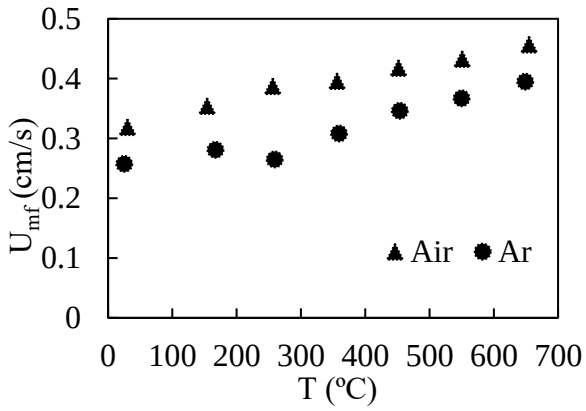

(c)

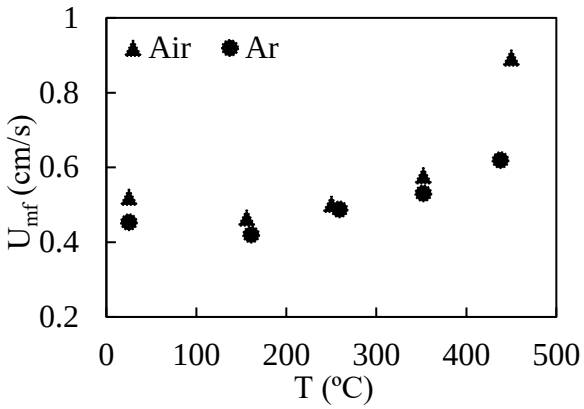

Figure 4.16: Variation of minimum fluidization velocity by temperature when fluidizing the particles with Air and Ar in the decreasing pass for: (a) FS226, (b) FCC86 and (c) GB71.

By looking at the variation of total bed pressure drop by U_g in Figure 4.18 it can be noticed that channeling is not happening until 450 ºC compared to 400 ºC in the case of fluidization with air in Figure 4.10.

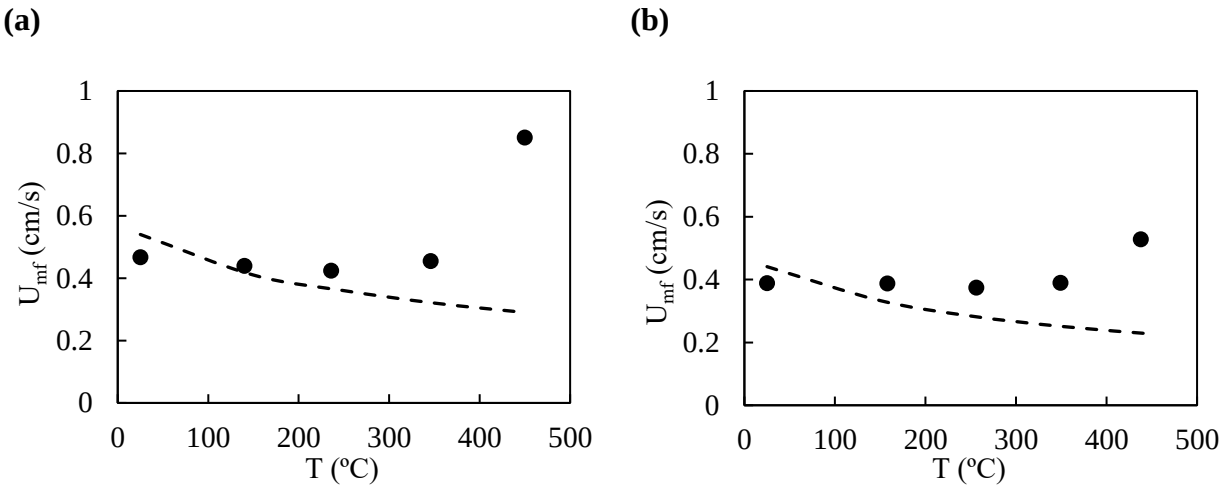

Figure 4.17 : Variation of minimum fluidization velocity of GB71 (●) by temperature fluidized with (a) air and (b) argon compared to the predictions achieved by the C-K equation (- - -).

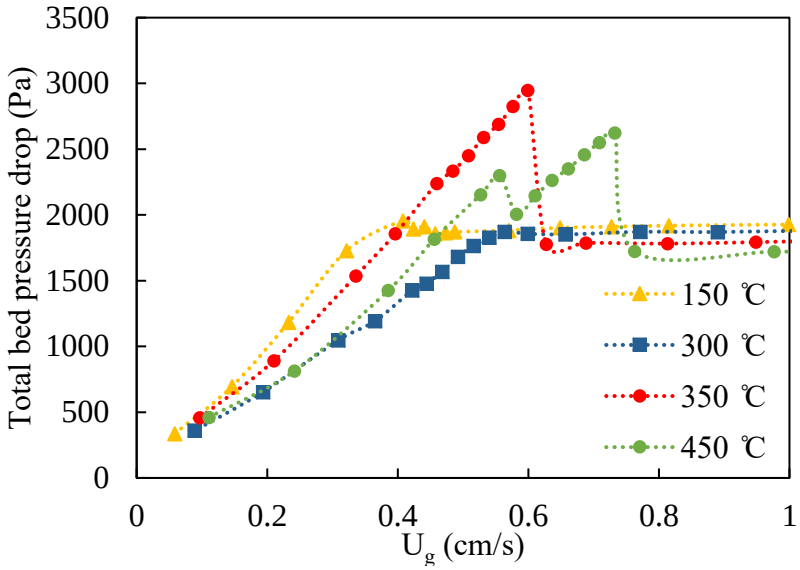

Figure 4.18: Variation of total bed pressure drop in the increasing superficial gas velocity pass at different temperatures for GB71 fluidized by Ar at 0 < Ug < 1 cm/s.

4.1.2 Indirect Measurement of IPFs

After proving the fact that IPFs are playing an important role in the fluidization of fine powders at elevated temperatures, now it is the time to go further with the presented data and estimate the magnitude of these IPFs in a fluidized bed. As it was mentioned earlier in 2.4.4 all the available measurement techniques are either complicated to apply, non-repeatable or even not well presenting the conditions in a real fluidization process, thus the results obtained from those approaches cannot be relied on. It will be extremely beneficial to be able to measure the level of IPFs in a fluidized bed without any intrusion and respecting the real conditions of the process. Therefore, in this section we are introducing a novel, simple and practical indirect measurement approach to accomplish the mentioned task.

In a fluidized bed, we can always back calculate the value of the drag force on a single particle or in the whole system by knowing the superficial gas velocity, properties of the gas and the particles, the type of the flow regime and the total pressure drop in our system. We use this fact as the basis of our indirect quantification method.

The difference between the value of the total drag force, back calculated through Equation (25) using the experimentally obtained U_{mf} affected by IPFs, and the same value obtained from a U_{mf} value calculated by a hydrodynamic based correlation that works well under the condition that there is no/negligible effect of IPFs, such as Carman-Kozeny, gives us the force that is needed to overcome the IPFs at minimum fluidization velocity. As for the starting point of this approach, it is extremely important to employ a correlation that adequately predicts the minimum fluidization velocity at room temperature. According to Figure 4.12, this was the case for GB71 particles at ambient temperature. However, we had to do a modification in the Carman-Kozeny correlation to use it for FCC86 particles. The modified format of Carman-Kozeny is presented in Equation (24). The modification is based on the fact that to obtain the Carman-Kozeny correlation, it has been considered that the gas flows through micro pipes that are created by the bed assembly in the form of bed voidage. Depending on the tortuosity of the flow path, the constant coefficient might be higher or lower than 180 [51]. In our case a value of 270 seems to give a better fit at ambient conditions. Next, considering the packing of the particles and the number of contact points of each particle with its neighboring particles gives us the value of the magnitude of IPFs between each two neighboring particles.

$$U_{mf} = \frac{\left(\varphi d_p\right)^2}{270} \frac{\rho_p - \rho_g}{\mu_g} g\left(\frac{\varepsilon_{mf}^3}{1-\varepsilon_{mf}}\right) \quad (24)$$

$$F_d = \nabla P A H \quad (25)$$

$$\nabla P = 180 \frac{\mu_g U_{mf}}{d_p^2} \frac{(1-\varepsilon_{mf})^2}{\varepsilon_{mf}^3} \quad (26)$$

In the case of GB71 particles, using the Equations (27) - (29) [141] to calculate the coordination number N_c, we obtain a value of $N_c = 6$ which represents a cubic structure for stacked particles in a way that each particle is connected to four particles on its sides and two particles at the top and the bottom presented in Figure 4.19.

$$N_c = (\frac{3.08}{\varepsilon})\text{-}1.13 \quad (27)$$

$$N_c = 1.126\, e^{3.196(1-\varepsilon)} + 0.860 e^{-3.5(1-\varepsilon)} \quad (28)$$

$$N_c = 1.61\varepsilon^{-1.48} \quad \varepsilon \leq 0.82 \quad (29)$$

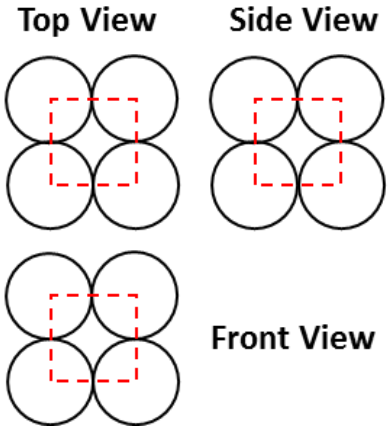

Figure 4.19: Cubic stacking structure of particles with $N_c = 6$

Thus, dividing the obtained total IPFs value by the number of particles is not far from reality and believed to be a good assumption to have the magnitude of individual IPFs between two single particles. We also increase the precision by considering the effect of the walls of the reactor. To consider the wall effect, we replaced it with a layer of stacked particles, if the level of IPFs between particles and wall is identical to that can be achieved between neighboring particles in the bed, and added the obtained number of particles to the real number of particles. However, by doing so we found that the difference is less than 0.5% which can be neglected. Thus, we did not consider this additional number of particles in our calculations.

The obtained values from this approach are plotted in Figure 4.20 for GB71 and FCC86 fluidized with air and argon. At a first glance, the order of magnitude of the measured forces are in the range of nN which is in accordance with the results reported in the works of Colbert et al. [66], Hakim et al. [64], Huang et al. [142], Li et al. [70] and Fatah [63].

In all cases the estimated value of IPFs is increasing by temperature and mimics the trend obtained earlier for the variation of U_{mf} by temperature. Comparing the graphs in Figure 4.20 (a) and (c) the effect of higher level of drag force exerted by argon compared to air resulted in a less increase of the level of IPFs in the case of fluidization with argon. The same comparison is valid for the comparison of Figure 4.20 (b) and (d). Estimated value of IPF increased with a smaller slope in the case of fluidization with argon. To have a clearer vision of the possible effect of the IPFs on the fluidization, the values of the ratio between this force and the weight of single particle (IPFs/W) is presented in Figure 4.21. It is clearly shown in Figure 4.21 (a) that at 450 ºC the ratio of IPFs/W is higher than 2 and this is where we had the defluidization of particles and formation of big chunks of agglomerates that we presented in Figure 4.13. However, this ratio was decreased to below 2 at 400 ºC in the case of fluidization with argon in Figure 4.21 (c) due to the elevated level of drag force in the system which counterbalances IPFs. Moreover, IPFs/W ratio for FCC has never reached more than 1.5 in any temperature using any fluidization gas which is in accordance with the sign of no agglomeration and defluidization during the experiments.

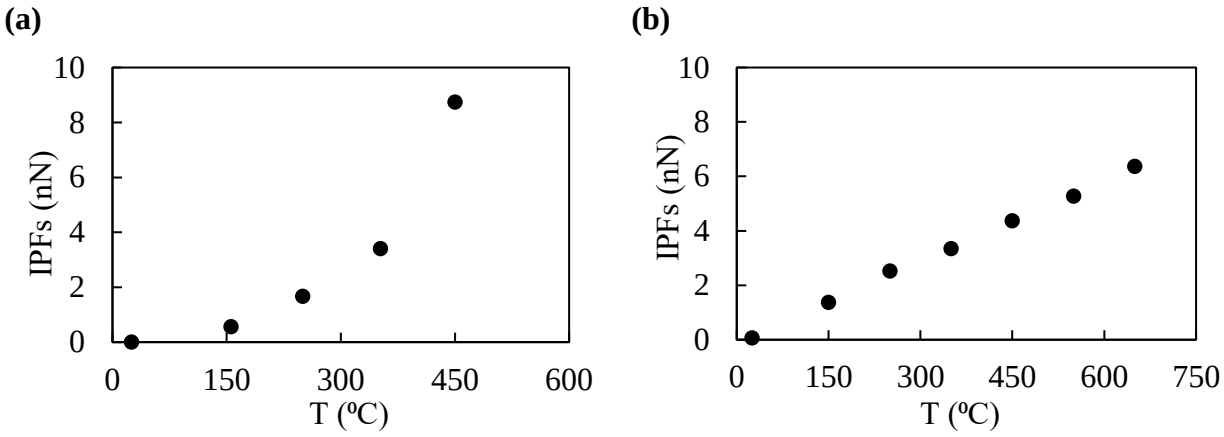

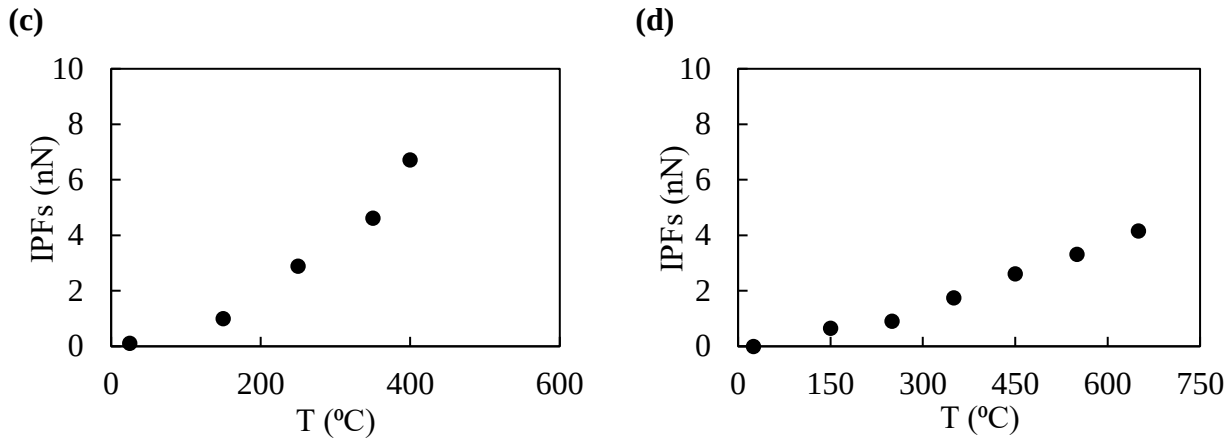

Figure 4.20: Individual IPFs value obtained for: (a) GB71 fluidized with Air, (b) FCC86 fluidized with Air, (c) GB71 fluidized with Argon and (d) FCC86 fluidized with Argon.

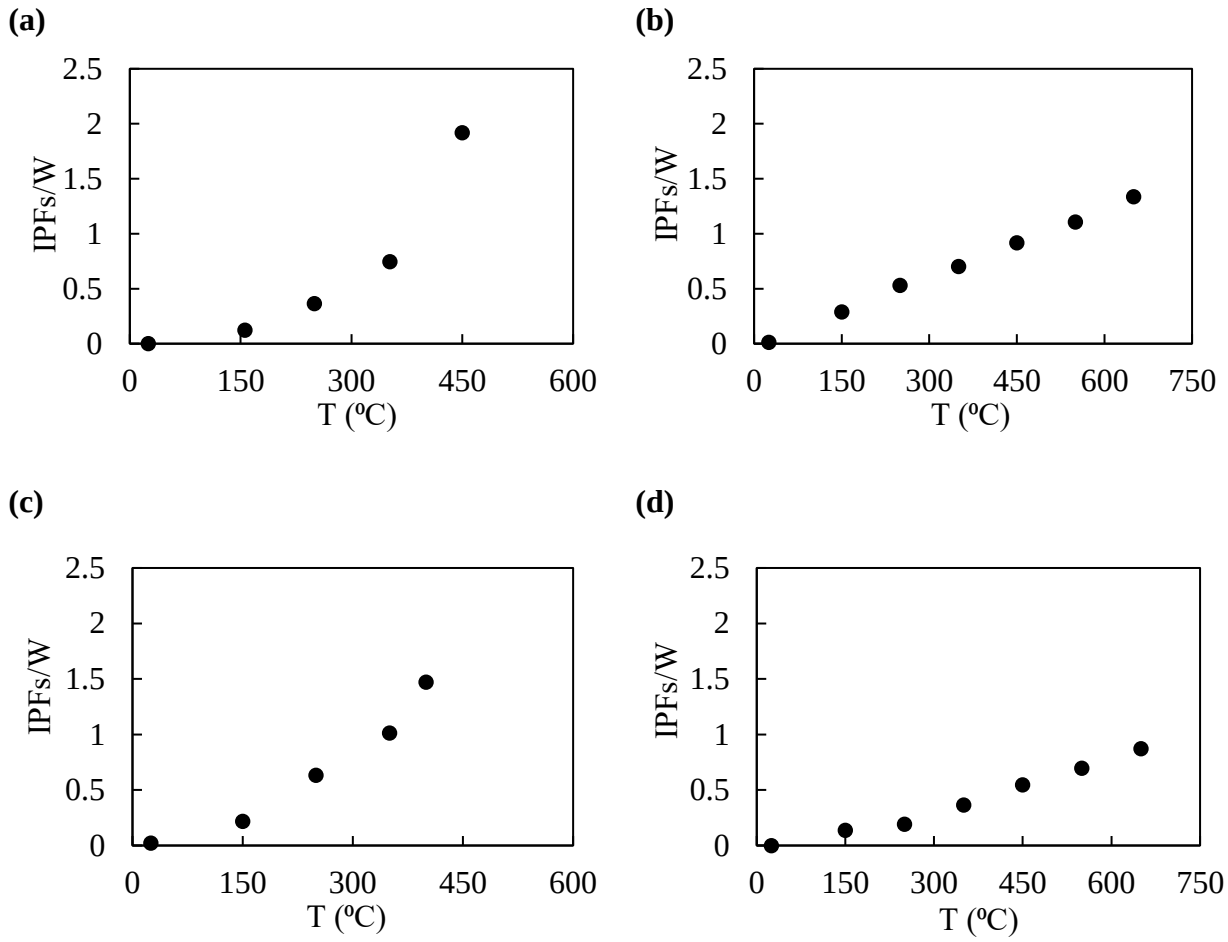

Figure 4.21: IPF/W value obtained for: (a) GB71 fluidized with Air, (b) FCC86 fluidized with Air, (c) GB71 fluidized with Argon and (d) FCC86 fluidized with Argon.

As stated and presented earlier in Figure 4.6, the presence of an overshoot in the value of pressure drop against superficial gas velocity for Geldart Group A particles is due to the presence of IPFs. We used this principal to verify our IPFs measurement results with a qualitative verification method. To do so, we measured the area between the values of pressure drop plotted against increasing and decreasing superficial gas velocity as well as the height of the peak for FCC86 and GB71 fluidized with Ar and Air as illustrated in Figure 4.22. For the case that we had channeling around U_{mf} we considered the height of the equivalent peak as if there were no channeling. The obtained values are presented in Figure 4.23. As highlighted inFigure 4.24, there is a similar trend

to those presented in Figure 4.20 and Figure 4.21 which again verifies qualitatively the approach that we used to obtain the IPF values in the previous step.

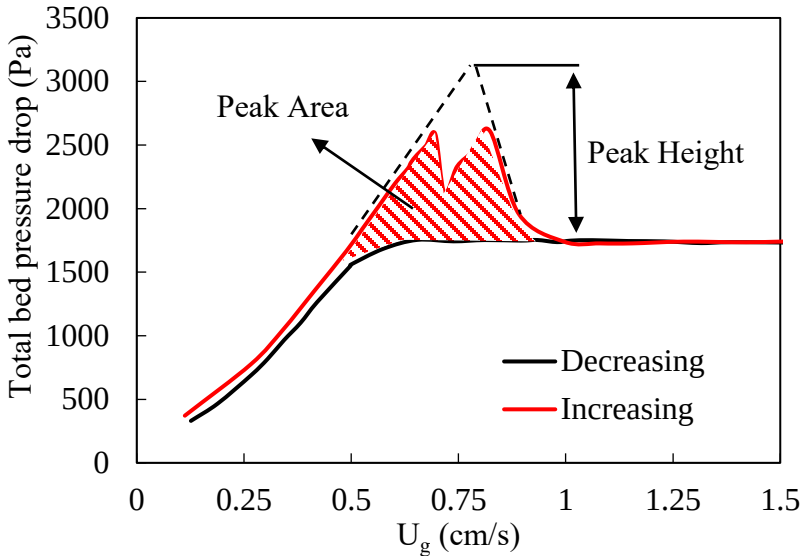

Figure 4.22: Peak area evaluation as a qualitative estimation of IPFs. GB71 fluidized with air at 400 ºC.

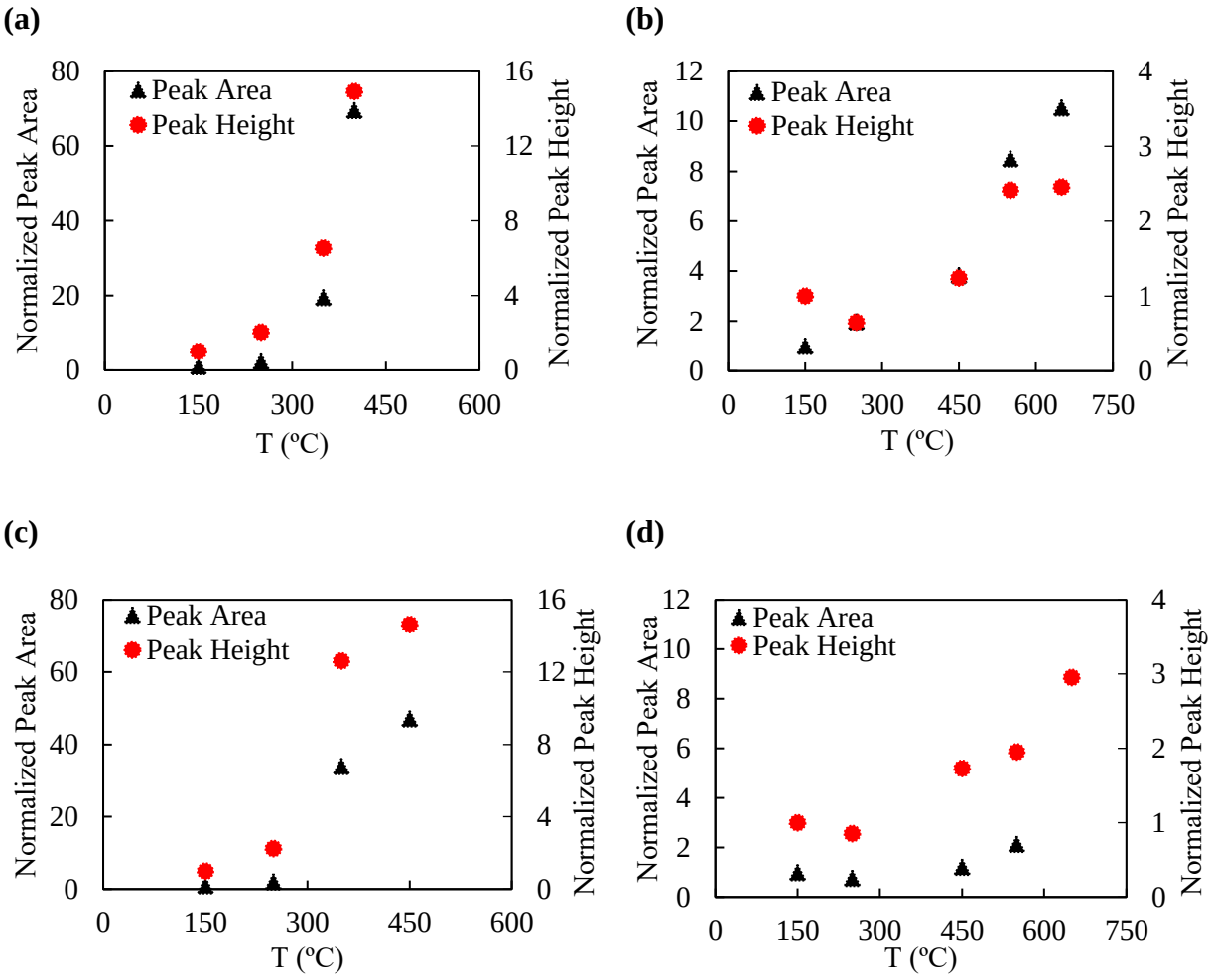

Figure 4.23: The variation of normalized peak height and peak area in the plot of total bed pressure drop against increasing gas velocity with temperature for: (a) GB71 fluidized with Air, (b) FCC86 fluidized with Air, (c) GB71 fluidized with Argon and (d) FCC86 fluidized with Argon.

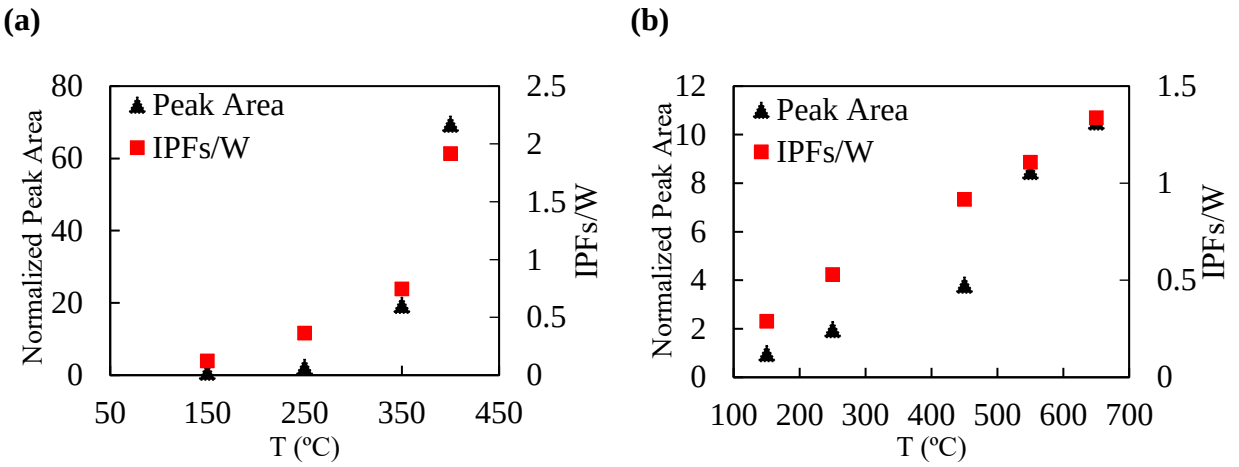

Figure 4.24 : The variation of normalized peak area and IPFs/W with temperature for: (a) GB71 and (b) FCC86 fluidized with air.

CHAPTER 5 CONCLUSION AND RECOMMENDATIONS

5.1 Conclusion

In this study, we achieved a better understanding of the effect of temperature on the level and magnitude of IPFs and HDFs and the importance of the ratio of IPFs/HDFs in the fluidization process of different particles. Highlighted conclusions of this study is presented in order of their appearance in the body of the work as follows.

- We Precisely measured U_{mf} and U_c of different powder samples with various physical properties from Geldart group A, B and border of B/D by analysis of the pressure signals, specifically plot of the total pressure drop versus increasing/decreasing superficial gas velocity and the standard deviation of in-bed pressure signal in the temperature range of 25 to 650 ºC.
- Experimental data showed that U_{mf} remains relatively unchanged with temperature for CS820 due to a competing effect of increasing gas viscosity and decreasing gas density in on the drag force exerted on particles while U_{mf} decreased for FS226 with temperature due to an increase in the viscosity of the fluidizing gas.
- Experimentally obtained U_{mf} values found to be in accordance with the values estimated by the correlation proposed by Chitester and Wen-Yu for CS820 and FS226 respectively.
- U_{mf} for FCC86 increased slightly by temperature which, considering the particle size, is believed to be because of the presence of IPFs.
- Water released at around 500 ºC in the case of fluidizing fresh FCC particles due to dihydroxylation process.
- U_{mf} values of GB71 showed a similar behaviour as FCC86 with a slight decrease up to 250 ºC and a more pronounced increase of U_{mf} at temperatures higher than 250 ºC.
- Severe agglomeration of particles happened for GB71 at temperatures higher than 400 ºC and the bed could not be saved from full defluidization even by increasing the gas velocity.

- Hydrodynamic based correlations such as Carman Kozeny failed to predict the values of U_{mf} for FCC86 and GB71 due to a high ratio of IPFs to HDFs at higher temperatures even when using a corrected value for the bed voidage considering the effect of IPFs on the packing of the particles.
- Using argon as the fluidizing agent decreased the values of U_{mf} for all the particles. It also reduced the severity of the effect of IPFs on GB71 at temperatures above 400 ºC. These are believed to be due to the higher viscosity of argon compared to air which provides higher HDFs in the system.
- The magnitude of IPFs estimated through a simple approach for FCC86 and GB71. We did so by back calculating and comparing two values of the drag force using the U_{mf} obtained experimentally and theoretically at a certain temperature.
- We found that IPFs increases by temperature for FCC86 and GB71 fluidized with air and argon and it exhibits the same trend as we obtained for the variation of U_{mf} by temperature for these particles.
- We also calculated and analyzed the area and the height of the peak in the plot of the total bed pressure drop against superficial gas velocity for FCC86 and GB71 fluidized with air and argon. Results showed the same behaviour that we obtained for the variation of IPFs by temperature in all cases.

5.2 Recommendations

In this research, we studied highlighted the importance and the effect of IPFs and HDFs on the hydrodynamic characteristics of gas-solid fluidized beds at high temperature and proposed a simple approach for the indirect measurement of IPFs. In addition to the achievements that we had in this work, some recommendations for future study are proposed as follows:

- Perform an experimental study in a bubble column reactor by application of different gases to highlight the influence of gas viscosity on the bubble size/stability in a multiphase reactor. Owing to the hydrodynamic similarity between a gas-solid fluidized bed and a

bubble column reactor the results obtained from this experiment help us to have a better understanding of the bubbling behaviour of fluidized bed of fine particles, e.g., FCC particles, at high temperature and verify the hypothesis that we provided for the effect of temperature on the bubbling behaviour of FCC86 in this work.

- Perform a series of experiments at ambient conditions employing different types of particles differing in size and density in gas-solid fluidized beds with different diameters to develop a correlation, which provides an appropriate prediction of U_c under various conditions, i.e., different particle properties and column diameters.
- Modification of hydrodynamic based correlations, e.g., the one obtained from the previous recommendation, to adequately predict a bed hydrodynamic parameter, e.g., U_c, at high temperature considering the effect of IPFs. A recommended approach could be to adapt the ratio of ($U_{mf,\ experimental}$ / $U_{mf,\ calculated}$) as a correction factor to introduce the effect of IPFs into the correlation.

BIBLIOGRAPHY

[1] P. Pagliai, S. J. R. J. R. Simons, and D. Rhodes, “Towards a fundamental understanding of defluidisation at high temperatures: A micro-mechanistic approach,” *Powder Technol.*, vol. 148, no. 2–3 SPEC. ISS., pp. 106–112, 2004.

[2] I. Tomasetta, “The effect of temperature on flow properties of powders,” UNIVERSITÀ DEGLI STUDI DI SALERNO, 2012.

[3] J. Zhu, B. Leckner, Y. Cheng, and J. Grace, “Fluidized Beds,” in *Multiphase Flow Handbook*, CRC Press, 2005, pp. 5–93.

[4] D. Kunii and O. Levenspiel, *Fluidization Enfineering*. 1991.

[5] X. Fan, D. J. Parker, Z. Yang, J. P. K. Seville, and J. Baeyens, “The effect of bed materials on the solid/bubble motion in a fluidised bed,” *Chem. Eng. Sci.*, vol. 63, no. 4, pp. 943–950, 2008.

[6] S. Gheorghiu and M.-O. Coppens, “Heterogeneity explains features of ‘anomalous’ thermodynamics and statistics.,” *Proc. Natl. Acad. Sci. U. S. A.*, vol. 101, no. 45, pp. 15852–15856, 2004.

[7] K. S. Lim, J. X. Zhu, and J. R. Grace, “Hydrodynamics of gas-solid fluidization,” *Int. J. Multiph. Flow*, vol. 21, no. Suppl, pp. 141–193, 1995.

[8] R. W. Pike, “Recent advances in the engineering analysis of chemically reacting systems. By L. K. Doraiswamy, Ed., Halsted Press, 1984, 611+X pp.,$49.95,” *AIChE J.*, vol. 32, no. 4, pp. 256–290, Apr. 1986.

[9] R. Cocco, S. B. R. Karri, and T. Knowlton, “Introduction to fluidization,” *Chem. Eng. Prog.*, vol. 110, no. 11, pp. 21–29, 2014.

[10] C. Zhu, Q. Yu, R. N. Dave, and R. Pfeffer, “Gas fluidization characteristics of nanoparticle agglomerates,” *AIChE J.*, vol. 51, no. 2, pp. 426–439, Feb. 2005.

[11] C. Zhu, G. Liu, Q. Yu, R. Pfeffer, R. N. Dave, and C. H. Nam, “Sound assisted fluidization of nanoparticle agglomerates,” *Powder Technol.*, vol. 141, no. 1–2, pp. 119–123, 2004.

[12] Q. Guo, Y. Li, M. Wang, W. Shen, and C. Yang, “Fluidization characteristics of SiO2 nanoparticles in an acoustic fluidized bed,” *Chem. Eng. Technol.*, vol. 29, no. 1, pp. 78–86, Jan. 2006.

[13] M. Ye, M. A. Van Der Hoef, and J. A. M. Kuipers, “The effects of particle and gas properties on the fluidization of Geldart a particles,” *Chem. Eng. Sci.*, vol. 60, no. 16, pp. 4567–4580, 2005.

[14] T. Kai and S. Furusaki, “Behavior of fluidized beds of small particles at elevated temperatures,” *J. Chem. Eng. Japan*, vol. 18, no. 2, pp. 113–118, 1985.

[15] B. Formisani, R. Girimonte, and L. Mancuso, “Analysis of the fluidization process of particle beds at high temperature,” *Chem. Eng. Sci.*, vol. 53, no. 5, pp. 951–961, Feb. 1998.

[16] W.-C. Yang, *Handbook of fluidization and fluid-particle systems*. 2003.

[17] J. Shabanian and J. Chaouki, “Pressure Signals in a Gas-Solid Fluidized Bed With Thermally Induced Inter-Particle Forces,” in *The 14th International Conference on Fluidization – From Fundamentals to Products*, 2013, vol. 259, pp. 135–152.

[18] A. Megaritis, R. C. Messenb??ck, I. N. Chatzakis, D. R. Dugwell, and R. Kandiyoti, “High-pressure pyrolysis and CO2-gasification of coal maceral concentrates: conversions and char combustion reactivities,” *Fuel*, vol. 78, no. 8, pp. 871–882, 1999.

[19] S. Porada, “The influence of elevated pressure on the kinetics of evolution of selected gaseous products during coal pyrolysis,” *Fuel*, vol. 83, no. 7–8, pp. 1071–1078, May 2004.

[20] L. A. C. Tarelho, D. S. F. Neves, and M. A. A. Matos, “Forest biomass waste combustion in a pilot-scale bubbling fluidised bed combustor,” *Biomass and Bioenergy*, vol. 35, no. 4, pp. 1511–1523, Apr. 2011.

[21] Z. Dong, M. Clark, T. Gunderson, W. C. Hecker, and T. H. Fletcher, “Swelling properties and intrinsic reactivities of coal chars produced at elevated pressures and high heating rates,”

Proc. Combust. Inst., vol. 30 II, no. 2, pp. 2213–2221, Jan. 2005.

[22] J. a. Laverman, I. Roghair, M. van Sint Annaland, and J. a. M. Kuipers, "Investigation into the hydrodynamics of gas–solid fluidized beds using particle image velocimetry coupled with digital image analysis," *Can. J. Chem. Eng.*, vol. 86, no. 3, pp. 523–535, Jun. 2008.

[23] P. E. R. Michl, "Method for fluidized bed polymerization." Google Patents, 1986.

[24] T. Xie, K. B. McAuley, J. C. C. Hsu, and D. W. Bacon, "Gas Phase Ethylene Polymerization: Production Processes, Polymer Properties, and Reactor Modeling," *Ind. Eng. Chem. Res.*, vol. 33, no. 3, pp. 449–479, 1994.

[25] G. Bruni, P. Lettieri, T. Elson, J. Yates, and D. Newton, "The effect of process conditions on the fluidization of gas fluidized beds," 2004.

[26] J. Shabanian and J. Chaouki, "Effects of Temperature, Pressure, and Interparticle Forces on the Hydrodynamics of a Gas-Solid Fluidized Bed," *Chem. Eng. J.*, vol. 313, pp. 580–590, 2016.

[27] T. M. Knowlton, "Pressure and temperature effects in fluid-particle systems," in *Pressure and temperature effects in fluid-particle systems*, 1992, pp. 27–46.

[28] S. Y. Wu and J. Baeyens, "Effect of operating temperature on minimum fluidization velocity," *Powder Technol.*, vol. 67, no. 2, pp. 217–220, Aug. 1991.

[29] Y. Zhou *et al.*, "Effects of interparticle forces on fluidization characteristics in liquid-containing and high-temperature fluidized beds," *Ind. Eng. Chem. Res.*, vol. 52, no. 47, pp. 16666–16674, Nov. 2013.

[30] P. Lettieri, J. G. Yates, and D. Newton, "The influence of interparticle forces on the fluidization behaviour of some industrial materials at high temperature," *Powder Technol.*, vol. 110, no. 1–2, pp. 117–127, 2000.

[31] J. M. Valverde, a Castellanos, P. Mills, and M. a S. Quintanilla, "Effect of particle size and interparticle force on the fluidization behavior of gas-fluidized beds.," *Phys. Rev. E. Stat. Nonlin. Soft Matter Phys.*, vol. 67, no. 5 Pt 1, p. 51305, 2003.

[32] Jaber Shabanian, “Hydrodynamics of a Gas-Solid Fluidized Bed At High Temperature in the Presence of Interparticle Forces,” École Polytechnique de Montreal, 2015.

[33] J. P. K. Seville, C. D. Willett, and P. C. Knight, “Interparticle forces in fluidisation: A review,” *Powder Technol.*, vol. 113, no. 3, pp. 261–268, 2000.

[34] W.-K. Lee, G. Jovanovic, and H. T. Kim, “The effect of interparticle forces on fluidization regimes in the magnetized fluidized beds,” *Korean J. Chem. Eng.*, vol. 16, no. 3, pp. 362–370, 1999.

[35] G. Bruni, P. Lettieri, D. Newton, and D. Barletta, “An investigation of the effect of the interparticle forces on the fluidization behaviour of fine powders linked with rheological studies,” *Chem. Eng. Sci.*, vol. 62, no. 1–2, pp. 387–396, Jan. 2007.

[36] J. Shabanian and J. Chaouki, “Hydrodynamics of a gas–solid fluidized bed with thermally induced interparticle forces,” *Chem. Eng. J.*, vol. 259, pp. 135–152, Jan. 2015.

[37] F. Alamolhoda, A. Shamiri, M. A. Hussain, R. Sotudeh-Gharebagh, and N. Mostoufi, “Early detection of agglomeration in a polyethylene fluidized bed at high temperature and pressure by vibration signature analysis,” *Chem. Eng. Res. Des.*, vol. 104, pp. 156–163, Dec. 2015.

[38] D. Song, F. Salama, J. Matta, and P. Mehrani, “Implementation of Faraday cup electrostatic charge measurement technique in high-pressure gas-solid fluidized beds at pilot-scale,” *Powder Technol.*, vol. 290, pp. 21–26, Jun. 2016.

[39] G. C. Brouwer, E. C. Wagner, J. R. van Ommen, and R. F. Mudde, “Effects of pressure and fines content on bubble diameter in a fluidized bed studied using fast X-ray tomography,” *Chem. Eng. J.*, vol. 207–208, pp. 711–717, 2012.

[40] D. Escudero and T. J. Heindel, “Bed height and material density effects on fluidized bed hydrodynamics,” *Chem. Eng. Sci.*, vol. 66, no. 16, pp. 3648–3655, Aug. 2011.

[41] O. Gundogdu, P. M. Jenneson, and U. Tuzun, “Nano particle fluidisation in model 2-D and 3-D beds using high speed X-ray imaging and microtomography,” *J. Nanoparticle Res.*, vol. 9, no. 2, pp. 215–223, 2007.

[42] S. Sanaei, N. Mostoufi, R. Radmanesh, R. Sotudeh-Gharebagh, C. Guy, and J. Chaouki, "Hydrodynamic characteristics of gas-solid fluidization at high temperature," *Can. J. Chem. Eng.*, vol. 88, no. 1, pp. 1–11, Feb. 2010.

[43] F. Fotovat, "Characterization of hydrodynamics and solids mixing in fluidized beds involving biomass, Ph.D. thesis," UNIVERSITÉ DE MONTRÉAL, 2014.

[44] J. Shabanian and J. Chaouki, "Local characterization of a gas-solid fluidized bed in the presence of thermally induced interparticle forces," *Chem. Eng. Sci.*, vol. 119, pp. 261–273, 2014.

[45] R. Radmanesh, R. Mabrouk, J. Chaouki, and C. Guy, "Effect of Temperature on Solids Mixing in a Bubbling Fluidized Bed Reactor," *Int. J. Chem. React. Eng.*, vol. 3, no. 1, pp. 1–16, Jan. 2005.

[46] J. Werther, "Measurement techniques in fluidized beds," *Powder Technol.*, vol. 102, no. 1, pp. 15–36, 1999.

[47] D. Geldart, "Types of gas fluidization," *Powder Technol.*, vol. 7, no. 5, pp. 285–292, 1973.

[48] J. Schweinzer and O. Molerus, "Bubble flow in pressurized gas/solid fluidized beds," *Chem. Eng. Technol. - CET*, vol. 10, no. 1, pp. 368–375, 1987.

[49] J. Li *et al.*, "Minimum and terminal velocity in fluidization of coal gasification materials and coal blending of gasification under pressure," *Fuel*, vol. 110, pp. 153–161, 2013.

[50] J. G. Yates and P. Lettieri, *Fluidized-Bed Reactors: Processes and Operating Conditions*, vol. 26. Cham: Springer International Publishing, 2016.

[51] L. G. Gibilaro and L. G. Gibilaro, "3 – Fluid flow through particle beds," in *Fluidization Dynamics*, 2001, pp. 14–30.

[52] L.-S. Fan and C. Zhu, *Principles of gas-solid flows*. Cambridge University Press, 2005.

[53] M. Rüdisüli, T. J. Schildhauer, S. M. A. Biollaz, and J. R. Van Ommen, "Scale-up of bubbling fluidized bed reactors - A review," *Powder Technol.*, vol. 217, pp. 21–38, 2012.

[54] G. H. Qian, I. Bágyi, I. W. Burdick, R. Pfeffer, H. Shaw, and J. G. Stevens, “Gas-solid fluidization in a centrifugal field,” *AIChE J.*, vol. 47, no. 5, pp. 1022–1034, May 2001.

[55] R. B. Bird, W. E. Stewart, and E. N. Lightfoot, *Transport Phenomena*, vol. 55. John Wiley & Sons, 2002.

[56] F. London and F. London, “The general theory of molecular forces,” *Trans. Faraday Soc.*, vol. 33, no. 0, p. 8, 1937.

[57] H. Krupp, “Particle adhesion theory and experiment,” *Adv. Colloid Interface Sci.*, vol. 1, no. 2, pp. 111–239, May 1967.

[58] L. Massimilla and G. Donsì, “Cohesive forces between particles of fluid-bed catalysts,” *Powder Technol.*, vol. 15, no. 2, pp. 253–260, 1976.

[59] S. Sánchez-Delgado, J. A. Almendros-Ibáñez, N. García-Hernando, and D. Santana, “On the minimum fluidization velocity in 2D fluidized beds,” *Powder Technol.*, vol. 207, no. 1–3, pp. 145–153, 2011.

[60] J. Visser, “Van der Waals and other cohesive forces affecting powder fluidization,” *Powder Technol.*, vol. 58, no. 1, pp. 1–10, May 1989.

[61] A. B. Yu, C. L. Feng, R. P. Zou, and R. Y. Yang, “On the relationship between porosity and interparticle forces,” *Powder Technol.*, vol. 130, no. 1–3, pp. 70–76, 2003.

[62] D. Turki and N. Fatah, “Behavior and fluidization of the cohesive powders: Agglomerates sizes approach,” *Brazilian J. Chem. Eng.*, vol. 25, no. 4, pp. 697–711, 2008.

[63] N. Fatah, “Study and comparison of micronic and nanometric powders: Analysis of physical, flow and interparticle properties of powders,” *Powder Technol.*, vol. 190, no. 1–2, pp. 41–47, Mar. 2009.

[64] L. F. Hakim, J. H. Blackson, and A. W. Weimer, “Modification of interparticle forces for nanoparticles using atomic layer deposition,” *Chem. Eng. Sci.*, vol. 62, no. 22, pp. 6199–6211, 2007.

[65] J. Schwedes, “Review on testers for measuring flow properties of bulk solids,” *Granul.*

Matter, vol. 5, no. 1, pp. 1–43, May 2003.

[66] M.-J. Colbert, M. Grandbois, and N. Abatzoglou, “Identification of inter-particular forces by atomic force microscopy and how they relate to powder rheological properties measured in shearing tests,” *Powder Technol.*, vol. 284, pp. 396–402, Nov. 2015.

[67] G. Bruni, D. Barletta, M. Poletto, and P. Lettieri, “A rheological model for the flowability of aerated fine powders,” *Chem. Eng. Sci.*, vol. 62, no. 1–2, pp. 397–407, Jan. 2007.

[68] G. Bruni, A. Colafigli, P. Lettieri, and T. Elson, “Torque Measurements in Aerated Powders Using a Mechanically Stirred Fluidized Bed Rheometer (msFBR),” *Chem. Eng. Res. Des.*, vol. 83, no. 11, pp. 1311–1318, Nov. 2005.

[69] G. I. Tardos, M. I. Khan, and D. G. Schaeffer, “Forces on a slowly rotating, rough cylinder in a Couette device containing a dry, frictional powder,” *Phys. Fluids*, vol. 10, no. 2, p. 335, 1998.

[70] Q. Li, V. Rudolph, B. Weigl, and A. Earl, “Interparticle van der Waals force in powder flowability and compactibility,” *Int. J. Pharm.*, vol. 280, no. 1–2, pp. 77–93, 2004.

[71] M. Rasteh, F. Farhadi, and A. Bahramian, “Hydrodynamic characteristics of gas-solid tapered fluidized beds: Experimental studies and empirical models,” *Powder Technol.*, vol. 283, pp. 355–367, 2015.

[72] O. Molerus, “Interpretation of Geldart’s type A, B, C and D powders by taking into account interparticle cohesion forces,” *Powder Technol.*, vol. 33, no. 1, pp. 81–87, Sep. 1982.

[73] J. S. M. Botterill, Y. Teoman, and K. R. Yuregir, “The Effect of Temperature on Fluidized Bed Behaviour,” *Chem. Eng. Commun.*, vol. 15, no. 1–4, pp. 227–238, Apr. 1982.

[74] J. S. M. Botterill, Y. Teoman, and K. R. Yüregir, “The effect of operating temperature on the velocity of minimum fluidization, bed voidage and general behaviour,” *Powder Technol.*, vol. 31, no. 1, pp. 101–110, Jan. 1982.

[75] R. R. R. R. Pattipati, C. Y. Y. Wen, and C. Y. W. R. R. Pattipati, “Minimum fluidization velocity at high temperatures,” *Ind. Eng. Chem. Process Des. Dev.*, vol. 20, no. 4, pp. 705–

707, Oct. 1981.

[76] M. F. Llop, F. Madrid, J. Arnaldos, and J. Casal, “Fluidization at vacuum conditions. A generalized equation for the prediction of minimum fluidization velocity,” *Chem. Eng. Sci.*, vol. 51, no. 23, pp. 5149–5157, 1996.

[77] Z. LIU, T. KAWAGUCHI, T. TANAKA, and Y. TSUJI, “The Effect of Temperature on the Minimum Fluidization Velocity Calculated by Distinct Element Method.,” *JSME Int. J. Ser. B*, vol. 45, no. 1, pp. 66–71, 2002.

[78] D. Geldart and R. R. Cranfield, “The gas fluidisation of large particles,” *Chem. Eng. J.*, vol. 3, pp. 211–231, 1972.

[79] M. Nakamura, Y. Hamada, S. Toyama, A. E. Fouda, and C. E. Capes, “An experimental investigation of minimum fluidization velocity at elevated temperatures and pressures,” *Can. J. Chem. Eng.*, vol. 63, no. 1, pp. 8–13, Feb. 1985.

[80] M. F. Llop, J. Casal, and J. Arnaldos, “Incipient fluidization and expansion in fluidized beds operated at high pressure and temperature,” in *Proceedings of the 8th International Conference on Fluidization*, 1995, pp. 131–138.

[81] K. Svoboda, J. Cermak, M. Hartman, J. Drahos, and K. Selucky, “Pressure fluctuations in gas-fluidized beds at elevated temperatures,” *Ind. Eng. Chem. Process Des. Dev*, vol. 22, no. 3, pp. 514–520, 1983.

[82] M. Hartman and K. Svoboda, “Predicting the effect of operating temperature on the minimum fluidization velocity,” *Ind. Eng. Chem. Process Des. Dev.*, vol. 25, pp. 649–654, 1986.

[83] T. Mii, K. Yoshida, and D. Kunii, “Temperature-Effects on the Characteristics of Fluidized Beds,” *J. Chem. Eng. Japan*, vol. 6, no. 1, pp. 100–102, 1973.

[84] R. Clift and J. R. Grace, “The mechanism of bubble break-up in fluidised beds,” *Chem. Eng. Sci.*, vol. 27, no. 12, pp. 2309–2310, Dec. 1972.

[85] J. Shabanian and J. Chaouki, “Fluidization characteristics of a bubbling gas-solid fluidized

bed at high temperature in the presence of interparticle forces," *Chem. Eng. J.*, vol. 288, pp. 344–358, 2016.

[86] M. F. Llop, J. Casal, and J. Arnaldos, "Expansion of gas-solid fluidized beds at pressure and high temperature," *Powder Technol.*, vol. 107, no. 3, pp. 212–225, 2000.

[87] J.-H. Choi, S. D. Kim, and J. R. Grace, "Entrainment Rate of Coarse Particles at Different Temperatures in Gas Fluidized Beds," *Can. J. Chem. Eng.*, vol. 85, no. April, pp. 151–157, 2007.

[88] J. H. Choi, J. E. Son, and S. D. Kim, "Solid Entrainment in Fluidized Bed Combustors," *J. Chem. Eng. JAPAN*, vol. 22, no. 6, pp. 597–606, 1989.

[89] S. Boggs, D. H. Damon, J. Hjerrild, J. T. Holboll, and M. Henriksen, "Effect of insulation properties on the field grading of solid dielectric DC cable," *IEEE Trans. Power Deliv.*, vol. 16, no. 4, pp. 456–461, 2001.

[90] N. S. Saxena, "Temperature and composition dependence of electrical conductivity of Se 90 In 10-x Sb x (x = 0 , 2 ," vol. 1, no. 1, pp. 43–52, 2009.

[91] W. O. Moughrabiah, J. R. Grace, and X. T. Bi, "Effects of pressure, temperature, and gas velocity on electrostatics in gas-solid fluidized beds," *Ind. Eng. Chem. Res.*, vol. 48, no. 1, pp. 320–325, 2009.

[92] T. A. Alsmari, J. R. Grace, and X. T. Bi, "Effects of superficial gas velocity and temperature on entrainment and electrostatics in gas-solid fluidized beds," *Chem. Eng. Sci.*, vol. 123, pp. 49–56, 2015.

[93] J. M. Valverde Millán, *Fluidization of Fine Powders*, vol. 18. Dordrecht: Springer Netherlands, 2013.

[94] J. H. Siegell, "High-temperature de fluidization," *Powder Technol.*, vol. 38, no. 1, pp. 13–22, Mar. 1984.

[95] P. Pagliai, S. J. R. Simons, and D. Rhodes, "A novel experimental study of temperature enhanced cohesive interparticle forces," *Powder Technol.*, vol. 174, no. 1–2, pp. 71–74,

2007.

[96] B. Formisani, R. Girimonte, and G. Pataro, “The influence of operating temperature on the dense phase properties of bubbling fluidized beds of solids,” *Powder Technol.*, vol. 125, no. 1, pp. 28–38, 2002.

[97] S. Rapagna, P. U. U. Foscolo, and L. G. G. Gibilaro, “The influence of temperature on the quality of gas fluidization,” *Int. J. Multiph. Flow*, vol. 20, no. 2, pp. 305–313, 1994.

[98] M. . Rhodes, X. . Wang, A. . Forsyth, K. . Gan, and S. Phadtajaphan, “Use of a magnetic fluidized bed in studying Geldart Group B to A transition,” *Chem. Eng. Sci.*, vol. 56, no. 18, pp. 5429–5436, 2001.

[99] K. Rietema, “Particle and Powder Characteristics,” in *The Dynamics of Fine Powders*, K. Rietema, Ed. Dordrecht: Springer Netherlands, 1991, pp. 19–38.

[100] M. J. Espin, J. M. VAlverde, M. A. S. Quintanilla, and A. Castellanos, “Stabilization of gas-fluidized beds of magnetic powders by a cross-flow magnetic field,” *J. Fluid Mech.*, vol. 680, pp. 80–113, Aug. 2011.

[101] P. Lettieri, D. Newton, and J. . G. Yates, “High temperature effects on the dense phase properties of gas fluidized beds,” *Powder Technol.*, vol. 120, no. 1–2, pp. 34–40, 2001.

[102] H.-Y. Y. Xie and D. Geldart, “Fluidization of FCC powders in the bubble-free regime: effect of types of gases and temperature,” *Powder Technol.*, vol. 82, no. 3, pp. 269–277, 1995.

[103] L. Massimilla, G. Donsì, and C. Zucchini, “The structure of bubble-free gas fluidized beds of fine fluid cracking catalyst particles,” *Chem. Eng. Sci.*, vol. 27, no. 11, pp. 2005–2015, 1972.

[104] J. A. A. Agbim, A. W. W. Nienow, and P. N. N. Rowe, “Inter-particle forces that suppress bubbling in gas fluidised beds,” *Chem. Eng. Sci.*, vol. 26, no. 8, pp. 1293–1294, Aug. 1971.

[105] J. P. K. Seville and R. Clift, “The effect of thin liquid layers on fluidisation characteristics,” *Powder Technol.*, vol. 37, no. 1, pp. 117–129, Jan. 1984.

[106] W. Y. Wu, A. Navada, and S. C. Saxena, “Hydrodynamic characteristics of a magnetically

stabilized air fluidized bed of an admixture of magnetic and non-magnetic particles," *Powder Technol.*, vol. 90, no. 1, pp. 39–46, 1997.

[107] L. J. McLaughlin and M. J. Rhodes, "Prediction of fluidized bed behaviour in the presence of liquid bridges," *Powder Technol.*, vol. 114, no. 1, pp. 213–223, 2001.

[108] K. Hilligardt and J. Werther, "Influence of temperature and properties of solids on the size and growth of bubbles in gas fluidized beds," *Chem. Eng. Technol. - CET*, vol. 10, no. 1, pp. 272–280, 1987.

[109] R. Girimonte and B. Formisani, "The minimum bubbling velocity of fluidized beds operating at high temperature," *Powder Technol.*, vol. 189, no. 1, pp. 74–81, 2009.

[110] G. Raso, M. D. Amore, and P. G. Lignola, "The influence of temperature on the properties phase at incipient fluidization of the particulate," vol. 72, pp. 71–76, 1992.

[111] R. Yamazaki, N. Ueda, and G. Jimbo, "Mechanism of Incipient in Bed At Elevated Temperature," pp. 251–257, 1986.

[112] R. Yamazaki, N.-S. S. Han, Z. F. Sun, and G. Jimbo, "Effect of chemisorbed water on bed voidage of high temperature fluidized bed," *Powder Technol.*, vol. 84, no. 1, pp. 15–22, Jul. 1995.

[113] G. H. Hong, R. Yamazaki, T. Takahashi, and G. Jimbo, "Minimum Fluidization Velocity in a Fluidized Bed at High Temperatures," *KAGAKU KOGAKU RONBUNSHU*, vol. 6, no. 6, pp. 557–562, 1980.

[114] C. Xu and J.-X. Zhu, "Effects of gas type and temperature on fine particle fluidization," *China Particuology*, vol. 4, no. 3–4, pp. 114–121, 2006.

[115] G. Bruni, P. Lettieri, D. Newton, and J. Yates, "The influence of fines size distribution on the behaviour of gas fluidized beds at high temperature," *Powder Technol.*, vol. 163, no. 1–2, pp. 88–97, Apr. 2006.

[116] H. Cui and J. Chaouki, "Effects of temperature on local two-phase flow structure in bubbling and turbulent fluidized beds of FCC particles," *Chem. Eng. Sci.*, vol. 59, no. 16, pp. 3413–

3422, 2004.

[117] A. Chehbouni, J. Chaouki, C. Guy, and D. Klvana, “Effect of temperature on the hydrodynamics of turbulent fluidized beds,” in *Proceedings of the 8th International Conference on Fluidization, Engineering Foundation*, 1995, pp. 149–156.

[118] D. C. Chitester, R. M. Kornosky, L.-S. S. Fan, and J. P. Danko, “Characteristics of fluidization at high pressure,” *Chem. Eng. Sci.*, vol. 39, no. 2, pp. 253–261, 1984.

[119] C. Y. Wen and Y. H. Yu, “A generalized method for predicting the minimum fluidization velocity,” *AIChE J.*, vol. 12, no. 3, pp. 610–612, May 1966.

[120] L. E. L. Sobreiro and J. L. F. Monteiro, “The effect of pressure on fluidized bed behaviour,” *Powder Technol.*, vol. 33, no. 1, pp. 95–100, 1982.

[121] P. C. Carman, “Fluid flow through granular beds,” *Trans. Chem. Eng.*, vol. 15, pp. 150–166, 1937.

[122] J. Kozeny, *Über kapillare leitung des wassers im boden:(aufstieg, versickerung und anwendung auf die bewässerung)*. Hölder-Pichler-Tempsky, 1927.

[123] C. L. Lin, M. Y. Wey, and S. D. You, “The effect of particle size distribution on minimum fluidization velocity at high temperature,” *Powder Technol.*, vol. 126, no. 3, pp. 297–301, 2002.

[124] M. Jiliang, C. Xiaoping, and L. Daoyin, “Minimum fluidization velocity of particles with wide size distribution at high temperatures,” *Powder Technol.*, vol. 235, pp. 271–278, 2013.

[125] J. F. Davidson, “The two-phase theory of fluidization: successes and opportunities,” in *AIChE Symp. Ser*, 1991, vol. 87, no. 281, pp. 1–12.

[126] K. Svoboda and M. Hartman, “Influence of Temperature on Incipient Fluidization of Limestone , Coal Ash and Corrundum,” *Ind. Eng. Chem. Process Des. Dev.*, vol. 20, pp. 319–326, 1981.

[127] P. D. Carl L. Yaws, “Viscosity of Gas,” in *Chemical Properties Handbook*, McGraw Hill Professional, Access Engineering, 1999, p. 473.

[128] J. van der Schaaf, J. C. Schouten, F. Johnsson, and C. M. van den Bleek, “Non-intrusive determination of bubble and slug length scales in fluidized beds by decomposition of the power spectral density of pressure time series,” *Int. J. Multiph. Flow*, vol. 28, no. 5, pp. 865–880, 2002.

[129] N. P. Cheremisinoff, “Review of experimental methods for studying the hydrodynamics of gas-solid fluidized beds,” *Ind. Eng. Chem. Process Des. Dev.*, vol. 25, no. 2, pp. 329–351, 1986.

[130] F. Ghasemi, J. Ruud van Ommen, and M. Sahimi, “Analysis of pressure fluctuations in fluidized beds. I. Similarities with turbulent flow,” *Chem. Eng. Sci.*, vol. 66, no. 12, pp. 2627–2636, 2011.

[131] J. van der Schaaf, J. C. Schouten, and C. M. van den Bleek, “Origin, propagation and attenuation of pressure waves in gas—solid fluidized beds,” *Powder Technol.*, vol. 95, no. 3, pp. 220–233, Mar. 1998.

[132] H. T. T. Bi, J. R. R. Grace, and J. Zhu, “Propagation of pressure waves and forced oscillations in gas-solid fluidized beds and their influence on diagnostics of local hydrodynamics,” *Powder Technol.*, vol. 82, no. 3, pp. 239–253, Dec. 1995.

[133] R. C. Zijerveld, J. C. Schouten, and C. M. Van den Bleek, “Characterization of fluidization regimes by time-series analysis of pressure fluctuations,” *Int. J. Multiph. Flow*, vol. 26, no. 4, pp. 663–715, 2000.

[134] J. Yerushalmi and N. T. Cankurt, “Further studies of the regimes of fluidization,” *Powder Technol.*, vol. 24, no. 2, pp. 187–205, Nov. 1979.

[135] A. Chehbouni, J. Chaouki, C. Guy, and D. Klvana, “Characterization of the Flow Transition between Bubbling and Turbulent Fluidization,” *Ind. Eng. Chem. Res.*, vol. 33, no. 8, pp. 1889–1896, Aug. 1994.

[136] H. T. Bi, N. Ellis, I. A. Abba, and J. R. Grace, “A state-of-the-art review of gas-solid turbulent fluidization,” *Chem. Eng. Sci.*, vol. 55, no. 21, pp. 4789–4825, Nov. 2000.

[137] H. T. Bi and J. R. Grace, “Effect of measurement method on the velocities used to demarcate the onset of turbulent fluidization,” *Chem. Eng. J. Biochem. Eng. J.*, vol. 57, no. 3, pp. 261–271, 1995.

[138] T.-Y. Y. Yang and L. ping Leu, “Study of transition velocities from bubbling to turbulent fluidization by statistic and wavelet multi-resolution analysis on absolute pressure fluctuations,” *Chem. Eng. Sci.*, vol. 63, no. 7, pp. 1950–1970, 2008.

[139] H. B. JOHNSON and F. KESSLER, “Kaolinite Dehydroxylation Kinetics,” *J. Am. Ceram. Soc.*, vol. 52, no. 4, pp. 199–203, Apr. 1969.

[140] R. L. Frost, “The Dehydroxylation of the Kaolinite Clay Minerals using Infrared Emission Spectroscopy,” *Clays Clay Miner.*, vol. 44, no. 5, pp. 635–651, 1996.

[141] H. Masuda, K. Higashitani, and H. Yoshida, *Powder Technology Handbook, Third Edition*. CRC Press, 2006.

[142] Q. Huang, A. Mesbah-Nejad, S. M. Tadayyon, P. Norton, H. Zhang, and J. Zhu, “Measurement of inter-particle forces by an interfacial force microscope,” *Particuology*, vol. 8, no. 5, pp. 400–406, 2010.

[143] P. Taylor, A. C. Hoffmann, and J. G. Yates, “Experimental Observations of Fluidized Beds At Elevated Pressures Experimental Observations of Fluidized,” *Chem. Eng. Commun.*, vol. 41, no. April 2013, pp. 37–41, Apr. 2007.

[144] B. U. Kozanoglu, J. Welti Chanes, D. García Cuautle, and J. P. Santos Jean, “Hydrodynamics of large particle fluidization in reduced pressure operations: An experimental study,” *Powder Technol.*, vol. 125, no. 1, pp. 55–60, 2002.

[145] J.-I. ichi Kawabata *et al.*, “Characteristics of Gas-Fluidised Beds Under Pressure.,” *J. Chem. Eng. Japan*, vol. 14, no. 2, pp. 85–89, 1981.

[146] P. A. Olowson, “Influence of pressure and fluidization velocity on the hydrodynamics of a fluidized bed containing horizontal tubes,” *Chem. Eng. Sci.*, vol. 49, no. 15, pp. 2437–2446, Aug. 1994.

[147] P. A. Olowson and A. E. Almstedt, “Influence of pressure on the minimum fluidization velocity,” *Chem. Eng. Sci.*, vol. 46, no. 2, pp. 637–640, 1991.

[148] P. a. A. Olowson and A. E. E. Almstedt, “Influence of pressure and fluidization velocity on the bubble behaviour and gas flow distribution in a fluidized bed,” *Chem. Eng. Sci.*, vol. 45, no. 7, pp. 1733–1741, 1990.

[149] A. Marzocchella and P. Salatino, “Fluidization of solids with CO2 at pressures from ambient to supercritical,” *AIChE J.*, vol. 46, no. 5, pp. 901–910, May 2000.

[150] C. Vogt, R. Schreiber, G. Brunner, and J. Werther, “Fluid dynamics of the supercritical fluidized bed,” *Powder Technol.*, vol. 158, no. 1–3, pp. 102–114, Oct. 2005.

[151] I. Sidorenko, “Pressure Effects on Fluidized Bed Behaviour,” Monash University Australia, 2003.

[152] I. Sidorenko and M. J. Rhodes, “Influence of pressure on fluidization properties,” *Powder Technol.*, vol. 141, no. 1–2, pp. 137–154, 2004.

[153] A. Mathur, S. C. Saxena, and Z. F. Zhang, “Hydrodynamic characteristics of gas-fluidized beds over a broad temperature range,” *Powder Technol.*, vol. 47, no. 3, pp. 247–256, 1986.

[154] M. Poletto, P. Salatino, and L. Massimilla, “Fluidization of solids with CO2 at pressures and temperatures ranging from ambient to nearly critical conditions,” *Chem. Eng. Sci.*, vol. 48, no. 3, pp. 617–621, 1993.

[155] H. W. W. Piepers, E. J. E. J. E. Cottaar, A. H. M. H. M. Verkooijen, and K. Rietema, “Effects of pressure and type of gas on particle-particle interaction and the consequences for gas-solid fluidization behaviour,” *Powder Technol.*, vol. 37, no. 1, pp. 55–70, Jan. 1984.

[156] P. A. A. Olowson and A. E. E. Almstedt, “Hydrodynamics of a bubbling fluidized bed: influence of pressure and fluidization velocity in terms of drag force,” *Chem. Eng. Sci.*, vol. 47, no. 2, pp. 357–366, Feb. 1992.

[157] I. H. H. Chan, C. Sishtla, and T. M. M. Knowlton, “The effect of pressure on bubble parameters in gas-fluidized beds,” *Powder Technol.*, vol. 53, no. 3, pp. 217–235, Dec. 1987.

[158] S. E. Olsson, J. Wiman, and A. E. Almstedt, “Hydrodynamics of a pressurized fluidized bed with horizontal tubes: Influence of pressure, fluidization velocity and tube-bank geometry,” *Chem. Eng. Sci.*, vol. 50, no. 4, pp. 581–592, Feb. 1995.

[159] J. Wiman and A. E. Almstedt, “Hydrodynamics, erosion and heat transfer in a pressurized fluidized bed: Influence of pressure, fluidization velocity, particle size and tube bank geometry,” *Chem. Eng. Sci.*, vol. 52, no. 16, pp. 2677–2695, 1997.

[160] J. Wiman and A. E. Almstedt, “Influence of pressure, fluidization velocity and particle size on the hydrodynamics of a freely bubbling fluidized bed,” *Chem. Eng. Sci.*, vol. 53, no. 12, pp. 2167–2176, 1998.

[161] W. Godlieb, N. G. G. Deen, and J. a. M. A. M. Kuipers, “On the relationship between operating pressure and granular temperature: A discrete particle simulation study,” *Powder Technol.*, vol. 182, no. 2, pp. 250–256, 2008.

[162] Z. Mansourpour, S. Karimi, R. Zarghami, N. Mostoufi, and R. Sotudeh-Gharebagh, “Insights in hydrodynamics of bubbling fluidized beds at elevated pressure by DEM-CFD approach,” *Particuology*, vol. 8, no. 5, pp. 407–414, 2010.

[163] P. Cai, S. P. Chen, Y. Jin, Z. Q. Yu, and Z. W. Wang, “Effect of operating temperature and pressure on the transition from bubbling to turbulent fluidization,” *Journal of Chemical Industry and Engineering (China)*, vol. 5. pp. 122–132, 1990.

[164] J. G. Yates, “Effects of temperature and pressure on gas-solid fluidization,” *Chem. Eng. Sci.*, vol. 51, no. 2, pp. 167–205, Jan. 1996.

[165] D. F. King, F. R. G. Mitchell, and D. Harrison, “Dense phase viscosities of fluidised beds at elevated pressures,” *Powder Technol.*, vol. 28, no. 1, pp. 55–58, Jan. 1981.

[166] J. R. F. Guedes de Carvalho, D. F. King, and D. Harrison, “Fluidizayion of Fine PArticles Under Pressure,” in *Proceedings of the 2nd Engineering Foundation Conference on Fluidization*, 1978, pp. 59–64.

[167] E. Cottaar and K. Rietema, “A theoretical study on the influence of gas adsorption on

interparticle forces in powders," *J. Colloid Interface Sci.*, vol. 109, no. 1, pp. 249–260, 1986.

[168] K. Rietema and H. W. Piepers, "The effect of interparticle forces on the stability of gas-fluidized beds—I. Experimental evidence," *Chem. Eng. Sci.*, vol. 45, no. 6, pp. 1627–1639, 1990.

[169] A. W. Weimer and G. J. Quarderer, "On dense phase voidage and bubble size in high pressure fluidized beds of fine powders," *AIChE J.*, vol. 31, no. 6, pp. 1019–1028, 1985.

[170] K. V. Jacob and A. W. Weimer, "High-pressure particulate expansion and minimum bubbling of fine carbon powders," *AIChE J.*, vol. 33, no. 10, pp. 1698–1706, Oct. 1987.

[171] K. V. Jacob and A. W. Weimer, "Normal bubbling of fine carbon powders in high-pressure fluidized beds," *AIChE J.*, vol. 34, no. 8, pp. 1395–1397, Aug. 1988.

[172] G. F. Barreto, J. G. Yates, and P. N. Rowe, "The effect of pressure on the flow of gas in fluidized beds of fine particles," *Chem. Eng. Sci.*, vol. 38, no. 12, pp. 1935–1945, Jan. 1983.

[173] J. R. F. G. de Carvalho, "Dense phase expansion in fluidised beds of fine particles: The effect of pressure on bubble stability," *Chem. Eng. Sci.*, vol. 36, no. 2, pp. 413–416, 1981.

[174] P. N. Rowe, P. U. Foscolo, A. C. Hoffmann, and J. G. Yates, "Fine powders fluidised at low velocity at pressures up to 20 bar with gases of different viscosity," *Chem. Eng. Sci.*, vol. 37, no. 7, pp. 1115–1117, 1982.

[175] J. Li and J. A. M. Kuipers, "Effect of pressure on gas-solid flow behavior in dense gas-fluidized beds: A discrete particle simulation study," *Powder Technol.*, vol. 127, no. 2, pp. 173–184, 2002.

[176] A. C. Hoffmann and J. G. Yates, "Experimental Observations of Fluidized Beds at Elevated Pressures," *Chem. Eng. Commun.*, vol. 41, no. 1–6, pp. 133–149, Apr. 1986.

[177] R. Clift, J. R. Grace, and M. E. Weber, "Stability of Bubbles in Fluidized Beds," *Ind. Eng. Chem. Fundam.*, vol. 13, no. 1, pp. 45–51, 1974.

[178] N. Mostoufi and J. Chaouki, "On the Axial Movement of Solids in Gas-Solid Fluidized Beds," *Chem. Eng. Res. Des.*, vol. 78, no. 6, pp. 911–920, Sep. 2000.

[179] M. Tsukada, D. Nakanishi, and M. Horio, “The effect of pressure on the phase transition from bubbling to turbulent fluidization,” *Int. J. Multiph. Flow*, vol. 19, no. 1, pp. 27–34, Feb. 1993.

[180] “Marzocchella 1996.pdf.” .

[181] J. Arnaldos and J. Casal, “Prediction of transition velocities and hydrodynamical regimes in fluidized beds,” *Powder Technol.*, vol. 86, no. 3, pp. 285–298, 1996.

[182] Y. Jin, Z. Q. Yu, Z. Wang, and P. Cai, “A Criterion for Transition from Bubbling to Turbulent Fluidization,” in *Fluidization V*, 1986, pp. 289–296.

[183] A. Chehbouni, J. Chaouki, C. Guy, and E. D. Klvana, “Effets de differents parametres sur les vitesses de transition de la fluidisation en regime turbulent,” *Can. J. Chem. Eng.*, vol. 73, no. 1, pp. 41–50, Feb. 1995.

APPENDIX A – EFFECT OF PRESSURE ON THE HYDRODYNAMICS OF GAS-SOLID FLUIDIZED BEDS

1. With No/Negligible IPFs

As mentioned before by increasing the pressure the magnitude of the drag force exerted from the fluid on the solid particles increases due to an increase in the density of the gas in the case of particles larger than 200 μm. It is for this size of particles that the inertia effect is more dominant than the viscous effect of the flowing gas [49], [76], [79], [80], [118], [120], [143]–[153] and the minimum fluidization velocity (U_{mf}) decreases by pressure (Figure 0.1).

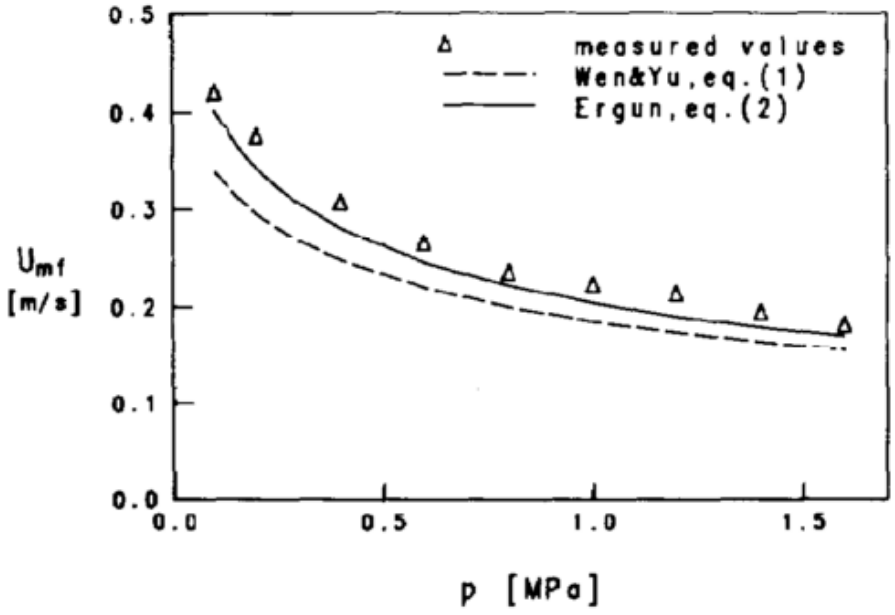

Figure 0.1: Variation of U_{mf} with pressure for 0.7 mm sand particles

It was also observed that by increasing the pressure to near critical conditions stability of the bed increased and a bubble-free regime was reached for Geldart group B particles [154]. The latter case occurred due to an increased level of Van der Waals IPFs coming from the adsorbed gas in the porousity of the particles [155]. However, instability of the bubbles has been observed in another work at high pressure due to an increase in bubble coalescence/break-up rate [156]. In general,

increasing the pressure helps the stability of the bed and provides a smoother fluidization thanks to smaller bubble size [39], [48], [81], [143], [148], [156]–[162].

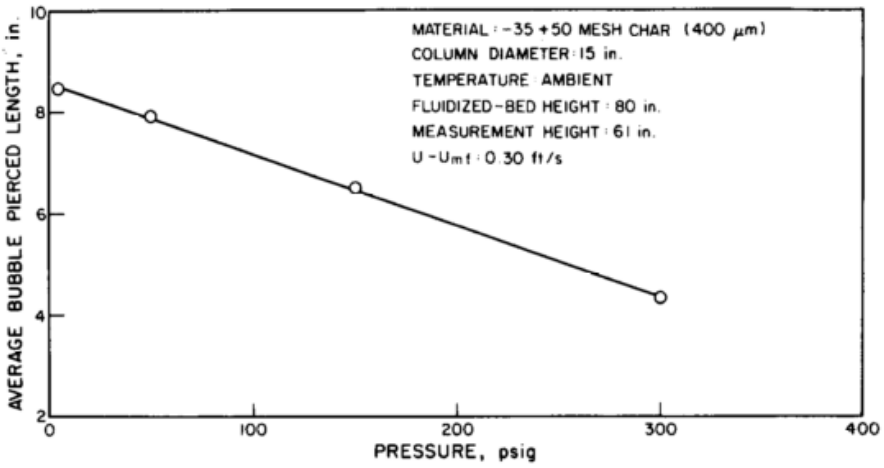

Figure 0.2: Variation of bubble size by pressure for 400 μm char particles fluidized by air [157].

This decrease in the bubble size can be explained using the mechanisms of bubble break-up in FB reactors. This phenomenon occurs by the formation of an indentation of particles on the roof of the bubble [84], [143]. Another mechanism implies that increasing the pressure increases the bubble rise velocity and decreases the terminal velocity of the particles results in an improved bubble break-up from the bottom of the bubble. The increasing effect of pressure on the bubble rise velocity has been reported along with non-uniform radial size distribution of the bubble size by Hoffmann et al. [143]. They showed the latter to be the main cause of formation of gross circulation in the bed working at high pressure.

As mentioned before, the magnitude of the drag force increases by pressure. This shifts the turbulent transition velocity (U_c) and the terminal velocity of the particles (U_t) to lower values which promote the level of entrainment and particle loss in high-pressure FBs [49], [118], [149], [163], [164].

A summary of the effects of pressure and temperature on U_{mf} and U_c is presented in Figure 0.3.

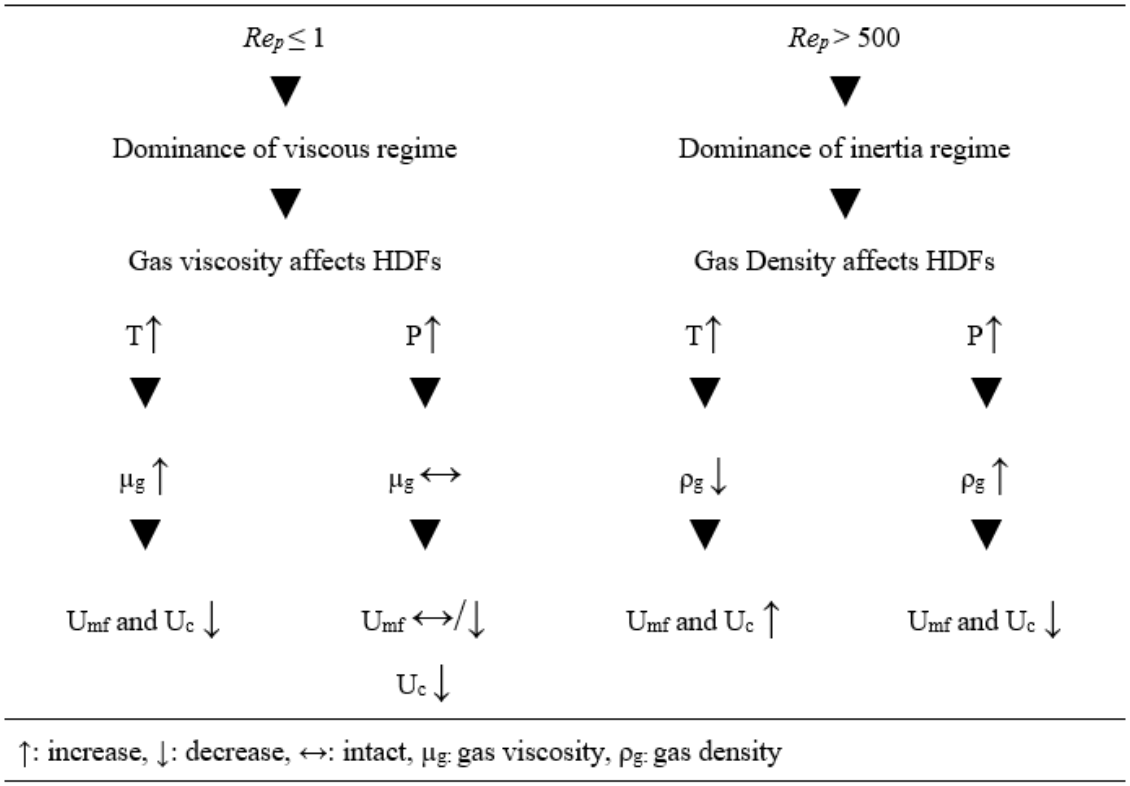

Figure 0.3: Summary of the effect of pressure and temperature on simple hydrodynamic parameters of fluidization in the absence of IPFs

With the Presence of IPFs

Fluidization of fine powders, i.e., Geldart group A particles, occurs at viscous flow regime. In this state, the magnitude of drag force exerted by the fluidizing gas on the particles depends only on the viscosity of the gas and since the viscosity does not change by pressure, drag force remains constant at different operating conditions [27]. As a result, U_{mf} and also ε_{mf} have been reported to be unaffected by pressure [118], [120], [152], [155], [165], [166]. On the other hand, increasing the pressure will expand the bubble-free fluidization region resulting in an increase in U_{mb} and ε_{mb}. This effect has been explained by an increase in the level of IPFs due to adsorption of the fluidizing gas into the pours on the surface of the particles by pressure which increases the elasticity modulus of the solid structure [155], [167], [168]. Another explanation that has been used to explain this effect is based on the change in the gas properties and the level of HDFs [169]–[171]. However,

both of these analogies should be considered at the same time to provide us with the capability of explaining the fluidization of fine powders at high pressure so that neglecting one of them will result in under/over estimation of hydrodynamic properties of such FB systems [149], [154], [170]. In general, for fine particles it has been found that increasing the pressure, makes the fluidization process smoother, i.e, lower bubble size and higher dense phase voidage and higher bed expansion [48], [155], [157], [165], [166], [172]–[175].

Also, according to the simple two phase flow, the excess gas after the fluidization state flows into the dense phase rather than bubbles at high pressure [156], [157], [165], [169], [174].

The change in the bubbling behavior at high pressure can be explained by the following theories: (i) at a bubble rise velocity more than the terminal velocity of the particles bubble breaks up through the insertion of particles into the wake of the bubble. For fine particles with low terminal velocity, this can happen at lower bubble rise velocity. So the stability of the bed becomes lower at high pressure [164], [176]. (ii) at high pressure, bubble roof becomes less stable due to a decrease in the kinematic viscosity of the dense phase which can be determined by the bed voidage. As pressure increase, the dense phase voidage also increases leading to an unstable bubble roof where bubble break up occurs [177].

The effect of pressure on U_c is based on the nature of solid movement in bubbling and turbulent regime. It is believed that particles at these regimes move as clusters rather than single particles. As a result, the increasing effect of pressure on the gas density leads to a decrease in the value of U_c [163], [178]–[180].

As a summary of the above-mentioned effects of pressure and temperature on the behavior of the bed, specifically the level of IPFs and HDFs, one can come to the conclusion that predicting the hydrodynamics of an FB system at extreme condition obliges us to consider both of these group of forces along each other at the same time. As a result, we can modify the available models and correlations in a way that can successfully predict the simple hydrodynamic parameters, such as U_{mf} and U_c. A summary of the effect of pressure and temperature on these parameters for a bed of fine particles is presented in Figure 0.4.

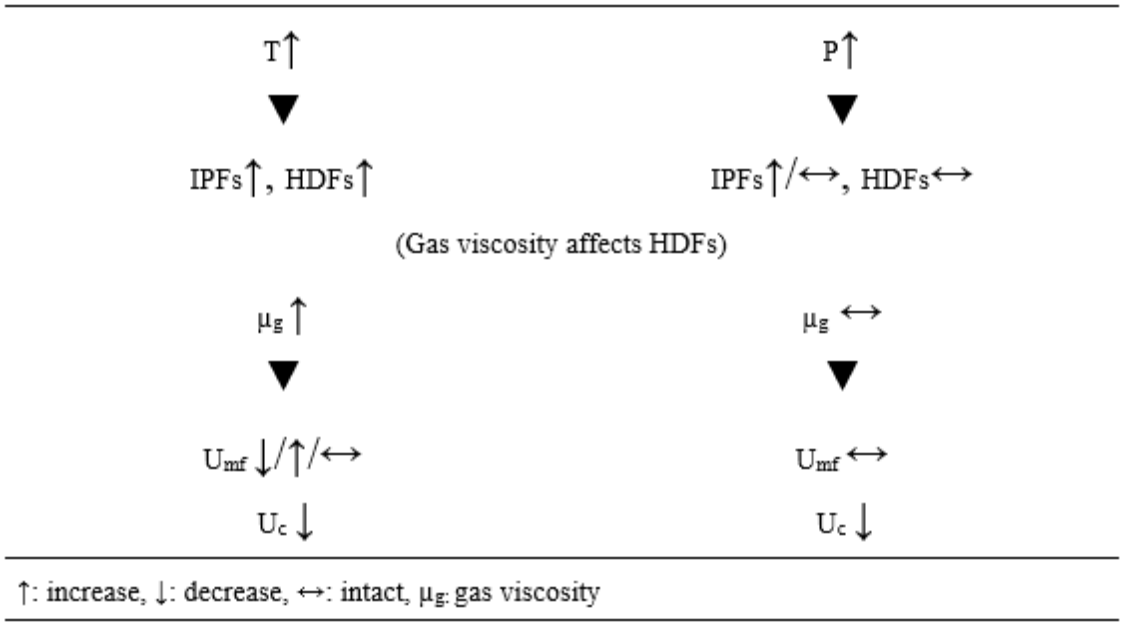

Figure 0.4: Summary of the effect of pressure and temperature on simple hydrodynamic parameters of fluidization in the presence of IPFs for fine particles.

APPENDIX B – CORRELATIONS FOR BUBBLING TO TURBULENT TRANSITION VELOCITY (U_C)

As mentioned before, pressure decreases the value of U_c while temperature can have an increasing or decreasing effect depending on the particle size in use, either by changing the drag force or by altering the bubbling behavior of the bed due to the change in HDFs. Most of the available correlations, including the ones that are presented in this section, are not considering the effect of the level of IPFs at extreme operating condition and fail to predict the hydrodynamic parameters precisely. Even at low temperature were the value of the ratio of IPFs/HDFs is negligible, they might not give a good prediction of the parameters of question. The precision of these correlation depends on many parameters such as operating conditions, setup dimensions and the properties of the fluidizing gas and solids. Below, can be found the correlation that has been used in this work to compare with our experimentally obtained U_c values.

Horio [181]**:**

$$Re_c = 0.936Ar^{0.427} \quad 54 < d_p < 2600\ \mu m \qquad (30)$$

Cai [163]**:** Cai et al. Proposed Equation (31) which is a modified version of the equation formerly proposed by Jin et al.[182] considering the effect of the diameter of the fluidized bed, D. Their correlation was tested for pressures in the range of 1 to 6 bar and different particle sizes. They have also reported an increase of U_c by temperature in the range of 50-450 ºC for Geldart group A, B, and D.

$$\frac{U_c}{(g d_p)^{0.5}} = \left[\frac{0.211}{D^{0.27}} + \frac{2.42\times10^{-3}}{D^{1.27}}\right]\left[\left(\frac{\rho_p - \rho_g}{\rho_g}\right)\frac{D}{d_p}\right]^{0.27} \qquad (31)$$

Chehbouni [183]**:** Chehbouni et al. claimed that they could predict the value of U_c with a goodness of fit of R^2=0.873 better than those of Horio (R^2=0.775) and Cai (R^2=0.703).

$$Fr_c = 0.463Ar^{0.145} \qquad 0.4 < Ar < 123316 \qquad (32)$$

$$50 < D < 200mm$$

A more elaborated list of correlations for U_c calculation is listed by Arnaldos and Casal [181].

APPENDIX C – U_C MEASUREMENT RESULTS

Before presenting any data, it should be kept in mind that the transition to the turbulent regime is affected directly by the bubbling behavior and the properties of the emulsion phase. By increasing the gas velocity at ambient condition in the bubbling fluidization regime, the increasing amount of gas going to the bubble phase creates larger bubbles. This phenomenon generally can be detected by a clear increase in the value of the standard deviation of pressure signals. This bubble growth continues to the point that the emulsion phase breaks up completely and there won't be any clear boundary between bubble and emulsion phase and the transition happens to the turbulent regime.

The Variation of the standard deviation of gauge pressure signals (STD_{gauge}) by the superficial gas velocity at different temperatures is presented in Figure 0.1 for FS226. At each temperature, this value increases in the bubbling fluidization regime because of the formation of larger bubbles. At the maximum value of (STD_{gauge}), which is defined as the transition velocity from bubbling to the turbulent regime (U_c), the emulsion phase breaks up completely due to the movement of large bubbles and STD_{gauge} starts to decrease upon increasing the superficial gas velocity. This phenomenon happens at different temperatures if IPFs are negligible.

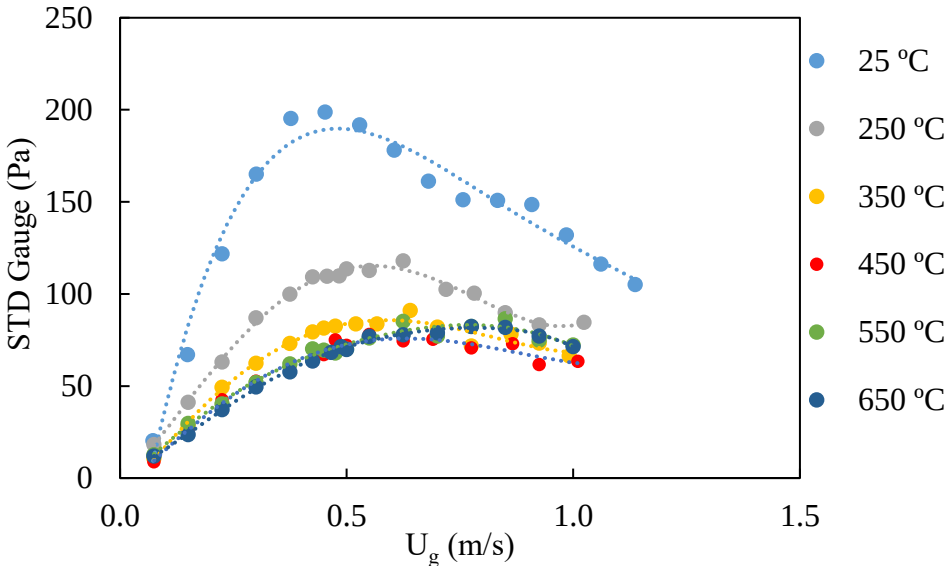

Figure 0.1: Variation of the standard deviation of gauge pressure signals by superficial gas velocity for FS226 fluidized by Air at different temperatures.

We can also see a decrease of STD_{gauge} by temperature in Figure 0.1. For FS226 and U_g values around U_c (high Reynolds number), gas density defines the level of drag force exerted on the fluidized particles. As the air density decreases by temperature, more gas should pass through the emulsion phase to keep the particles in a well-fluidized state [85]. Therefore, at a constant value of U_g, lower amount of gas passes through the bed in bubbles and the bubble size decreases. This decrease in the bubble size has been explained also by the easier formation of indentations of particles on the roof of the bubbles which leads t a higher rate of bubble break-up through this mechanism[85]. Also, a decreased level of drag force, more gas flow is needed to have a higher number of smaller bubbles to completely break up the emulsion phase. This increasing trend of U_c by temperature is presented in Figure 0.2.

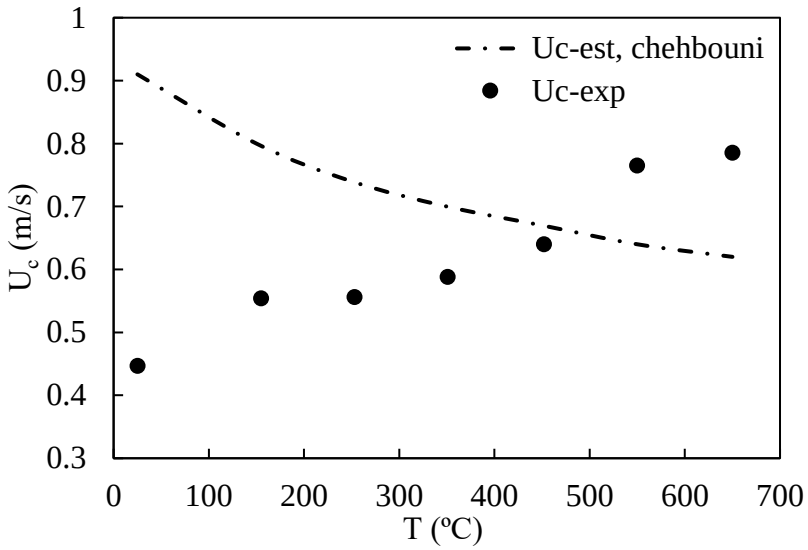

Figure 0.2: Variation of U_c by temperature for FS226 fluidized by Air compared to the predicted value by Chehbouni et al. [183].

To verify the effect of air density on the increasing trend of U_c we did the same experiment with larger particles, CS820, which are at the border of Geldart group B/D region. The Variation of STD_{gauge} by the superficial gas velocity at different temperatures is presented in Figure 0.3 for CS820. The same behaviour can be observed also for CS820 for which the effect of gas density is more pronounced. STD_{gauge} values at a certain superficial gas velocity decreased with temperature

and, the transition velocity is postponed to higher values. For CS820 it is interesting to mention that at 650 ºC, it is hard to distinguish the transition velocity due to the insufficient drag force compared to the weight of the particles. Also, the voidage of emulsion phase for coarse particles is inherently high compared to fine particles. Hence, the complete breakage of the emulsion phase does not change the situation considerably. As a consequence, it will be difficult to distinguish a deterministic transition point from bubbling to turbulent regime at high temperature for CS820. In this case, the bed is in a continuous bubbling regime until the system reaches to the transport regime [44], [85].

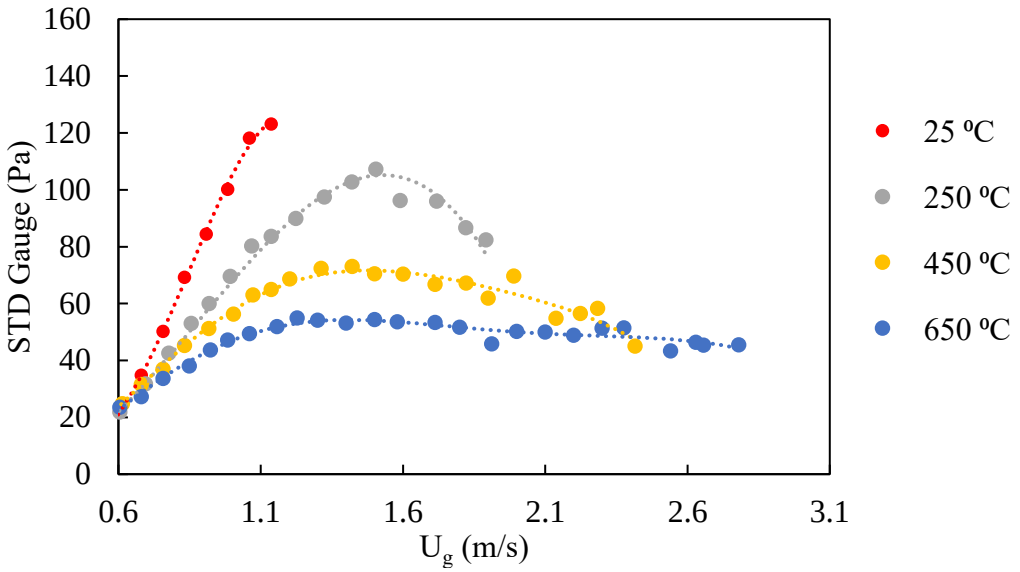

Figure 0.3: Variation of the standard deviation of gauge pressure signals by superficial gas velocity for CS820 fluidized by Air at different temperatures.

The Variation of STD_{gauge} by the superficial gas velocity at different temperatures is presented in Figure 0.4 for FCC86. For this size of the particle in the presented range of U_g gas viscosity defines the level of drag force exerted by the air on the FCC particles. As the gas viscosity increases by temperature, a higher level of drag force is applied to the particles. At a constant U_g, the terminal velocity of particles becomes lower than the bubble rise velocity which enhances the bubble break up through the bubble split from the bottom. As the gas viscosity is increased by temperature, even small bubbles have enough power to pass through the emulsion phase and make the transition to

the turbulent regime. This explains the decreasing trend of STD_{gauge} by temperatures in Figure 0.4. In general, it is expected that the transition from bubbling to turbulent regime occurs at a lower U_g at high temperature due to higher level of drag force exerted on the particles by the fluidizing agent and an increase in the bed voidage [116]. However, for FCC86, this was the case until we increased the temperature up to 350 °C as presented in Figure 0.5. A further increase in the temperature leads to an increase in U_c. This trend inversion can be explained by taking a closer look at the variation of STD_{gauge} by the temperature at high values of U_g presented in Figure 0.6.

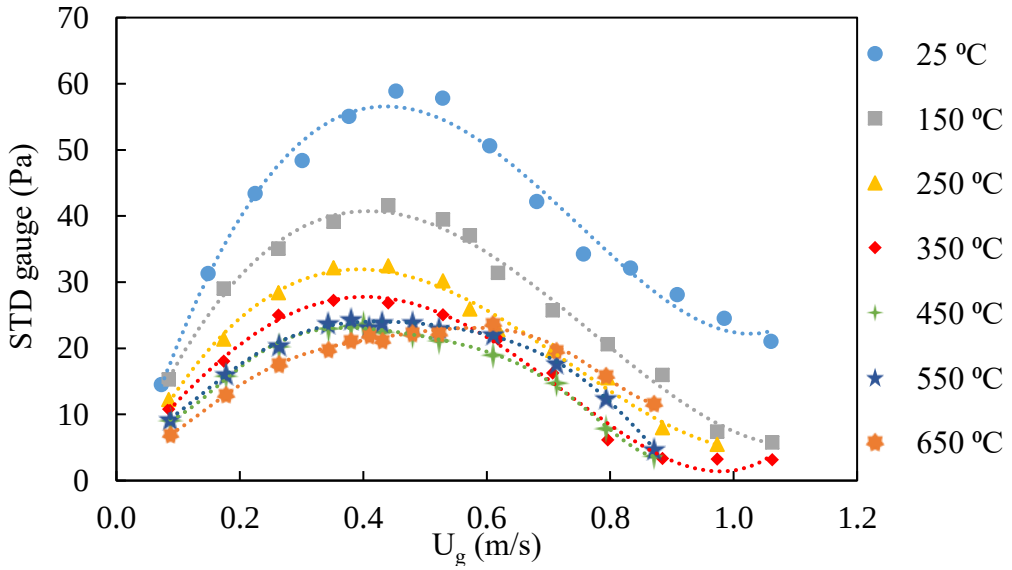

Figure 0.4: Variation of the standard deviation of gauge pressure signals by superficial gas velocity for FCC86 fluidized by Air at different temperatures.

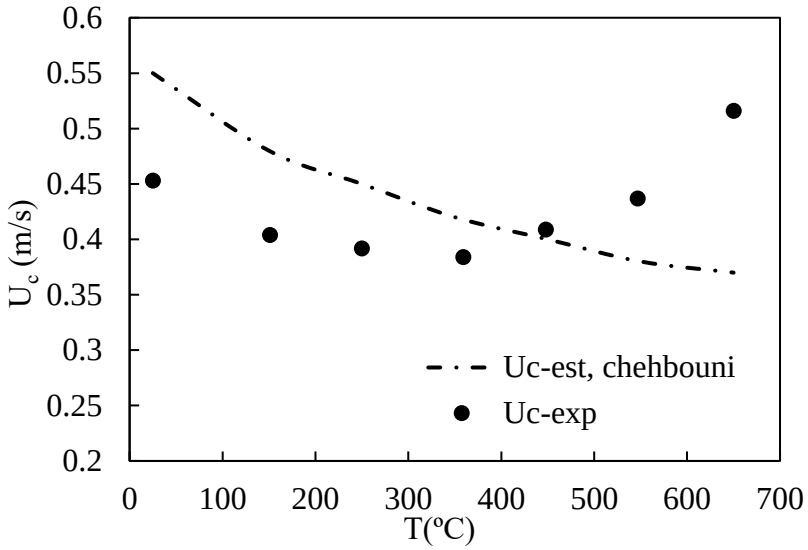

Figure 0.5: Variation of U_c by temperature for FCC86 fluidized by Air compared to its value estimated by Chehbouni et al. [183].

By increasing the temperature the value of STD_{gauge} did not drop after the maximum point as fast as it occurred at lower temperatures. This observation implies that the emulsion phase is resisting against the complete breakage by the bubbles. Also, bubble size is not changing significantly from 450 to 650 ºC from looking at the values of STD_{gauge} which confirms also the increased resistance of emulsion phase against the complete breakage. This increased resistance of the emulsion phase against breakage can be explained by the effect of IPFs on the fluidization characteristics of fine particles at high temperature. A higher level of IPFs increases the resistance of emulsion phase so there should be more flow of gas to compensate for the small bubbles [85].

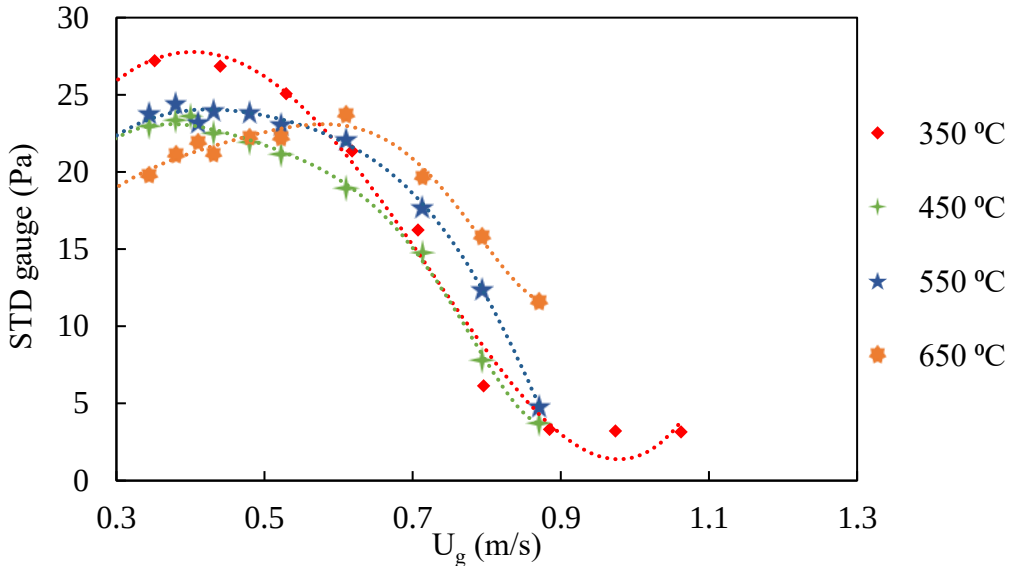

Figure 0.6: Variation of the standard deviation of gauge pressure signals by superficial gas velocity for FCC86 fluidized by Air at T > 350 ºC and $U_g > U_c$.

In the case of GB71 particles, also, there is a significant decrease in the bubble size at constant U_g when we increased the temperature from ambient to 150 ºC as can be observed from the increased value of STD_{gauge} in Figure 0.7. However, there is no significant change from 250 to 450 ºC due to the increased level of IPFs by temperature. Referring back to the Table 3.1 GB71 has the lowest melting point among the other powders deployed in this experiment. Similar to FCC86 an increased level of IPFs increases the resistance of the emulsion phase against rupture [44], [85]which is the reason for a constant U_c by temperature presented in Figure 0.8. However, it is not easy to find the maximum point for the graphs plotted at 250, 350 and 450 ºC in Figure 0.7. In another word, we could have adopted even higher values for U_c at these temperatures but here the incipient transition velocity has been chosen.

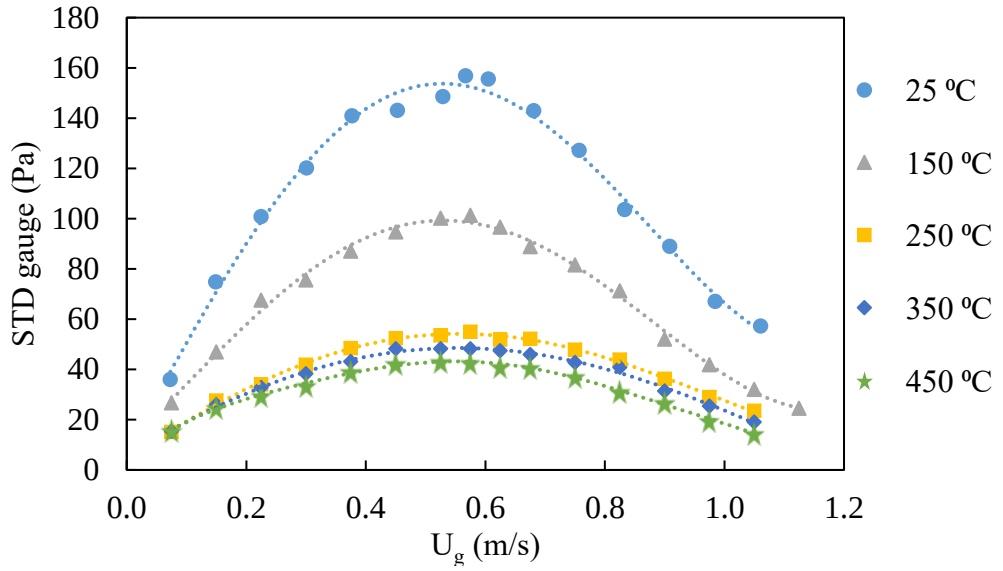

Figure 0.7: Variation of the standard deviation of gauge pressure signals by superficial gas velocity for GB71 fluidized by Air at different temperatures.

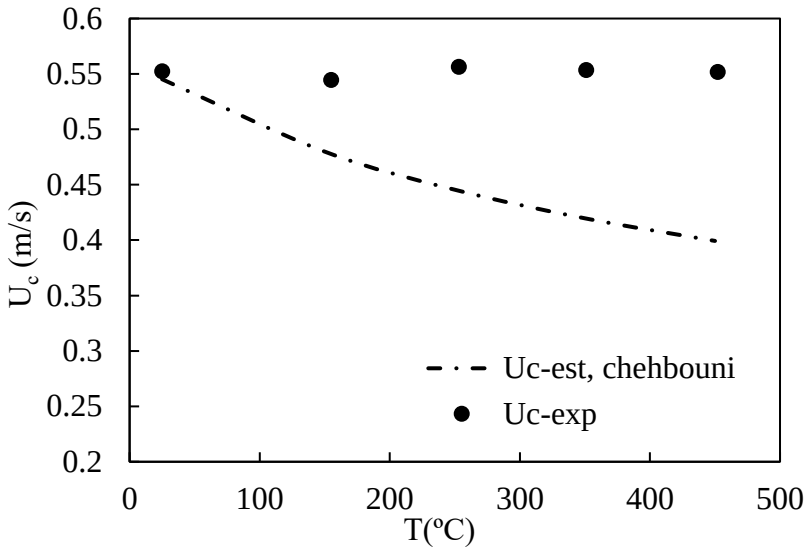

Figure 0.8: Variation of U_c by temperature for GB71 fluidized by Air compared to its value estimated by Chehbouni et al. [183].

Deploying argon as the fluidizing agent decreases the bubble size (lower values of STD_{gauge}) at all temperatures as presented in the case of FS226 in Figure 0.9. Argon has both higher viscosity and density compared to air resulting in smaller bubble size when compared at a constant gas velocity

with air which results in an increased level of drag force and U_c in all cases as presented in Figure 0.10.

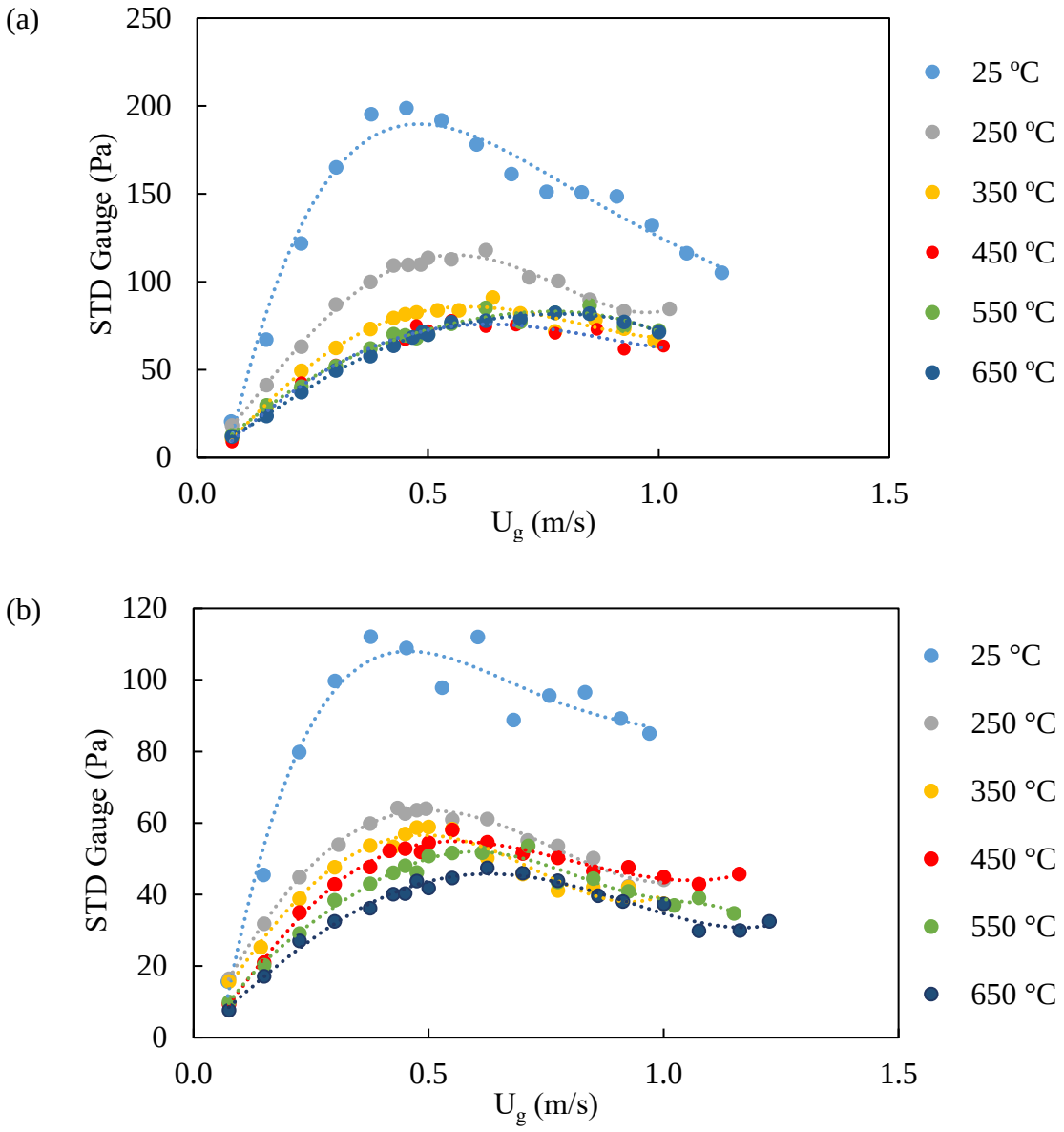

Figure 0.9 : Variation of the standard deviation of gauge pressure signals by superficial gas velocity for FS226 at different temperatures fluidized by: (a) air and (b) argon

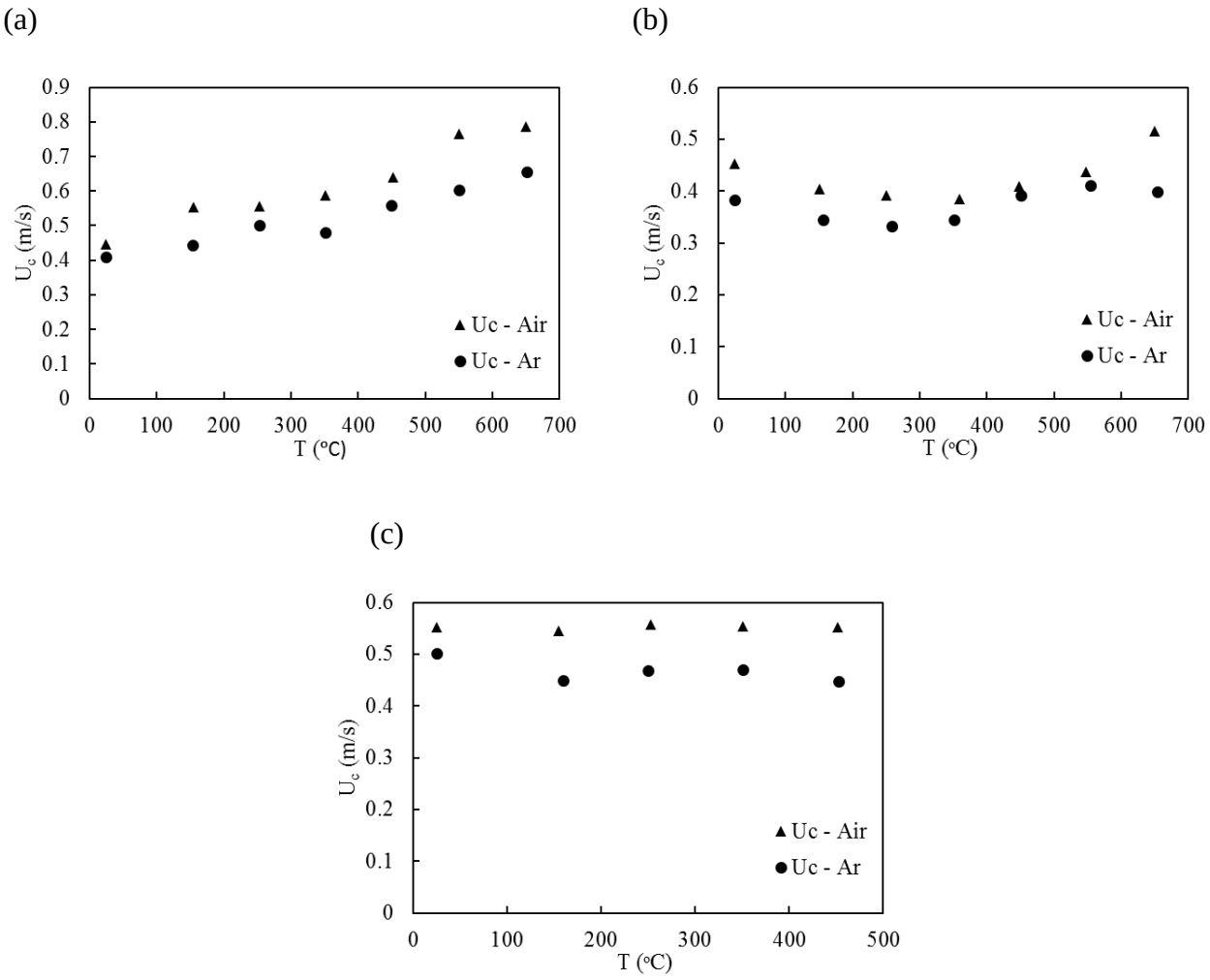

Figure 0.10: Variation of U_c of: (a) FS226 (b) FCC86 and (c) GB71 by temperature for fluidization with Air and Ar.

Up to now we have only compared our experimentally obtained U_c values with those predicted by Chebouni's correlation and there was no good agreement in any of the cases presented above, not even the trend was predicted well. To have a better insight of the capability of different correlation in this regard, the experimental data of FCC86 is compared with the correlations proposed by Chehbouni, Cai and Horio in Figure 0.11. According to Arnoldos et al. [181] these correlations

found to have a better prediction for the type of particles that we employed. Also the correlation proposed by Chehbouni is considering the diameter of the bed which can highly affect the value of U_c. As you can see the other correlations are incapable of predicting the experimental data similarly. This difference between the predicted and measured values at high temperature can be explained to be as a direct result of the impact of IPFs however, this is not the case at ambient temperature. Therefore, one should first develop a correlation based on the present experimental data to at least have good prediction at ambient/moderate temperatures and as an extension to the model, modify it with the consideration of the impact of IPFs on the fluidization of particles.

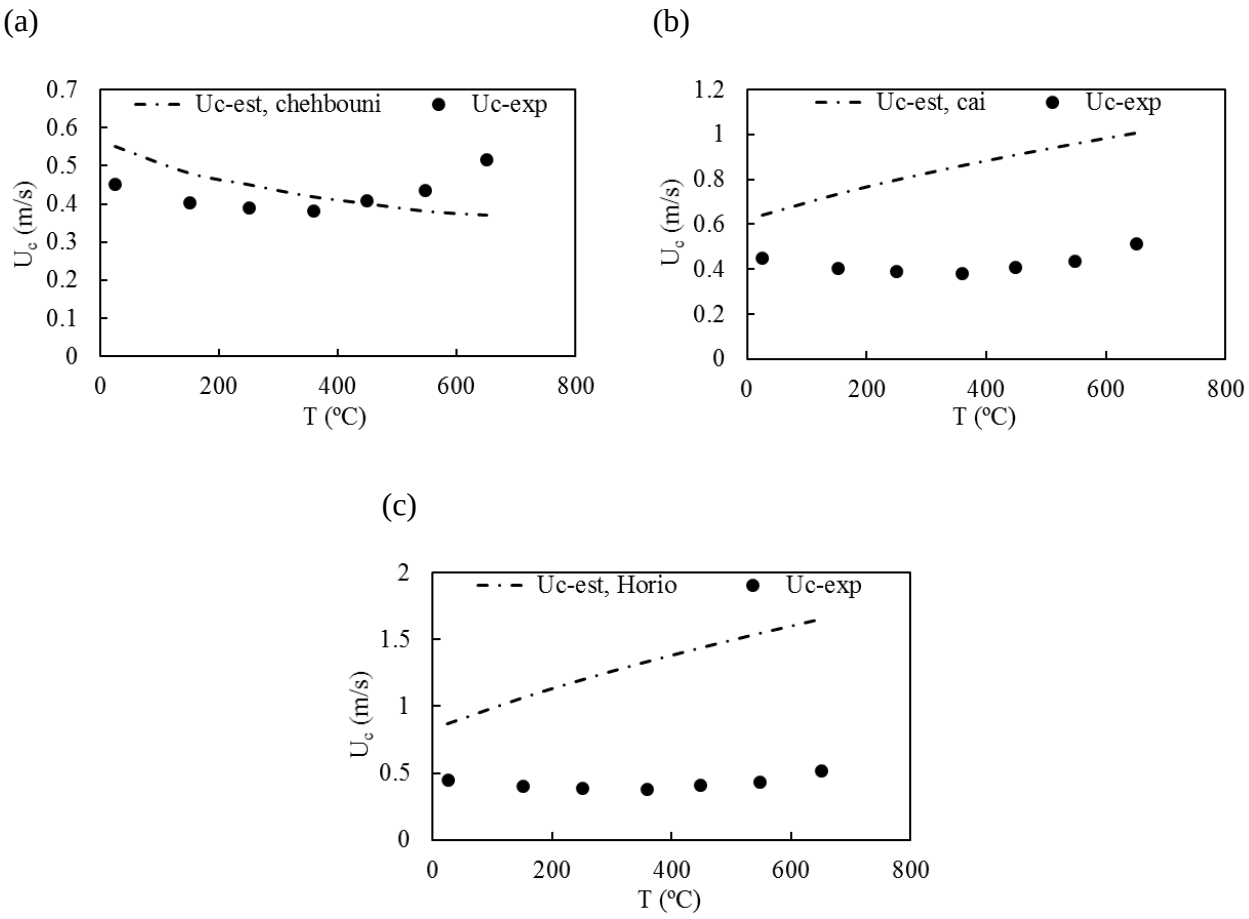

Figure 0.11: Variation of U_c by temperature for FCC86 fluidized by Air compared to its value estimated by: (a) Chehbouni et al. [183], (b) Cai et al. [163] and (c) Horio et al. [181].

Concluding Remarks

- U_c values of FS226 particles increased by temperature due to a decrease of the gas density and bubble size which delays the transition from bubbling to turbulent regime. This was also verified by the variation of U_c by temperature for CS820.
- For FCC86 particles, U_c values first decreased and then decreased by increasing the operating temperature. This dual trend found to be affected by the ratio of IPFs/HDFs at different temperatures.
- The increasing trend of U_c for FCC86 found to be due to the increased resistance of emulsion phase against bubble growth due to elevated levels of IPFs.
- U_c measurements for GB71 similarly increased by temperature due to the increase of IPFs by temperature.